

ORGANIC ELECTRONICS

BY

SELF-ASSEMBLY

Dissertation

zur Erlangung des akademischen Grades

Doktor der Naturwissenschaften (Dr. rer. nat.)

im Fach Chemie der Fakultät für Biologie, Chemie und Geowissenschaften

der Universität Bayreuth

vorgelegt von

Andreas Ringk

geboren in Homberg/Efze

Bayreuth 2012

Die vorliegende Arbeit wurde in der Zeit von August 2008 bis Dezember 2012 am Lehrstuhl für Makromolekulare Chemie I der Universität Bayreuth unter der Betreuung von Prof. Dr. Peter Strohriegl angefertigt.

Vollständiger Abdruck der von der Fakultät für Biologie, Chemie und Geowissenschaften der Universität Bayreuth genehmigten Dissertation zur Erlangung des akademischen Grades Doktor der Naturwissenschaften (Dr. rer. nat.).

Datum der Einreichung: 10.12.2012

Datum des wissenschaftlichen Kolloquiums: 22.03.2013

Prüfungsausschuss:

Erstgutachter: Prof. Dr. Peter Strohriegl

Zweitgutachter: Prof. Dr. Anna Köhler

Vorsitzender: Prof. Dr. Karl-Heinz Seifert

Prof. Dr. Stephan Förster



This research forms part of the research programme of the
Dutch Polymer Institute (DPI), project #627

“SUMM, SUMM.”

P. SCHÖRGEL



ABBREVIATIONS

AFM	atomic force microscopy
AMOLED	active matrix organic light emitting diode
a.u.	arbitrary unit
C	capacitance
CMOS	complementary metal oxide semiconductor
cps	counts per seconds
DOS	density of states
e	fundamental unit of charge
eV	electron volt
GIXD	grazing incidence X-ray diffraction
GIZO	gallium indium zinc oxide
HOMO	highest occupied molecular orbital
I_d	drain current
i. e.	that is (<i>id est</i>)
L	length
LUMO	lowest unoccupied molecular orbital
m	meter
NMOS	n-type metal-oxide-semiconductor
OFET	organic field effect transistor
OLED	organic light emitting diode
OSC	organic solar cell
OPV	organic photo voltaic
PTCDA	perylene tetracarboxylic dianhydride
PBI	perylene bisimide
PMOS	p-type metal-oxide-semiconductor
R	resistance

RFID	radio frequency identification tag
r. m. s.	root mean square
SAM	self-assembled monolayer
SAMFET	self-assembled monolayer field-effect transistor
SEM	scanning electron microscopy
SKPM	scanning kelvin probe microscopy
S_N2	bimolecular nucleophilic substitution
t	thickness
q	density of charges
V	volt
V_{dd}	supply voltage
$V_{d(s)}$	drain voltage
V_g	gate voltage
V_{th}	threshold voltage
W	width
XPS	X-ray photoelectron spectroscopy
XRR	X-ray reflectivity
Φ	work function
Φ_B	Schottky barrier
μ	charge mobility
Å	angstrom

TABLE OF CONTENTS

1	Summary	1
2	Introduction	9
3	Aim of the Thesis	29
4	Overview of the Thesis	31
5	References	49
6	N-Type Perylene to fill Voids in Solution Processed Nanoparticulate Zinc Oxide Thin Films	59
7	N-Type Self-Assembled Monolayer Field-Effect Transistors and Complementary Inverters	75
8	N-Type Self-Assembled Monolayer Field-Effect Transistors for Flexible Organic Electronics	111
9	Appendix	137
10	List of Publications	151

The target of low-priced and bendable electronic devices spurred academia, as well as, industry to develop novel high-performance materials for application in field-effect transistors. A crucial requirement for those materials is solubility in common solvents, enabling simple device fabrication steps such as printing, on large areas. Inorganic oxides and organic materials received attention because of their high performance and good solution processability. Whereas organic hole conducting materials (p-type) already exhibit high performance with mobilities similar to amorphous silicon, reliable electron transporting materials (n-type) are still a challenge. Both types of semiconductors, however, are needed to enable the well established complementary metal oxide semiconductor (CMOS) technique commonly used in silicon based electronic circuits. This thesis deals with the synthesis of new materials and their applications in n-type field-effect transistors in order to improve device performance by using simple fabrication procedures at low temperatures.

The first approach deals with field-effect transistors based on zinc oxide nanoparticles. Stable dispersions of zinc oxide nanoparticles allow the fabrication of zinc oxide transistors by solution processes. Despite the high intrinsic electron mobilities of zinc oxide, a large surface to volume ratio of nanoparticles often prevents their use as active material in field-effect transistors. Dangling zinc bonds are present at the surface, which act as electron donor, leading to increased conductivity. Switching the transistor off becomes challenging. The use of a tailored perylene bisimide, chemically linked to pyrrolidone groups, allowed the passivation of the dangling zinc bonds at the particle surface. Mixing of this perylene bisimide into nanoparticulate zinc oxide dispersions allowed transistor fabrication by spin-coating at low temperatures. On/off-ratios of the

resulting transistors could be enhanced by 3 orders of magnitude to 10^3 , so that zinc oxide nanoparticles turn into a semiconductor.

The second approach represents the main part of this thesis focusing on n-type self-assembled monolayer field-effect transistors (SAMFETs). It is known that approximately 90% of charge transport in field-effect transistors is managed just by an ultra-thin layer close to the dielectric. Due to the absence of bulk current, on/off-ratios in SAMFETs are enhanced without disadvantages to charge mobility or threshold voltage. The molecules for SAMFET applications typically consist of a semiconducting core, an endcapper on one side, and a reactive group on the other side, which is fixed to the core via a spacer. In this thesis, the well known perylene bisimides were chosen as semiconducting core. A branched alkyl tail acted as endcapper, whereas a linear C11-alkyl tail takes over the spacer part. As reactive group a phosphonic acid was chosen, which enables covalent fixation to aluminium oxide, a common dielectric for transistor applications. SAMFETs were fabricated by submerging transistor substrates into a dilute solution of the active molecule. During the immersion, the perylene bisimides reacts spontaneously to the aluminium oxide dielectric, forming a monomolecular layer. X-ray photoelectron spectroscopy (XPS) revealed a dense, homogeneous, and smooth monolayer on top of aluminium oxide. X-ray reflectivity (XRR) measurements confirmed the expected three regions, endcapper, semiconducting core, and spacer, perpendicularly ordered to the surface. In plane order was investigated by grazing incidence measurements (GIXD), which resulted in a nano-crystalline layer. SAMFETs showed bulk like electron mobilities of $10^{-3} \text{ cm}^2/\text{Vs}$. High on/off-ratios up to 10^5 and low threshold voltages were achieved. SAMFETs with channel length up to $100 \mu\text{m}$ were measured for the first time. The fact that all measured transistors, short channel as well as long channel, were working, indicated a high degree of reproducibility. Furthermore, by combining n-type and p-type SAMFETs, the first CMOS-bias inverter, solely based on SAMFETs, with large gain values up to 15, was realized.

To further improve SAMFET performance, the branched alkyl tail was replaced by a short linear fluorinated alkyl tail, with the intention to increase the surface coverage of the chromophores by a more slender design of the molecule. SAMFETs were fabricated with the same simple method as described above. XPS measurements showed a complete coverage of an organic layer with a thickness matching perfectly the simulated length of the molecule. In contrast to the previous SAMFETs, the phosphorous was located mainly

at the aluminium oxide surface and not, as before, throughout the organic layer. The fluorine atoms were detected at the top of the layer. Both observations are indicative for higher order of the monolayer. XRR measurements gave a consistent structure of the layer. A three layer structure was found in which the electron density of the outer layer was enhanced, due to the presence of electron rich fluorine atoms. The thicknesses of all three layers were in good agreement to the calculated distances. Furthermore, GIXD studies revealed an amorphous SAM on top of aluminium oxide, optimal for charge transport without disturbing grain boundaries.

The new SAMFETs were also highly reproducible and showed electron mobilities on the order of 10^{-3} cm²/Vs, low onset voltages, and high on/off-ratios in the order of 10^6 . Besides SAMFETs on common non-flexible silicon substrates, comparable n-type SAMFETs were also fabricated on polymer based substrates for the first time. Furthermore, a unipolar bias inverter was built, paving the way towards flexible *organic electronics by self-assembly*.

In summary, all three publications of this thesis deal with the synthesis of semiconducting perylene bisimides and their implementation in n-type field-effect transistors. Reliable transistors and the first integrated CMOS-like circuits based solely on SAMFETs with high performances were achieved, made by simplest solution processes at low temperatures.

Der Wunsch nach preisgünstigen und flexiblen elektronischen Bauteilen ist für Forschungseinrichtungen sowie für die Industrie Ansporn, nach neuen Hochleistungsmaterialien für Anwendungen in Feld-Effekt Transistoren zu suchen. Eine wichtige Voraussetzung solcher Materialien ist deren Löslichkeit in gängigen Lösungsmitteln, wodurch elektronischen Bauteile mittels einfacher Methoden, wie beispielsweise durch Drucken, hergestellt werden können. Anorganische, nanopartikuläre Oxide und organische Materialien erlangten große Aufmerksamkeit aufgrund Ihrer guten Eigenschaften und einfachen Prozessierbarkeit aus Lösung. Während organische Lochleiter bereits hohe Ladungsträgermobilitäten erreichen, die mit amorphem Silizium vergleichbar sind, sind bisher nur wenige elektronenleitende Materialien mit hohen Mobilitäten bekannt. Beide Arten von Halbleitern werden jedoch für die etablierte CMOS-Technik (complementary metal oxide semiconductor) benötigt, die in den meisten elektronischen Schaltungen zur Anwendung kommt. Diese Arbeit handelt von der Synthese neuer Materialien und deren Anwendung in elektronenleitenden Feld-Effekt Transistoren, welche ausschließlich durch einfache, lösungsbasierte Prozesse bei niedrigen Temperaturen hergestellt werden wobei gleichzeitig die Eigenschaften der Transistoren verbessert werden.

Der erste Ansatz handelt von Feld-Effekt Transistoren aus Zinkoxid Nanopartikeln. Stabile Dispersionen von Zinkoxid Nanopartikeln erlauben die Herstellung von Zinkoxid Transistoren durch lösungsbasierende Prozesse. Trotz hoher intrinsischer Elektronenmobilitäten ist das große Oberflächen-Volumen-Verhältnis der Zinkoxid Nanopartikel hinderlich für deren Anwendung als Material in Feld-Effekt Transistoren. An der Oberfläche befinden sich ungesättigte Zinkbindungen welche als

Elektronendonatoren wirken. Dadurch wird die Leitfähigkeit erhöht. Das Ausschalten eines solchen Transistors wird dadurch erschwert. Die Verwendung eines maßgeschneiderten Perylenbisimides, chemisch verbunden mit Pyrrolidon Einheiten, ermöglichte eine Passivierung der ungesättigten Zinkvalenzen an der Partikeloberfläche. Die Beimischung dieses Perylenbisimides zu Zinkoxid Dispersionen erlaubte die Transistorherstellung mittels Spin-Coating bei niedrigen Temperaturen. Die an/aus-Verhältnisse der resultierenden Transistoren konnten um drei Größenordnungen auf 10^3 gesteigert werden.

Der zweite Ansatz spiegelt den Hauptteil dieser Arbeit wieder und beschäftigt sich mit elektronenleitenden, selbst-assemblierenden Feld-Effekt Transistoren welche aus einer Moleküllage bestehen (self-assembled monolayer field-effect transistors, SAMFETs). Es ist bekannt, dass ungefähr 90% des Ladungstransports in Feld-Effekt Transistoren in einer ultradünnen Schicht, nahe dem Dielektrikum, stattfindet. Aufgrund der Abwesenheit von Volumenströmen ist das an/aus-Verhältnis in SAMFETs erhöht, ohne Nachteile auf Mobilität oder Schwellspannung. Die Moleküle für Anwendungen in SAMFETs bestehen aus einem halbleitenden, aromatischem Kern, einer Alkylkette auf der einen Seite und einer reaktiven Gruppe auf der anderen Seite, welche mittels eines Spacers an den Kern gebunden ist. In dieser Arbeit wurden Perylenbisimide als halbleitende Kerne verwendet. Ein verzweigter Alkylrest fungiert zunächst als Endcapper, während eine C11-Alkylkette als Spacer fungiert. Als reaktive Gruppe wurde die Phosphonsäure gewählt, welche eine kovalente Fixierung auf Aluminiumoxid ermöglicht, ein übliches Dielektrikum in Feld-Effekt Transistoren. Die SAMFETs wurden durch Eintauchen der Substrate in verdünnte Lösungen der Bisimide hergestellt. Während des Eintauchens reagiert die Phosphonsäure mit den OH-Gruppen des Aluminiumoxid Dielektrikums, wodurch eine monomolekulare Schicht aufgebaut wird. XPS (X-ray photoelectron spectroscopy) Untersuchungen ergaben eine dichte, homogene und ebene Monolage auf Aluminiumoxid. XRR (X-ray reflectivity) Messungen bestätigten die erwarteten, senkrecht geordneten drei Regionen von Endcapper, halbleitendem Kern und Spacer. Die Ordnung innerhalb der Schicht wurde mittels GIXD (grazing incidence X-ray diffraction) untersucht, und ergab eine nanokristalline Schicht. Die SAMFETs zeigten Elektronenmobilitäten von $10^{-3} \text{ cm}^2/\text{Vs}$, hohe an/aus-Verhältnissen von 10^5 , und niedrige Schwellspannung von 3 V. Außerdem wurden zum ersten Mal SAMFETs mit Kanallängen bis 100 μm gemessen. Die Tatsache, dass alle gemessenen Transistoren, mit

kurzen sowie mit langen Kanälen, funktionierten, beweist einen hohen Grad an Reproduzierbarkeit. Des Weiteren wurde der erste, einzig auf SAMFETs basierende, CMOS-Spannungs Inverter mit hohen Verstärkungsfaktoren von bis zu 15, realisiert.

Um die Eigenschaften der SAMFETs zu verbessern, wurde der verzweigte Alkylrest durch eine kurze, lineare fluorierte Kette ersetzt. Die Intention war die Oberflächenbedeckung durch ein schlankeres Design des Moleküls zu erhöhen. Die SAMFETs wurden mit der oben beschriebenen, einfachen Methode hergestellt. XPS Messungen zeigten eine dichtere Bedeckung des Dielektrikums durch das neue Perylenebisimid. Die Schichtdicke stimmte hierbei perfekt mit der simulierten Länge des Moleküls übereinstimmt. Im Gegensatz zu den vorangegangenen SAMFETs findet man den Phosphor hauptsächlich an der Aluminiumoxidoberfläche und nicht zusätzlich in der organischen Schicht. Die Fluoratome hingegen wurden hauptsächlich an der Oberfläche der Schicht detektiert. Beide Beobachtungen weisen auf bessere Anordnung der Moleküle innerhalb der Monolage hin. XRR Untersuchungen ergaben einen übereinstimmenden Aufbau der Monolage. Die Monolage kann in drei separate Schichten unterteilt werden wobei die Elektronendichte der äußeren Schicht, aufgrund der Anwesenheit elektronenreicher Fluoratome, erhöht war. Die Schichtdicken aller drei Lagen stimmten mit den berechneten überein. Des Weiteren zeigten GIXD Messung eine amorphe Monolage ohne störende Korngrenzen von kristallinen Bereichen.

Es konnten SAMFETs mit hoher Ausbeute hergestellt werden. Es wurden Elektronenmobilitäten in der Größenordnung von $10^{-3} \text{ cm}^2/\text{Vs}$, niedrige Durchschlagsspannungen und hohe an/aus-Verhältnisse im Bereich von 10^6 erhalten. Neben den üblichen SAMFETs auf starren Silizium Substraten wurden zum ersten Mal auch funktionierende n-type SAMFETs Polymersubstraten hergestellt. Des Weiteren wurde ein unipolarer Spannungsinverter aufgebaut, ein wichtiger Schritt in Richtung flexibler organischer Elektronik basierend auf SAMFETs.

Zusammenfassend beschäftigen sich alle drei Veröffentlichungen dieser Arbeit mit der Synthese von halbleitenden Perylenebisimiden und deren Anwendung in elektronenleitenden Feld-Effekt Transistoren. Hochreproduzierbare Transistoren mit hohen Ladungsträgermobilitäten und an/aus-Verhältnissen bei niedrigen Schwellspannungen wurden ebenso wie die ersten integrierten CMOS-Schaltkreise durch einfaches Self-Assembly aus Lösung hergestellt.

An apparatus for controlling electric currents was proposed by Lilienfeld already during the twenties.^[1] He patented a device where an electronic flow between two conductive terminals could be modified by a third potential between these terminals. The device was planned in order to amplify the *transfer* of charges by controlling the *resistance* with an applied potential. As a consequence, a portmanteau was born which gave this device its name: *transistor*.^[2]

Basically, a transistor can be regarded as a capacitor in which two plates are separated by an insulator. One plate consists of a semiconducting material which is placed between two ohmic contacts, the other plate is a conducting material (see figure 1). The contacts are called source- and drain-electrodes, the insulator is a dielectric and the conductive plate is named gate-electrode. By applying an electric potential to the gate electrode the semiconductor becomes conductive and enables a charge transfer from source- to drain-electrode. The first prototype transistor was demonstrated by Shockley, Bardeen, and Brattain in the Bell laboratories in 1947.^[3] In 1958 the three inventors were awarded the Nobel Prize in physics because of the huge impact of their findings. Putting together more than one transistor in a single device initiated the field of integrated circuits.^[4] So far semiconducting materials were only able to conduct electrons and only unipolar n-type circuits with high power consumption could be built. The discovery of hole conductors (p-type) allowed the realization of the complementary metal-oxide semiconductor (CMOS) technique, which requires pairs of p- and n-type transistors.^[5] Low power consumption and high noise immunity were the results. Following Moore's law, transistors became simultaneously smaller and improved at a lower price to enable new high performance computer systems.^[6] Most recently Intel has accomplished a major

success for practical usage by introducing a completely new transistor generation onto the market. This architecture allows dense packing of 1.4 billion so called tri-gate transistors with a size of 22 nm onto a 160 mm² die.^[7] Recently, the miniaturization of transistors reached the physical limit. Fuechsle et al. realized a single-atom transistor by doping silicon with an individual phosphorous atom.^[8]

Silicon based transistors will be the leading technology for high performance electronics in the foreseeable future.

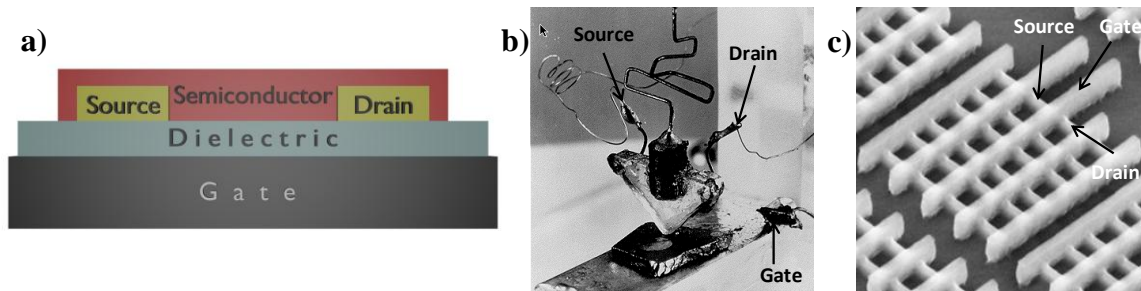


Figure 1: a) Layout of a typically field effect transistor containing source-, drain-, gate-electrodes, the semiconductor and dielectric. b) Picture of the first working transistor made in the bell laboratories in 1947.^[9] c) 22 nm tri-gate transistors recently commercialized by Intel.^[10]

Since the sixties, inorganic metal oxide semiconductors e.g. tin oxide^[11] or zinc oxide^[12] have been studied as active material in field-effect transistors. The performance of these devices was considerably low but the use of transparent semiconductors promised a new field for application. The performance of metal oxide thin-film transistors rises year by year. Nomura et al., for example, presented gallium indium zinc oxide (GIZO) transistors with excellent device characteristics showing electron mobilities up to 80 cm²/Vs.^[13] However, during device fabrication high temperatures up to 1400°C were needed. In order to prevent plastic incompatible high temperatures and multiple fabrication steps, the focus shifted to solution based processes. Usage of soluble precursors or nanoparticles are two main routes to allow simple methods as spraying,^[14] spin-coating^[15] or ink-jet printing^[16] to form metal oxide layers. Here, the challenges are the preparation of printable precursor solutions,^[17] instabilities concerning the large surface area of nanoparticles,^[18] and high temperatures of several hundred degrees during a post-bake step. Nevertheless, Kim et al. showed that solution processes is even combinable with polymer substrates to realize high performance and optical transparent transistors on flexible plastic substrates.^[19]

In the late 1970s, Heeger, Diarmid and Shirakawa presented a new material for which they were honored with the Nobel Prize in chemistry in 2000. By doping polyacetylene with halogens, the first electrical conductive organic polymer was demonstrated.^[20] Many groups paid great attention to this new field, which grew so fast that first organic solar cells^[21] (OSC) and organic light emitting diodes^[22] (OLEDs) became reality. Mechanical properties of organic materials promise a huge market for low cost and energy saving displays or flexible circuits. Good solubility of organics in common solvents allows cheap printing of large area electronics such as solar cells. A conjugated π -electron system is the basic requirement for organic polymers or small molecules in order to conduct positive or negative charges. Such planar systems are achievable by alternation of carbon-carbon single and double bonds where the carbon atoms are sp^2 -hybridized, so that p_z -orbitals can overlap to delocalize the electron density over several atoms along the molecule. Due to the fact that the overlap of two p_z -orbitals is less, π -bonds are weaker than σ -bonds, which are formed by the overlap of two sp^2 -orbitals. In π -conjugated materials the π -orbitals usually form the Highest Occupied Molecular Orbitals (HOMO) and the Lowest Unoccupied Molecular Orbital (LUMO). A high HOMO-level is suitable for p-type materials, whereas a low LUMO level is desirable for n-type materials. A big pool of synthetic strategies allows modification of the materials to get tailored properties by chemical adjustment. Matching orbital-levels by chemical modification is an essential advantage of organic semiconducting materials to optimize optoelectronic properties. These features, i. e., -flexibility, printability and modifiability- make organic materials a competitor of metal oxides to fill niches which are difficult to access with silicon.

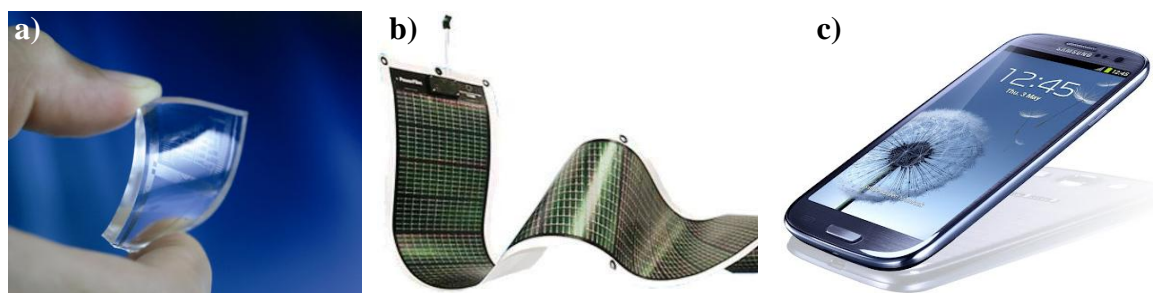


Figure 2: Applications for organic semiconductors. **a)** Organic circuits on a bendable polymer substrate.^[23] **b)** Flexible organic photovoltaik.^[24] **c)** Samsung Galaxy S3 smart phone incorporate an organic based super-AMOLED display.^[25]

An example par excellence is Samsung's active-matrix organic light-emitting diode (AMOLED) display, brought onto the consumer market in 2010. The industrial realization of organic solar cells is also at the edge of commercialization. Animated by

the world's increasing energy consumption, companies around the world work on how to beat the efficiency record of about 10%.^[26] Materials for organic field-effect transistors have already achieved performances comparable to amorphous silicon. Possible applications, such as pixel drivers in displays or circuits in radio-frequency identification tag (RFID), are feasible.

The initial part of this thesis describes the improvement of nanoparticulate zinc oxide field-effect transistors. That was done by surface modification of zinc oxide nanoparticles using a tailored organic compound in a low temperature process.

The second part forms the main part of this thesis and deals with n-type self-assembled monolayer field-effect transistors (SAMFETs) based on heterosubstituted perylene bisimides. Self-assembly is a promising method for large area device fabrication at low temperatures by using only a minimum amount of the active semiconducting material. This has already been demonstrated successfully for p-type materials. The aim is to develop novel n-type materials for SAMFET applications in order to push this new field towards the CMOS-technique and to enable robust organic electronics made by self-assembly.

2.1 Organic Field-Effect Transistors

The basic units in organic field-effect transistors are the electrodes source, drain, and gate, a dielectric layer and a semiconductor. A schematic is shown in figure 3. The gate can also be used as substrate and consists in principle of any conductive material. Highly doped silicon wafers are commonly used as gate electrode and thermally grown silicon dioxide forms the insulating dielectric layer. On top of the dielectric the electrodes, typically patterned by photolithography, are deposited.

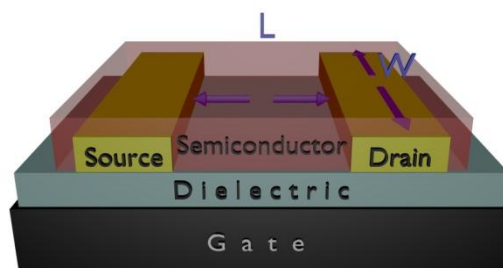


Figure 3: Scheme of a bottom-gate, bottom-contact organic field-effect transistor. The gate-electrode is separated by a dielectric layer from the source- and drain-electrodes. A semiconductor is between these electrodes to enable a pathway for charges. The length (L) is defined as the distance between source and drain. The width (W) is the length of the electrodes.

A semiconductor can be placed between the transistor electrodes by, for example, spin-coating or drop-casting. The source- and drain-electrodes should form ohmic contacts to the semiconducting material within the channel. For p-type materials, these contacts should have a low work function (Φ) in order to enable an efficient transfer of holes between semiconductor and electrode. For n-type materials, a high work function is favorable to get a better injection of electrons into the LUMO-level of the semiconductor without huge contact resistance. Gold ($\Phi \sim 5.1 \text{ eV}$)^[27] is a good contact material for p-type OFETs, whereas aluminum ($\Phi \sim 4.28 \text{ eV}$)^[27] or calcium ($\Phi \sim 2.9 \text{ eV}$)^[27] are convenient for n-type materials. However, due to its inertness and easy processability, e.g. for lithography processes, gold is often also used for n-type OFETs. In this case injection barriers are accepted. The channel is defined by the channel width (W) and the channel length (L), which stands for the distance between source- and drain-electrodes. To get higher currents, finger transistors are often used in which interpenetrating electrodes form a broad channel width of typically 1 - 20 μm at a channel length of 1 - 20 μm .

In the following part, the working principle of an organic field-effect transistor will be described, which is illustrated in figure 4. By applying a potential only to the source- and drain-electrodes no current is measurable. The device is in the off-state and the semiconductor acts as insulator (Fig. 4a). Only low off-currents occur as a result of a slight conductivity of the material. If a potential is applied to the gate-electrode (V_g), the potential drops over the dielectric to the semiconductor, due to the “field-effect”, resulting in a band-bending. Charges injected from the source electrode into the semiconductor generate a thin charge accumulation layer close to the dielectric. Depending on the semiconductor and the gate bias, holes or electrons can be generated. A negative gate-bias accumulates holes; a positive bias accumulates electrons (Fig. 4b). The semiconductor becomes conductive and first all deep traps are filled. Increasing the gate bias up to the threshold voltage (V_{th}), the semiconductor gets mobile charge carriers, which enable an electrical current (I_d) through the transistor channel by applying a drain voltage (V_d). That drain current increases linearly with the drain voltage (Fig. 4c). At a certain voltage where the equation $V_d \geq V_g - V_{th}$ is complied, the pinch-off point is reached (Fig. 4d). The potential of the gate is now the same as the potential inside the semiconducting layer close to the drain electrode. Further increase in V_d shifts the pinch-off point slightly in the direction of the source-electrode and a depletion zone is formed (Fig. 4e). If the transistor

length (L) is much longer than the width of the depletion zone, no further increase of the current can be observed by increasing V_d , due to the resistance of the depletion zone. A high potential inside the depletion zone between drain-electrode and pinch-off point occurs, which results in a space-charge limited current. The resistance between source-electrode and pinch-off point remains constant - no current increase can be observed. I_d saturates, and becomes independent of the drain voltage and can be modulated only by the gate voltage.

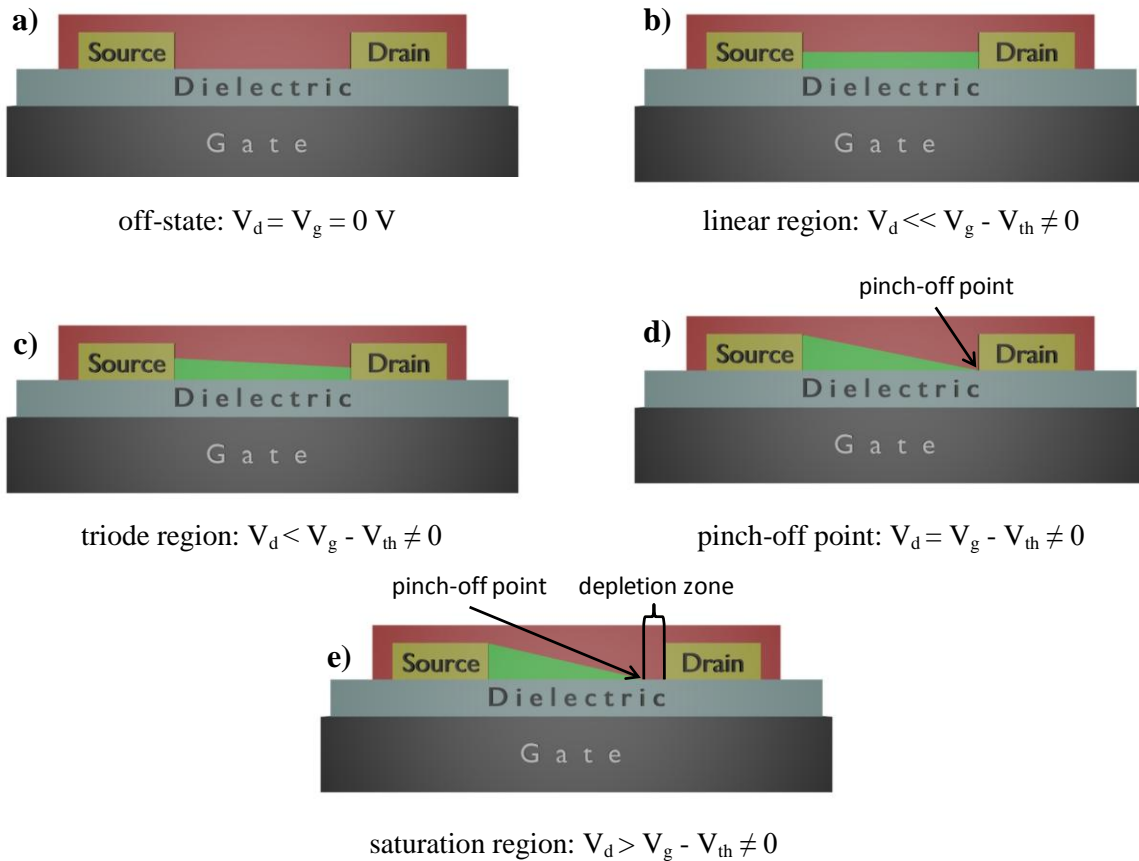


Figure 4: Schematic illustration of the working-principle of an organic field-effect transistor. **a)** The transistor is switched off. Drain- and gate-voltage are equal to zero, so that the semiconductor acts as insulator. **b)** By applying only a gate-voltage, the charge carrier concentration within the channel increases and an accumulation layer (green) is generated. **c)** An additional drain-voltage leads to an electrical current flowing from the source through the semiconductor into the drain-electrode. **d)** Reaching the pinch-off point the potential inside the channel close to the drain-electrode is equal to the gate-bias. **e)** Further increase in the drain-voltage results in a depletion zone where the drain-current becomes independent of the drain-voltage.^[28]

To analyze transistors, two main characteristics are needed: output and transfer. For the output characteristic, the gate voltage is kept constant and the drain voltage is swept; whereas for measuring the transfer characteristic, the gate voltage is swept while holding the drain bias constant. The resulting I - V -curves can also be described theoretically.^[29] If

a voltage is applied to the gate, a uniform accumulation layer is generated close to the dielectric across the semiconductor (Fig. 4b). By applying a drain-voltage (V_d), the charge density inside the channel at a specific position x is proportional to the voltage difference $V_g - V_{(x)}$. With the capacitance C of the dielectric, the number of charges inside the channel, the fundamental unit of charge e , and the thickness of the charged layer t , and the areal density of charges q can be described with equation 1:

$$q_{ind(x)} = n_{(x)}et = C(V_g - V_{(x)}) \quad (1)$$

In organic transistors, the semiconductor is often not conductive at $V_g = 0V$ because of charge trapping or mismatches between electrodes and semiconductor. In order to include this behavior, the threshold voltage (V_{th}) is used, so that equation 1 becomes equation 2:

$$q_{ind(x)} = n_{(x)}et = C(V_g - V_{th} - V_{(x)}) \quad (2)$$

By applying a voltage to the drain electrode which is lower than the gate bias, a linear charge concentration gradient occurs (Fig. 4d). Under this condition the average value of the charges in the middle of the layer turns from equation 2 into equation 3 (gradual channel approximation). To the left, the concentration is higher, and to the right, the concentration is lower, so that integration over the complete channel results in the half concentration:

$$q_{ind(x)} = n_{(x)}et = C(V_g - V_{th} - \frac{V_d}{2}) \quad (3)$$

Ohm's law can be written as shown in equation 4:

$$\frac{I_d}{tW} = \sigma \frac{V_d}{L} \rightarrow I_d = (n_{av}et)\mu V_d \quad (4)$$

Here, σ is the conductivity, μ is the charge mobility, and n_{av} is the average concentration of charges in the channel. Now equation 3 can substituted into equation 4 to obtain equation 5:

$$I_d = \frac{W}{L} C_{ox} \mu [(V_g - V_{th}) - \frac{V_d}{2}] V_d \quad (5)$$

For reason of simplicity, equation 5 is transformed into equation 6.

$$I_d = \frac{W}{L} C_{ox} \mu [(V_g - V_{th}) V_d - \frac{V_d^2}{2}] \quad (6)$$

Equation 6 is a description of the current in the linear regime where the drain current $V_d \leq (V_g - V_{th})$ (Fig. 4c). Here, the current scales linearly with the gate voltage, and quadratically with the drain voltage. The term inside the brackets multiplied with C_{ox} is the average areal charge density in the transistor channel. For $V_d \ll (V_g - V_{th})$, the $V_d/2$ term becomes negligible and can be dropped.

$$I_d = \frac{W}{L} C_{ox} \mu [(V_g - V_{th}) V_d] \quad (7)$$

To calculate the mobility in the linear regime, the first derivative of equation 7 is used.

$$\left. \frac{\partial I_d}{\partial V_g} \right|_{V_d} = \frac{W}{L} C_{ox} \mu_{lin} V_d \Rightarrow \mu_{lin} = \frac{\partial I_d}{\partial V_g} \frac{L}{W C_{ox} V_d} \quad (8)$$

If the drain voltage is increased, so that $V_d \leq V_g - V_{th}$, the channel is pinched and a depletion zone occurs close to the drain electrode, so that no increase in current can be observed. The current becomes constant and is no longer a function of the drain voltage. To describe this behavior $V_d = V_g - V_{th}$ is substituted into equation 6:

$$I_{d,sat} = \frac{W}{2L} C_{ox} \mu_{sat} (V_g - V_{th})^2 \quad (9)$$

To calculate the charge mobility in the saturation regime, $\sqrt{I_d}$ is plotted versus the gate voltage. From the slope of the resulting graph, the mobility can be determined with equation 10:

$$\mu_{sat} = \left(\frac{\partial \sqrt{I_{d,sat}}}{\partial V_g} \right)^2 \frac{2L}{W C_{ox}} \quad (10)$$

The x-intercept of the slope gives the threshold voltage (Fig. 5b). Besides the mobility and threshold voltage, the on/off-ratio is the third important value for transistors. The fourth often used value is the sub threshold swing S which is defined as:

$$S = \frac{dV_g}{d(\log I_d)} \quad (11)$$

High charge mobilities and on/off-ratios and a low threshold voltage and threshold swing are desirable. All these values are commonly determined from the transfer characteristics.

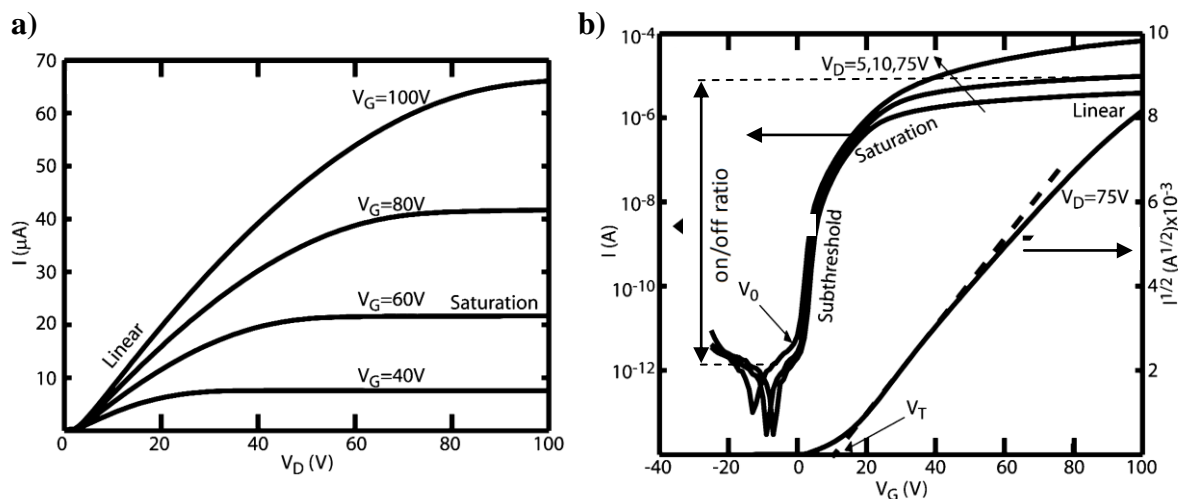


Figure 5: Examples of I-V-curves for an organic field effect transistor. **a)** Output characteristics for gate- voltages up to 100 V. **b)** Transfer characteristics with drain voltages of 5 V, 10 V, and 75 V. The lower curve shows $\sqrt{I_d}$ versus the gate voltage, V_0 is defined as onset voltage, V_T is the threshold voltage.^[29]

2.2 Charge injection and transport in organic field-effect transistors

Charge injection into and charge transport through the organic semiconductor plays a crucial role with respect to device performance. Both aspects are discussed in the following passage.

2.2.1 Charge injection into organic semiconductors

The injection of charges from a metal electrode into organic semiconductors is an important aspect for OLEDs,^[30] OPV,^[31] as well as OFETs.^[32] In OFETs, injection has huge impact, in particular for short channel devices having channel lengths shorter than $\sim 5\mu\text{m}$. One reason is the challenge of creating ohmic contacts between metals and organic semiconductors. In inorganic semiconductors, for example, ohmic contacts are made by controlled doping of the semiconductor, leading to neat charge injection. In contrast, due to device instabilities and migration of counterions, doping of organic semiconductors is more difficult. As a result, Schottky-barriers (Φ_B) are often formed at the interface between metal and organic semiconductor, leading to contact resistance. If an electrical

field is applied to an organic transistor, an electron can be injected into the semiconductor. Simultaneously, a positive mirror charge is left in the metal electrode. An electrical field between these charges occurs, which makes further electron injections more difficult (built-in potential; Fig. 6).^[33]

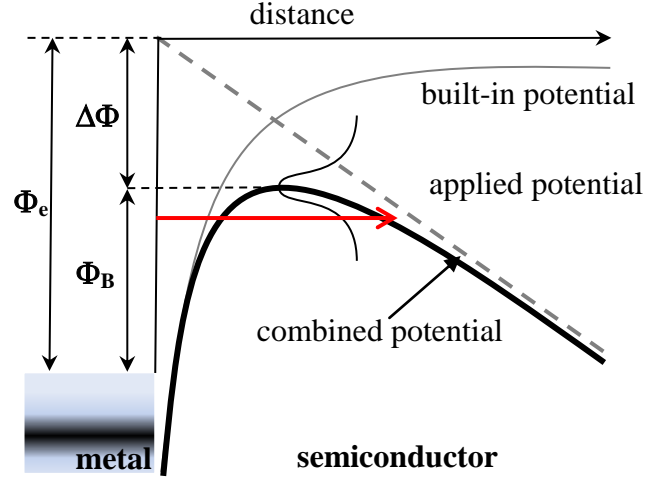


Figure 6: Energy band diagram of charge injection from a metal contact into a disordered organic semiconductor. After applying a potential (grey dashed line), electrons are injected into the semiconductor, leaving behind positive charges in the metal electrode. A built-in potential (grey line) occurs, which hampers further charge injection. The result of both potentials is called Schottky-barrier (Φ_B), which is lower than the metal work function (Φ_e) by the amount $\Delta\Phi$. Because organic semiconductors are often disordered, charge injection (red arrow) into deep states becomes possible, lowering the barrier further.^[33,34]

Bürgi et al. showed that if the barrier is less than 0.3 eV, contact resistance is not determined by the Schottky barrier at the metal/organic interface but by the bulk-transport in the vicinity of the contacts.^[35] If the barrier exceeds the value of 0.3 eV, then the source resistance is larger than the drain resistance, which means that the contact resistance is determined mainly by the physics of carrier injection. Furthermore, the Schottky-barrier (Φ_B) is slightly reduced, due to molecular disorder within the organic semiconductor. Disorder in organic leads to a broader gaussian distribution of the density of states (DOS), which enables new pathways through deep states in the DOS (Fig. 6 red arrow).^[34]

The mathematical description in the previous chapter assumes ohmic contacts where no contact resistant occurs. In this optimized case the transistor current in the linear regime can be described with equation 5 where I_d is the drain current, W the channel width, L the channel length, C_{ox} the capacitance, μ the charge carrier mobility, V_g the gate voltage, and V_{th} the threshold voltage.

$$I_d = \frac{W}{L} C_{ox} \mu [(V_g - V_{th}) - \frac{V_d}{2}] V_d \quad (5)$$

Taking the source and drain resistance (R) into account, the mobility in the linear regime is described with equation 12.^[36,37]

$$\mu = \mu_0 \frac{L}{L + WC_{ox}R\mu_0(V_g V_{th} \frac{V_d}{2})} \quad (12)$$

The intrinsic mobility (μ_0) is constant, whereas the determined mobility (μ) is a function of the channel length (L). Equation 12 displays that for longer channel length the mobility approaches a limit. For shorter channels, the contact resistance has much stronger influence. Charge mobility drops, leading to lower transistor switching speeds.^[37] Similar results were also shown for the saturation regime.^[38] To obtain lower contact resistance different metals can be used for the contacts, in order to match the fermi-levels of the metal with the orbital energies of the organic semiconductor. For n-type semiconductors low work function contacts, for p-types a high work function contact is desirable, in order to inject, electrons, or holes, respectively. Further strategies for lowering contact resistance are the use of self-assembled monolayers, e.g. thiols^[39] on electrodes or change of device architecture.^[36,40]

2.2.2 Charge transport through organic semiconductors

Organic semiconducting materials are typically molecules having an extended π -electron system. In those systems, overlapping π -orbitals are present, which enable charge delocalization along the molecule. These molecules can be classified into electron and hole transporting materials according to whether majority charge carriers are present. Electron withdrawing groups lower the HOMO and LUMO level, whereas electron donating groups enhances the HOMO and LUMO level. Low LUMO-levels are favorable for electron injection and transport, high HOMO-levels, in contrast, are required for hole injection and conduction. The mobility of electrons in organic materials is for practical cases much smaller than of holes, because of the high sensitivity of electrons towards trap-states.^[41] Therefore, high purities and well ordered structures are required to lower the density of traps states.^[42] Oxygen and water are supposed to be the main reasons for trap generation under ambient conditions.^[43] To prevent charge trapping with respect to water and oxygen low LUMO-levels less than 4.0 eV are essential.

The three dimensional order in organic materials is often lower than in inorganic materials. Thus, the band model where charges are delocalized over several atoms as in metals or metal oxide semiconductors is not suitable to describe charge transport in

disordered systems. Different models, such as the polaron transport^[44] or the Scher-Montroll formalism,^[45] were proposed. However, the most important theory for charge transport in disordered organic systems has been introduced by Bässler.^[46] Because of local disorder and the resulting individual environment of each molecule, their energy levels are not monoenergetic. A gaussian distribution of local states is assumed where the charges are fixed in an orbital located at one molecule. The charge transport itself takes place by hopping among molecules.

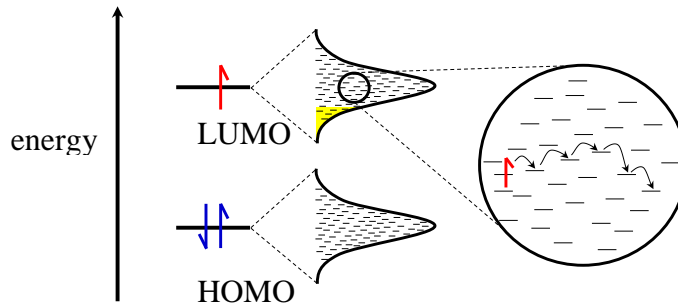


Figure 7: The “hopping mechanism” for an n-type semiconductor according to Bässler.^[46] Because of disorder, a gaussian distribution of energy levels is assumed. The electron (red) is localized in a LUMO level at one molecule and can hop to the next molecule after applying an electrical field. Depending on their energy, the lowest states of the LUMO levels can act as trap (highlighted in yellow).

A broad energy distribution leads to a broader density of states, so that more highest and lowest states are present. Impurities and low crystallinity can be responsible for the unfavorable broadening of the DOS. The deepest states can trap charges due to their low energy and in this way reduce device performance. To prevent charge trapping by chemical traps, high purity is needed. Also remarkable is that charge transport in crystalline organic materials depends strongly on the molecular orientation^[47] and crystal axis.^[48] For materials reaching mobilities up to $1 \text{ cm}^2/\text{Vs}$ ^[49] or higher,^[48] the band model becomes accurate. Here, the mobility goes down with increasing temperature, which is a fingerprint for band like charge transport. However, the charge transport mechanism in organic materials is not yet understood in all details and still under discussion.

2.3 Transistor architectures

Different transistor architectures are known. Bottom-gate bottom-contact transistors are often used, as only one step, the deposition of the semiconductor onto the preformed substrate, is needed to complete the device. Those substrates are commercially available, which is ideal for fast material screening and device optimization. The electrodes are typically made of gold. The low work function of gold matches well with the HOMO

levels of p-type materials. For n-type materials, gold electrodes can be modified with thiols in order to increase the work function for better electron injection.^[39]

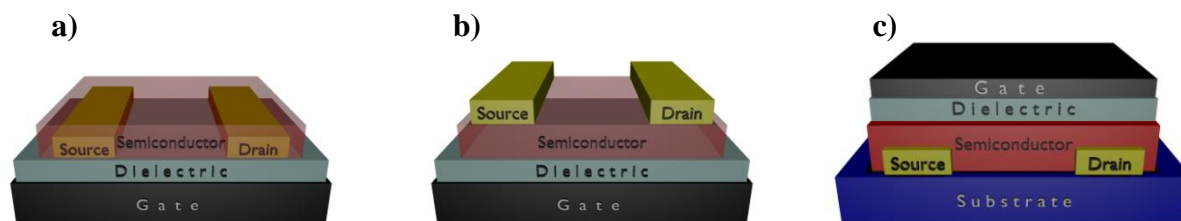


Figure 8: Most important transistor architectures. **a)** The bottom-gate bottom-contact, **b)** bottom-gate top-contact structure **c)** and top-gate bottom-contact configuration.

The electrodes in top-contact bottom-gate devices are typically evaporated through a shadow mask on top of the organic semiconductor. To prevent destruction and penetrating of metal atoms into the organic layer, a careful metal evaporation is required. As a result, complete and dense metal electrodes cover the organic, so that the contact resistance in top-contact bottom gate transistors is approximately one order of magnitude lower compared to bottom-contact devices.^[36] The most challenging device architecture discussed here is the bottom-contact top-gate configuration. Here, the gate electrode is deposited on top of the organic semiconductor so that the semiconductor is encapsulated between the substrate and the dielectric with gate electrode. This encapsulation increases device stability under ambient conditions.^[50,51] Also the contact resistance can be reduced in this setup.^[52] Nevertheless, the elaborate device fabrication makes this architecture more difficult to realize so that the bottom-gate bottom-contact device is the most widely used transistor device. In the following chapter materials for n-type transistors are discussed.

2.4 Rylene bisimides for electronic devices

A widely used class of electron transporting materials are the rylene based diimides. The basic building block is a naphthalene unit. This unit can be connected at the 1,1' or 8, 8' position with further naphthalene units to build up oligo(peri-naphthalene)s. Finally, the rylene bisimides are formed by termination of those naphthalenes with two bisimides groups. Typical examples are shown in figure 9. Chemical modification by organic synthesis allows a broad variation of the tails at the imide group or of substituents attached to the rylene skeleton in order to adjust solubility, packing behavior or optoelectronic properties. High electron mobilities, and desirable chemical, thermal, and

photochemical stability makes this class of molecules attractive as active material in organic photovoltaics,^[53] organic light-emitting diodes,^[54] dye lasers^[55] or field-effect transistors.^[56]

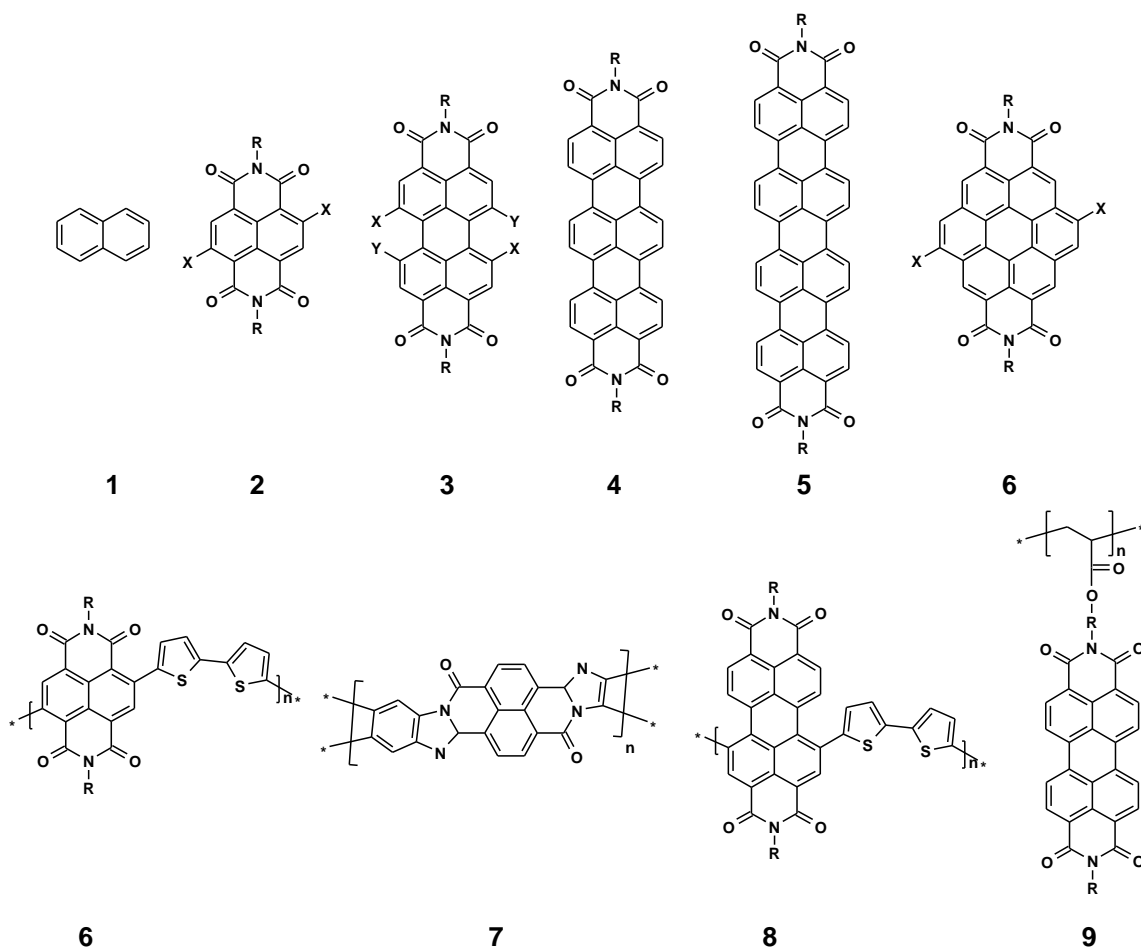


Figure 9: Chemical structures of rylene based materials for organic field-effect transistors: the basic building block naphthalene (1), naphthalene bisimide (2),^[57] perylene bisimide (3),^[58,59] terrylene bisimide (4),^[60] quaterylene bisimide,^[61] coronene bisimide (6),^[62] naphthalene bisimides based polymers (6,7),^[63,64] and perylene bisimide (8,9) based polymers.^[65,66]

2.4.1 Perylene bisimides for OFET applications

Perylene bisimides are the best investigated rylene for organic field-effect transistors. Their excellent stability and packing behavior makes perylene bisimides useful candidates for high performance transistors. Ambient stability of perylene bisimides can be reached by chemical modification. Therefore, two different strategies are useful: attaching linear fluorinated alkyl chain to the imide nitrogen results in a close packed structure which is claimed to create an intrinsic atmospheric barrier.^[56] The second strategy lowers the

LUMO-level of the molecule by introducing electron withdrawing groups to the perylene core, in order to prevent reactions with trapping species e.g. oxygen or water.^[43]

The raw material for perylene bisimides is acenaphthene **9** (Fig. 10), which can be obtained by extraction of coal tar. Further oxidation with vanadium oxide yields naphthalic anhydride **10**. With aqueous ammonia, naphthalimide **11** is formed in a quantitative condensation reaction. An alkaline fusion reaction is used to transfer **11** into the perylene core. This is done in molten alkali via a bimolecular nucleophilic substitution of two naphthalimide units to achieve **12** after precipitation into water.

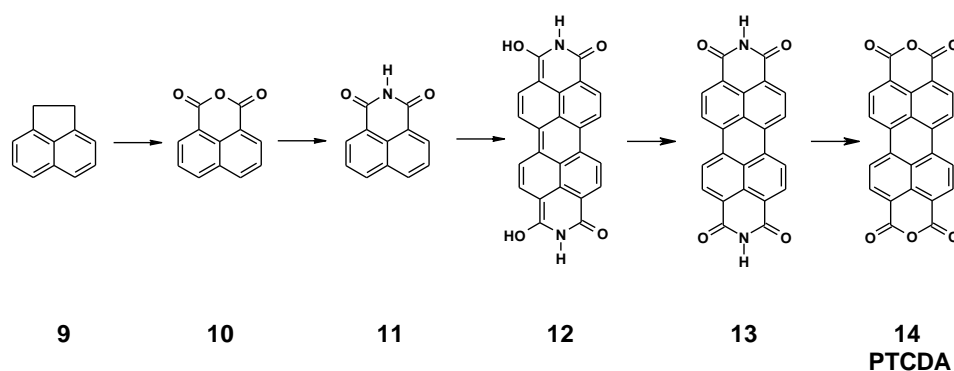


Figure 10: Chemical synthesis of 3,4,9,10-Perylenetetracarboxylic dianhydride **14**, which is commonly used as commercial available starting material for the synthesis of homo- and heterosubstituted perylene bisimides.^[67]

Compound **12** is oxidized with air or peroxide to the bisimide **13**, which is finally hydrolyzed in concentrated sulfuric acid at temperatures in excess of 200°C to the product 3,4,9,10-perylenetetracarboxylic dianhydride **14**.

In principle, perylene bisimides can be divided into homo- and hetero substituted bisimides. Homo substituted perylene bisimides bear the same tail on both imide nitrogens. These bisimides can be obtained in a simple one step condensation reaction of PTCDA **14** with primary amines (Fig. 11; step I) in high yields. To get hetero substituted perylene bisimides, two different routes are principally used which are also depicted in figure 11. In both cases, commercially available PTCDA **14** is used as starting material (Fig 11). In route A, the dianhydride PTCDA reacts first with an amine to the homosubstituted bisimide **b**. A partial saponification under strongly basic conditions to the monoimide monoanhydride **c** is described by Langhals et al.^[68] In the last step, the recovered anhydride group reacts with another amine to form the hetero substituted perylene bisimide **d**. During the alternative route B the mono potassium salt **e** is formed

by complete hydrolysis of **PTCDA 14** by potassium hydroxide and subsequent titration with acetic acid. Here, the potassium salt acts as protective group so that in the following step only the left anhydride group is able to react with ammonia to the mono imide **f**. In the following step the recaptured anhydride moiety reacts with an amine to bisimide **g**. This species has an acidic hydrogen at the imide group, which can be abstracted under basic conditions. After H-abstraction the formed anion allows an S_N2 reaction with bromides to obtain the heterosubstituted bisimides **d**.

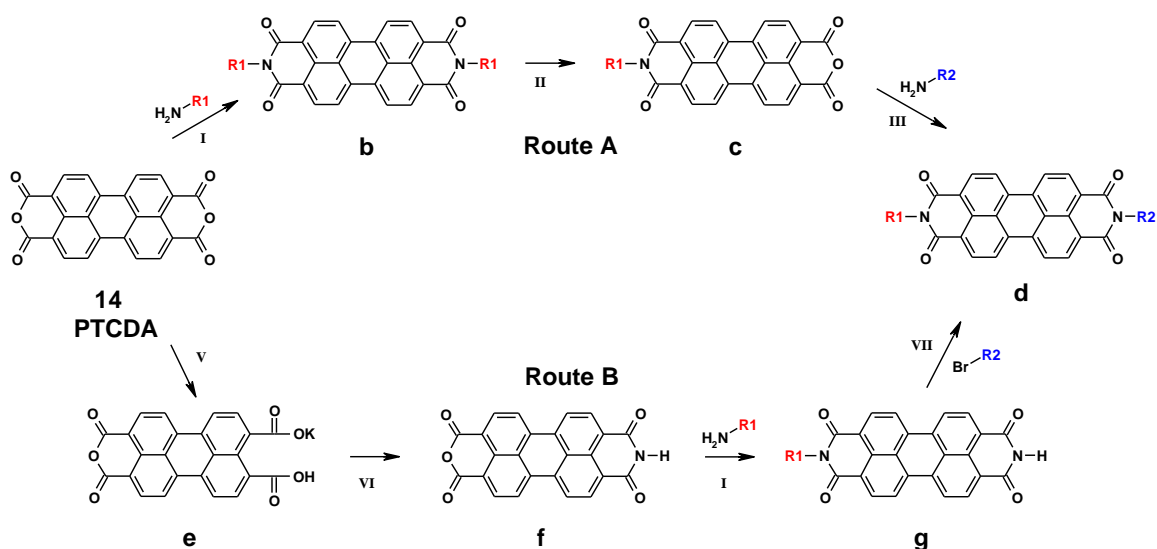


Figure 11: Two chemical strategies towards homo- and hetero substituted perylene bisimides.^[69,70,71,72]

2.5 Self-assembled monolayer field-effect transistors

Whitesides defined self-assembly as the autonomous organization of components into patterns or structures without human intervention.^[73] The concept of self-assembly is used in nature,^[74] as well as in man-made technical application^[75] and can be principally divided into two major forms of self-assembly: dynamic and static. Patterns formed by dynamic self-assembly are only stable if the system dissipates energy e.g. biological cells. Systems made by static self-assembly are at an equilibrium and do not dissipate energy.^[73]

Self-assembled monolayers (SAMs) belong to the type of static self-assembly. Here a covalent bond is formed between molecules and surface via a reactive group building up a two-dimensional monomolecular layer just by immersing a substrate into a solution of the

active material. A reactive group in the molecule reacts spontaneously with the surface. Depending on the substrate, different anchor groups are useful. The most extensively studied SAMs are thiols on gold.^[76]

SAM-formation attracted huge interest because of its manifold fields of application. SAMs allows dramatic changes of material properties e.g. wetting behavior^[77] or the engineering metal work functions,^[78,39] control over corrosion^[79] and crystallization of deposited organic materials,^[80,81] and changing characteristics in electronic devices^[82,83,84] and much more.

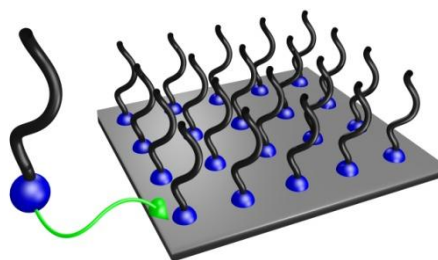


Figure 12: Schematic illustration of a molecule having a reactive group (blue) and a tail (black). The reactive group allows a spontaneous fixation to a surface in order to form a monolayer.

Ultra thin layers are also attractive in the field of organic field-effect transistors. Studies have shown that for a working transistor only a few layers of the organic semiconductor are needed.^[85,86,87,88] Even monolayer field-effect transistors were fabricated from small molecules,^[89,90] as well as from polymers^[91,92] by different techniques. The use of self-assembly in order to get semiconducting monolayers for transistor applications offers a huge step forward towards low cost large area electronics by a simple low temperature process. The first so called self-assembled monolayer field-effect transistor (SAMFET) was made by Tulevski et al. using a chatechol based molecule (see figure 13) chemisorbed onto aluminum oxide.^[93] The monolayer in which the molecules are standing upright allow a gate modulated hole transport for sub-100 nm transistors. However, the electrical performance and device yield of working transistors having channel lengths longer than 60 nm was still low. Far smaller SAMFETs were achieved by Guo et al. using a hexabenzocoronene derivative as semiconductor bonded via acid chloride moieties to silicon dioxide.^[94] Here, the electrodes consist of a single-walled carbon nanotubes. An ultrafine lithography process allows cutting of these nanotubes. The resulting nanogaps represent transistor channels with lengths in the range of 2-6 nm. Parallel stacks of 4-12 molecules between the electrodes enable hole transport with mobilities of $1 \text{ cm}^2/\text{Vs}$ and on/off ratios of 10^5 . Mottaghi et al. were able to build up

thiophene based short channel SAMFETs on silicon dioxide getting hole mobilities up to $3.5 \times 10^{-3} \text{ cm}^2/\text{Vs}$.^[95] Phosphonic acids anchor groups were used by Hutchins et al. to fix a quinquethiophene derivative covalently to aluminum oxide dielectrics by spin coating.^[96] Mobilities on the order of $10^{-6} \text{ cm}^2/\text{Vs}$ were obtained for a wide range of channel lengths up to 80 μm . Nevertheless, all SAMFETs described up to this point are either difficult to fabricate or exhibit relatively low performances. The best SAMFETs so far were realized by Smits et al.^[97] They used a quinquethiophene derivative with an ethyl end-capper at one side and an undecyl-spacer bearing a terminal chlorosilane group at the other side. The tailored chemical structure of the molecule was the result of a compromise between sufficient solubility and a highly extended chromophore system. Grazing incidence X-ray diffraction studies revealed a herringbone arrangement of the chromophores,^[98] typical for oligothiophenes. Bottom-gate, bottom-contact transistor substrates were submerged into a solution of the active molecule at room temperature for 24 hours. A condensation reaction of the liquid crystalline molecule with hydroxy groups of the surface leads to a covalently fixed, dense, and smooth 3.5 nm thick monolayer on top of the silicon dioxide. After immersion, decent transistor characteristics were obtained showing almost no hysteresis. High on/off ratios of 10^6 and mobilities up to $0.04 \text{ cm}^2/\text{Vs}$ were measured, on par with quinquethiophene single-crystalline thin-film transistors.^[99] The high performance of the molecules and the reliability of the fabrication process allows also fabrication of first integrated circuits based on SAMFETs e.g. a unipolar bias inverter and a 7-stage ring oscillator. The most complex device was a 15-bit code generator. This device combines more than 300 single SAMFETs simultaneously addressed. Furthermore, it has been shown that the molecule forms ordered semiconducting layers also on polymer surfaces.^[100] The demonstration of integrated circuits on foil is a promising step forward towards flexible low cost electronics based on SAMFETs. The unique high performance of this quinquethiophene derivative allows further detailed studies, in order to solve fundamental questions. Such monolayer allows direct measurements of the active layer in organic field-effect transistors without disturbance by the bulk material. The effect of charge carrier confinements on charge transport,^[101] measuring the density of states by scanning kelvin probe microscopy (SKPM),^[102] as well as optical investigations,^[103] are examples for what SAMFETs are useful, in order to get new fundamental informations about charge transport in 2-dimensional organic materials.

All SAMFETs described here so far are based on p-type materials. However, the established circuit design for integrated circuits is based on the complementary metal oxide semiconductor (CMOS) technique. High noise immunity can be obtained by combining p-type and n-type together in one device. Due to the fact that one transistor is always off, the power consumption of CMOS-circuits is quite low. These two advantages made CMOS to the most widely used technique for integrated circuits.

Novak et al. described the first n-type SAMFET so far.^[104] They fixed a C60-fullerene derivative via a phosphonic acid group onto an aluminum oxide dielectric by self-assembly. High resolution transmission electron microscopy confirmed a 2.5 nm thick organic layer on top of the substrate which is comparable to the calculated molecular length. The resulting bottom-gate top-contact field-effect transistors showed field-effect mobilities of 10^{-4} cm²/Vs, a threshold voltage of 3 V, and on/off-ratios of 2×10^4 .

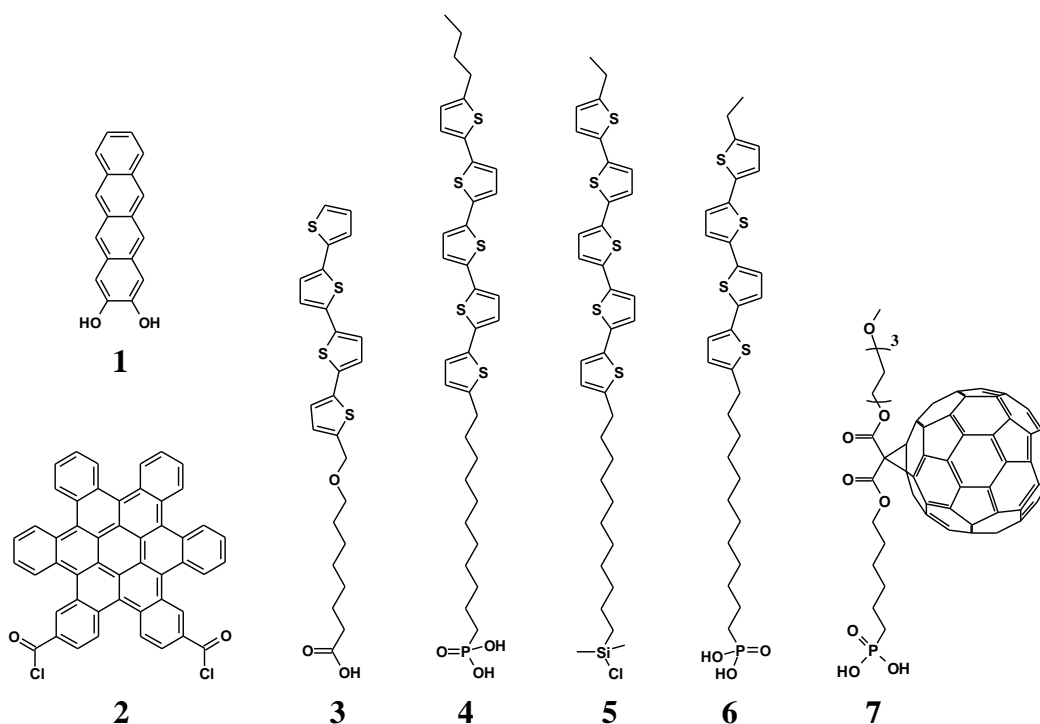


Figure 13: Chemical structures of molecules designed for SAMFET applications. (1) End functionalized tetracene for anchoring onto aluminumoxide,^[93] (2) Hexabenzocoronene for ultra-small transistor channels,^[94] (3) Thiophene based molecule for SAMFETs on aluminum oxide,^[95] (4) Thiophene based molecule for SAMFETs made by spincoating,^[59] (5) high performance thiophene based molecule for SAMFETs on silicon dioxide,^[97] (6) Thiophene based molecule for low voltage SAMFETs,^[104] (7) fullerene based molecule as the first n-type material for SAMFETs.^[104]

The development of new soluble semiconducting materials is crucial for the realization of flexible low-cost electronics, made by simple fabrication processes. Inorganic nanoparticles, as well as organic materials, are suitable candidates for cheap, solution based processes, e.g. printing. Whereas, organic hole conducting compounds (p-type) already exhibit reasonable device performances, reliable electron transporting materials (n-type) are still needed in order to build up circuitry with the well established complementary metal oxide semiconductor (CMOS) logic. The aim of this thesis is the synthesis of organic compounds and their application in n-type field-effect transistors. In order to realize flexible devices easy device fabrication steps at low temperatures are desirable. For this approach two strategies were pursued: modification of inorganic zinc oxide nanoparticles by organic materials, and fabrication of self-assembled monolayer field-effect transistors (SAMFETs). For both strategies, perylene bisimides with different linker groups were synthesized. In order to modify zinc oxide nanoparticles, linkers were chosen, which passivate dangling bonds at the surface of zinc oxide nanoparticles. Dangling zinc bonds are known as electron donors, facilitating electron conduction even if the transistor is switched off. Passivation of these unwanted bonds is supposed to reduce the off-current and to enable nanoparticulate zinc oxide field-effect transistors.

The main focus of this thesis is on n-type self-assembled monolayer field-effect transistors (SAMFETs). Self-assembly is a promising bottom-up approach for simple, large area device fabrication at low temperatures. Furthermore, the absence of bulk current in SAMFETs makes them attractive for transistors with high on/off-ratios, maintaining other important transistor parameters, such as high charge carrier mobility and low threshold voltage.

The thesis contains three papers which are presented in chapters six to eight. One paper is added to the appendix in chapter nine. Three have been already accepted, one is intended for submission to *Organic Electronics*.

All chapters deal with the synthesis and characterization of semiconducting perylene bisimides and their application in n-type field-effect transistors. The perylene bisimides used in this thesis were tailored to modify inorganic oxides. Therefore, linker groups were chemically introduced, which can form either non-covalent or covalent bonds to oxide surfaces, in order to enhance transistor performance and to enable simple solution based fabrication processes. For this purpose two strategies were pursued: passivation of inorganic nanoparticles and direct self-assembly of semiconducting monolayers onto inorganic dielectrics.

Chapter six deals with n-type field-effect transistors based on zinc oxides nanoparticles. In general, the surface plays a crucial role in determining the properties of nanoparticles, due to their extreme surface to volume ratio. Typically, dangling zinc bonds are present at zinc oxide surfaces. These bonds act as electron donating groups, leading to an increased intrinsic conductivity. Therefore, nanoparticulate zinc oxide thin film transistors show low on/off-ratios with no field-effect behavior. Selective modification of zinc oxide surfaces was done by organic compounds, to fill voids between nanoparticles on the one side, and to passivate the oxide surface on the other, leading to semiconducting behavior of zinc oxide nanoparticles.

The main part of this thesis is presented in chapters seven to nine, which deal with self-assembly of monolayers (SAMs) and their application as 2-dimensional electron transport layer in so-called self-assembled monolayer field-effect transistors (SAMFETs).

It is known that charge transport in organic field-effect transistors is managed only by a few layers very close to the dielectric. Therefore, the absence of bulk layers in SAMFETs shows no significant negative influence on the device performance. The absence of bulk material even decreases the off-current, which is favorable for the transistor performance. In these chapters it is shown that a covalently fixed, dense, and semiconducting monolayer is spontaneously formed between source and drain electrode, and is enough for reliable n-type organic field-effect transistors. Therefore, molecules were synthesized, having a semiconducting core connected via a spacer to a reactive group, which allows a covalent fixation onto transistor dielectrics. Precise studies using several techniques revealed a complete, homogeneous, and smooth 2-dimensional semiconducting sheet on top of inorganic oxide dielectrics, paving the way to highly reproducible and well performing organic electronics by self-assembling.

All organic compounds were synthesized, purified, and analyzed using standard techniques. For analyzing the morphology of nanoparticulate thin films, scanning electron microscopy (SEM) was chosen. The length of several molecules was calculated using Avogadro 1.0.3 software. Roughness of SAMFETs was investigated by atomic force microscopy (AFM). X-ray photoelectron spectroscopy (XPS) was used to determine surface coverage, molecular composition, molecular orientation, and thickness of self-assembled monolayers. Furthermore, X-ray reflectivity (XRR) studies were done to itemize out of plane order of the monolayers. Grazing incidence X-ray diffraction (GIXD) measurements were performed in order to get information about in-plane order of the SAMs. Electrical characterizations were carried out at room temperature under either vacuum, or nitrogen atmosphere.

The organic semiconductors which were synthesized in this thesis belong to the well known class of perylene bisimides (PBIs). High thermal stability, good packing behavior, and possible modification by chemical synthesis are the main reasons why this class of material was chosen.

Chapter six presents the first approach of this thesis where a perylene bisimide is used to modify zinc oxide nanoparticles. The advantage of zinc oxide nanoparticles is their solution processability, which makes them useful for spin coating or printing processes. However, transistors made from pure nanoparticulate zinc oxide dispersions show characteristics with high on as well as off currents. No gate modulation of the drain current was observed. One reason for this intrinsic conductivity are dangling zinc bonds

at the surface of zinc oxide. These unsaturated zinc bonds act as electron donating group. Providing electrons in the material means an increase in conductivity of the n-type semiconductor, even if no gate voltage is applied. The high surface to volume ratio in nanoparticles continues to deteriorate transistor performance. Due to the presence of these charge carriers, it is impossible to switch the transistors off - the transistors are always in the on-state. Consequently, low on/off-ratios make such transistors unsuitable for electronic circuits. It has been proven that pyrrolidone moieties form non-covalent bonds to dangling zinc bonds in zinc oxide. In order to prevent large amounts of insulating material, these groups were fixed to a perylene bisimide core, which is an n-type semiconductor by its own and can fill voids between the n-type zinc oxide particles. A second perylene bisimide was synthesized as reference, bearing two inert perfluorinated alkyl tails, which do not inter with the zinc oxide. Mixing the fluorinated reference compound together with zinc oxide nanoparticles did not lower the high intrinsic conductivity of zinc oxide nanoparticles. It was shown that in contrast the perylene bisimide with pyrrolidone linkers can turn the zinc oxide into a semiconductor with n-type field-effect transistor behavior.

The second approach, constituting the main part of the thesis, is presented in chapters seven to nine. In these chapters perylene bisimides were tailored for the application in self-assembled monolayer field-effect transistors (SAMFETs). In contrast to the perylene bisimides described in the previous paragraph, these bisimides are heterosubstituted. On one side of the perylene bisimide core an end-capper was attached in order to control stacking behavior and solubility. On the other side a linear alkyl spacer was introduced, functionalized with a terminal anchor group. As anchor group, phosphonic acid was chosen to enable covalent fixation onto aluminum oxide surfaces, which is often used as dielectric in transistor devices. For high solubility a branched alkyl tail was used as end-capper in the first case. The target molecule PBI-PA was obtained after six reaction steps in high yield. For the SAMFET fabrication, transistor substrates with aluminum oxide dielectrics were submerged into a dilute solution of PBI-PA. A covalently fixed monolayer was spontaneously formed during the immersion by a condensation reaction of the phosphonic acid with the hydroxide groups of the aluminum oxide surface. After this self-assembly process, organic transistors presented bulk-like electron mobilities and high on/off-ratios together with the desired low threshold voltages. The fact that a gate modulated drain current was obtained for all measured transistors, including devices with

channel length up to 100 μm , indicates a high reproducibility. Furthermore, an n-type SAMFET was connected with a p-type SAMFET to a CMOS-bias inverter, demonstrating, for the first time, the opportunity of complementary logic for SAMFETs.

Chapter eight shows a way to increase SAMFET performance by tailored chemical modification of the self-assembled molecule. Here, the branched alkyl tail was replaced by a short linear fluorinated alky tail. The linear shape of the tail allowed a denser packing of the perylene chromophores on the surface. Higher coverage led to a more complete passivation of hydroxyl groups at the surface, which are known to act as trap states. As a result, monolayers with high electron mobilities and on/off-ratios were obtained, showing reduced hysteresis. Additionally, measurements of n-type SAMFETs and the realization of the first SAMFET based NMOS-bias inverter, both on polymer based substrates, proved the practicality of n-type SAMFETs, for flexible organic electronics.

In the following, the key-results of the individual publication are summarized. Further detailed information about synthesis or analytical studies can be found in the publications and accompanying supporting informations.

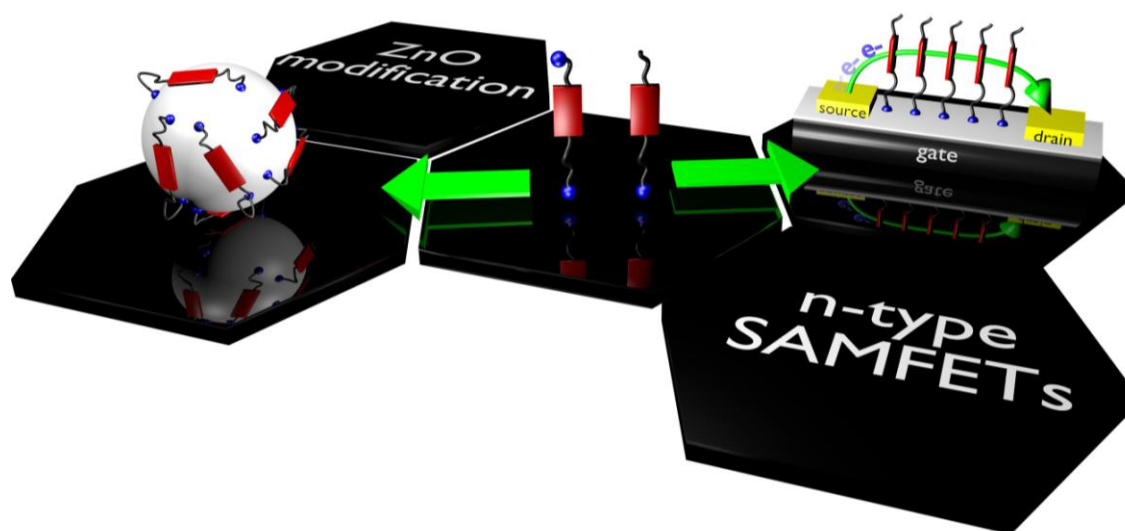


Figure 14: Schematic illustration of two approaches used in this thesis to realize n-type organic field-effect transistors: surface modification of ZnO-nanoparticles and n-type self-assembled monolayer field-effect transistors (SAMFETs).

4.1 N-type perylene to fill voids in solution processed nanoparticulate zinc oxide thin films

For the paper in chapter six, two perylene bisimides were synthesized in order to suppress the intrinsic conductivity and to fill voids between zinc oxide nanoparticles by mixing organic and inorganic compounds. The surface sensitivity in nanoparticulate thin layers is enhanced, due to the large surface to volume ratio. Atmospheric surface adsorbates are known to influence field-effect transistor behavior in a negative way. Furthermore, voids between neighboring nanoparticles disturb charge pathways between source and drain electrodes. Both peculiarities of nanoparticles have negative impact on the transistor performance. To overcome the disadvantages of zinc oxide nanoparticles a special chemical linker was used to passivate the particle surface. In order to fill voids, the linker is connected to an n-type perylene bisimide. The chemical structures of the molecules used here are depicted in figure 15.

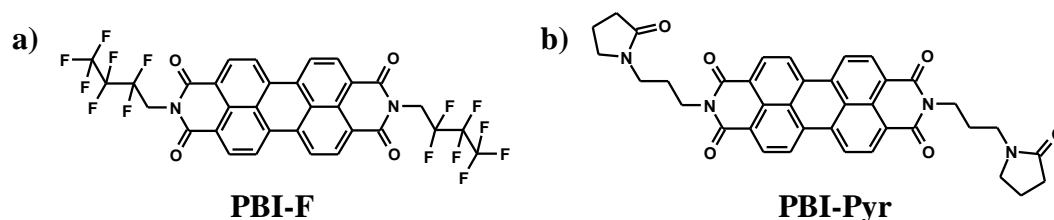


Figure 15: Chemical structures of two perylene bisimides. **a)** PBI-F with perfluorinated alkyl tails. **b)** PBI-Pyr with two pyrrolidone moieties.

The organic substances were synthesized in a condensation reaction of perylene-3,4,9,10-tetracarboxylic dianhydride with the corresponding amine, whereas zinc oxide nanoparticles were provided from Evonik Industries. Nanoparticulate zinc oxide dispersions were made using methoxyethanol as surfactant. Thin films were made by spin coating. To be compatible with polymer substrates, the temperature was maintained at a low level during all fabrication steps, never exceeding 125°C.

The perylene bisimide PBI-F (in the paper the molecules are named PDI-F and PDI-Pyr) has two linear fluorinated alkyl tails (see figure 15). Spin coating of PBI-F and zinc oxide nanoparticle composites resulted in inhomogeneous thin films. The perylene bisimide formed aggregates, leading to precipitates. The conductivity of such films decreased by increasing PBI-F content, which is attributed to the reduced number of percolation pathways, due to PBI-F aggregates. Furthermore, the inactive fluorinated tails had no effect on the dangling zinc bonds, which were still present, so that the PBI-F composite films showed rather ohmic

than semiconducting properties. A gate modulation of the drain current was not observed (Fig. 16a).

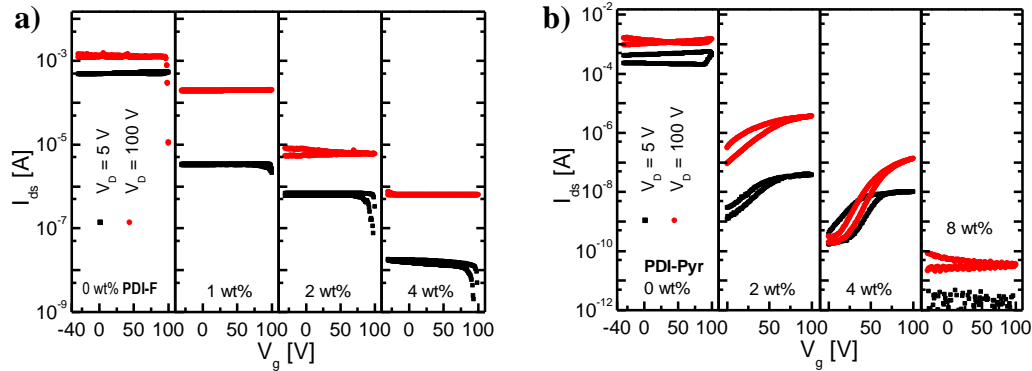


Figure 16: Transfer characteristics of PBI-F (left) and PBI-Pyr (right) zinc oxide hybrid transistors. The concentration of the perylene bisimides is varied between 0–8 weight-%. All transistors containing PBI-F as organic compound exhibit no gate modulation of the drain current. PBI-Pyr composites in contrast show semiconducting properties for devices with 4 and 8 weight%.

In contrast to inactive PDI-F, the bisimide PBI-Pyr contains two active pyrrolidone moieties. These groups are known to bind to dangling zinc bonds at zinc oxide surfaces. Dangling zinc bonds at zinc oxide surfaces act as electron donors, which are supposed to be responsible for intrinsic charge transport. PBI-Pyr was chosen to passivate the surface of the zinc oxide nanoparticles in order to decrease the conductivity in the off-state. The perylene core itself acts as n-type semiconductor and can be embedded in voids between nanoparticles, generating new conducting percolation pathways for electrons. As shown in figure 16b, addition of 2 weight-% of PBI-Pyr to the zinc oxide dispersion already resulted in semiconducting field-effect transistors. An increase of the amount of PBI-Pyr up to 4 weight-% showed further improvement. At this point the transistor conducted actually no charges in the off-state, also for high drain biases, as the density of thermally active charge carriers is reduced. Higher concentrations of PBI-Pyr led to a dramatic drop of the transistor current also in the on-state. The reason for this observation is once more the precipitation of the organic compound, which lowers the amount of conduction pathways. These results show that controlled addition of well chosen additives allows a transformation of conducting into semiconducting zinc oxide.

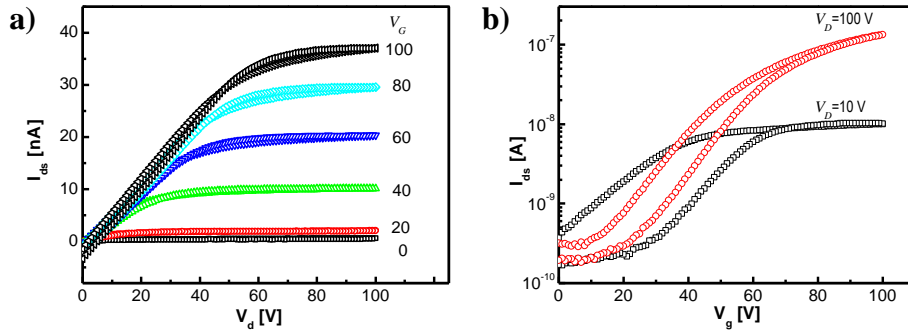


Figure 17: a) Output and b) transfer characteristics of a nanoparticle zinc oxide field-effect transistor with 4 weight-% of PBI-Pyr. The electron mobility of the device is $7.5 \times 10^{-5} \text{ cm}^2/\text{Vs}$, the on/off-ratio is 10^3 .

4.2 N-type self-assembled monolayer field-effect transistors and complementary inverters

It is known that approximately 90% of charge transport in organic field effect transistors is managed by the first layer on top of the dielectric. Therefore, a single monolayer should be sufficient for reliable transistors. Unwanted bulk currents would be eliminated, which decreases the on/off-ratios in organic field-effect transistors. This chapter describes the novel, heterosubstituted perylene bisimide PBI-PA, designed for monolayer field - effect transistors, fabricated by a simple self-assembly process at low temperatures. For those self-assembled monolayer field-effect transistors (SAMFETs), the perylene bisimide provides a branched alkyl tail at one side to enable sufficient solubility. At the other side a linear alkyl spacer bearing a terminal phosphonic acid unit was attached. The C_{11} -spacer allows a certain degree of flexibility, whereas the phosphonic acid enables a covalent fixation to the aluminum oxide surface. The chemical structure of PBI-PA is shown in the inset of figure 19. Transistors were made by submerging pre-structured substrates with aluminum oxide dielectrics into a dilute solution of PBI-PA. After 24 hours, the substrates were taken out of the solution, rinsed with solvent in order to get rid of unwanted precipitates, dried on a hotplate, and subsequently characterized. Figure 18 presents an atomic force microscopy (AFM) height image of a plane SAMFET channel, embedded between source and drain electrodes.

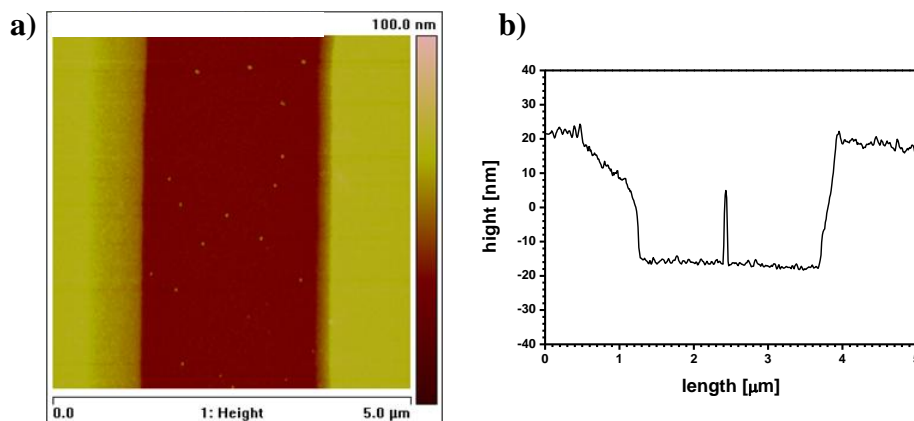


Figure 18: a) Atomic force microscopy height image of a SAMFET channel. The yellow areas to the left and right are the source and drain electrodes. The smooth channel in the middle exhibits some 20 nm high islands which are supposed to be substrate defects. b) Cross section through the transistor channel.

The surface coverage and thickness of the organic layer was investigated by X-ray photoelectron spectroscopy (XPS). These measurements revealed a complete coverage and a thickness of the organic layer of 3.1 nm, which is in good agreement with the calculated molecular length of PBI-PA.

Out of plane order was studied using X-ray reflectivity (XRR) measurements. These studies were also verified by theoretical calculations, using a three layer model. The results revealed an organic monolayer on top of aluminum oxide which itself can be divided into three separate regions (see figure 19). The third region corresponds to the branched end-capper, the second region corresponds to the aromatic core, and the first region close to the dielectric corresponds to the aliphatic spacer. The obtained thicknesses are in good agreement with the estimated lengths. Also the electron densities reflect a consistent layer structure, where the electron density of the middle layer is noticeable enhanced, due to the present of electron rich elements such as nitrogen and oxygen. The electron density of the first region is also slightly enhanced compared to the third layer. The reason for this observation is the presence of phosphorous and oxygen, which originates from the phosphonic acid linker group.

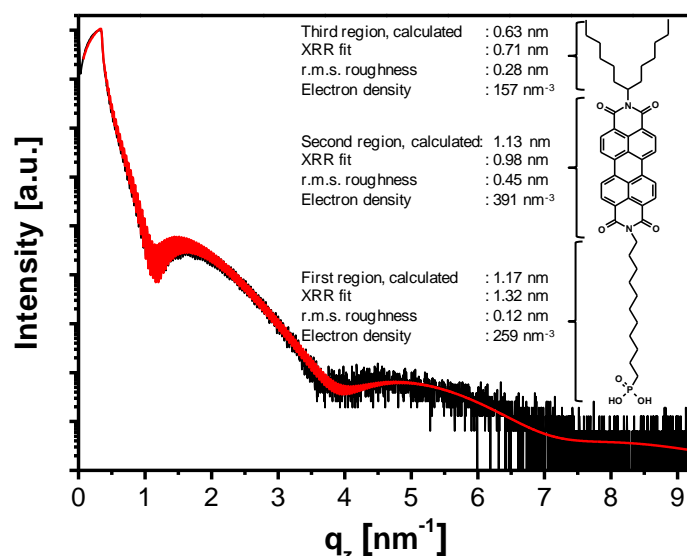


Figure 19: X-ray reflectivity investigation of PBI-PA monolayers. The black curve shows the experimental results, the red line gives the model calculation. The inset shows the chemical structure of PBI-PA.

The in-plane order of PBI-PA monolayers was investigated by grazing incidence X-ray diffraction measurements (GIXD). A broad diffraction peak (q_{xy}) at 17.5 nm^{-1} is observed, corresponding to a perylene-perylene distance of 3.6 \AA (see figure 20), typically known for this class of molecules. The relatively wide diffraction signal indicates low crystallinity of the monolayer. The width of the diffraction peak of 2 nm^{-1} results in a correlation length of 3.1 nm . However, XRR and GIXD investigations revealed a twisted arrangement of PBI-PA, perpendicular ordered with respect to the aluminum oxide.

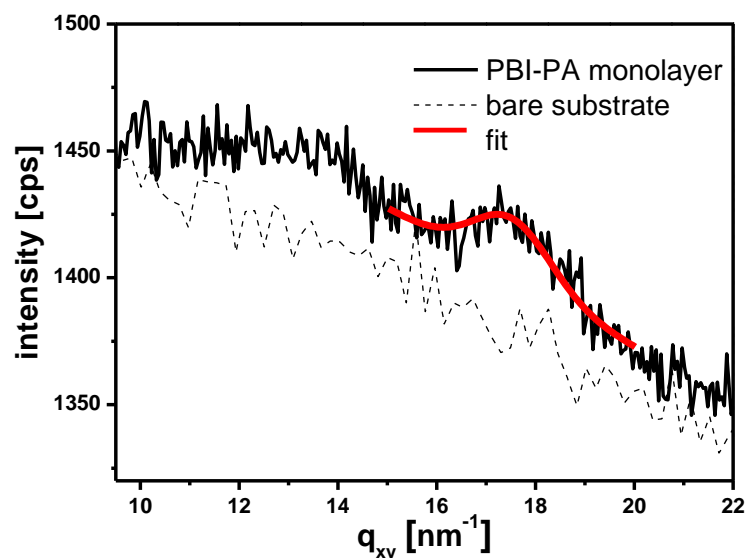


Figure 20: Grazing incidence X-ray diffraction (GIXD) measurements of a bare aluminum oxide substrate (dotted curve), a self-assembled PBI-PA monolayer onto aluminum oxide (black curve), and a fit (red curve) for clarification.

Electrical characterizations of several bottom-gate bottom-contact transistors were carried out under inert atmosphere. A typical output and transfer characteristic of a PBI-PA SAMFET is presented in figure 21. The device has a channel length of 20 μm and a width of 1000 μm . The calculated electron field-effect mobility is $1.5 \times 10^{-3} \text{ cm}^2/\text{Vs}$. An on/off-ratio in the order of 10^4 and a threshold voltage close to zero was observed. All measured devices showed gate modulation of the drain current, i.e. device yield of 100%.

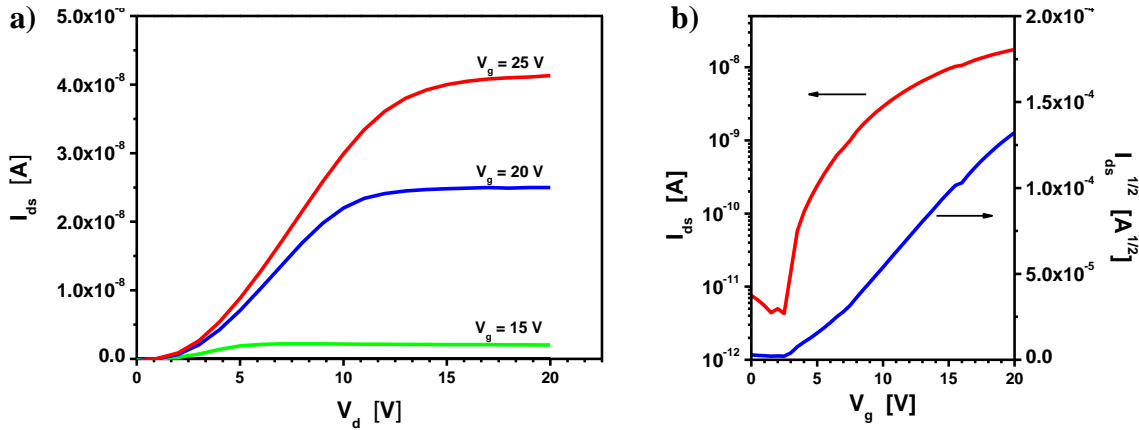


Figure 21: Field-effect characteristics of a PBI-PA SAMFET. **a)** Output characteristics of a PBI-PA SAMFET with a channel length/width ratio of $40\mu\text{m}/1000\mu\text{m}$. The gate voltage is varied in 5 V per step, the drain voltage is varied from 0 V to 20 V. **b)** Transfer characteristics of the same device in the saturation regime. The gate voltage was varied from 0 V to 20 V.

It is remarkable that a field-effect is observed for short channel as well as for long channel transistors, so that, for the first time, well performing SAMFETs, having channel lengths up to 100 μm were described. Channel length dependence measurements of the electron mobility showed an increase of mobility for short channel transistors up to 40 μm . At this point, the mobility began to become constant. Such a saturation of the mobility is a fingerprint for a complete surface coverage of the active material, enabling charge transport through percolation pathways also over long distances.

To assure robust and low power circuits, the complementary metal oxide semiconductor (CMOS) technique is crucial. In CMOS-logic pairs of p-type and n-type transistors are combined to one device in which power dissipation only occurs during switching processes. In order to build-up a SAMFET based CMOS bias inverter, a quinquethiophene derivative is used for the p-type SAMFET, whereas a PBI-PA SAMFET is used as the corresponding n-type device. Mobilities of both transistors were matched by adjusting transistor channel lengths. Both devices were connected by hand in a complimentary layout as shown in figure 22b. The input voltage was varied from 10 V to 30 V in 5 V per step. The resulting bias inverter characteristics are shown in figure 22a. At a

supply voltage of 30 V, a high gain value of 15 with the “trip-point” at around 23 V of V_{in} was obtained. Noise margin and gain received in this bipolar bias inverter was larger than for unipolar PMOS inverter previously reported and on par with conventional organic CMOS.

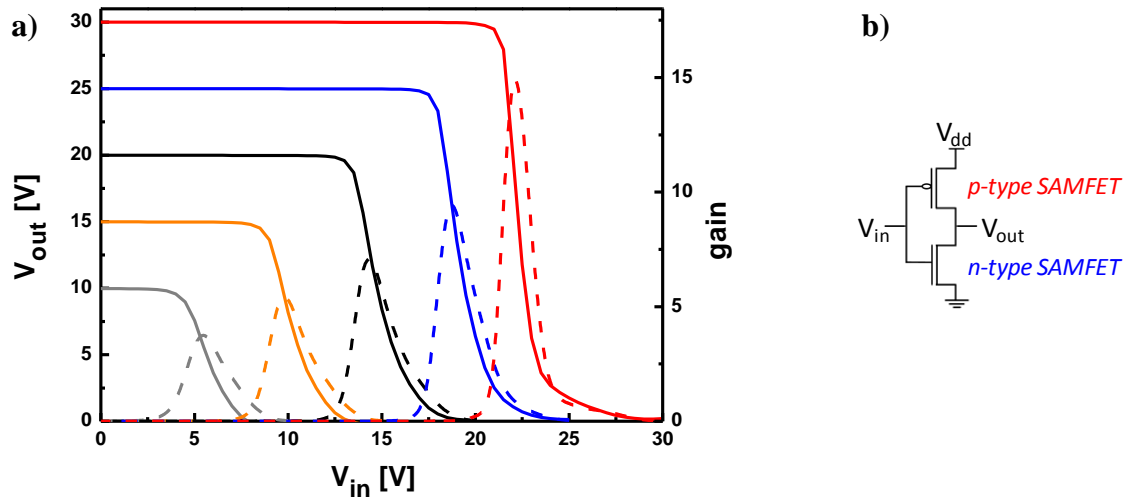


Figure 22: a) Characteristics of a SAMFET based bipolar bias inverter. The supply voltage (V_{dd}) was varied from 10 V to 30 V in 5 V per step, the input voltage is swept from 0 V to 30 V. The individual gain is presented as dashed line. b) Diagram of a CMOS bias inverter used in this thesis.

4.3 N-Type self-assembled monolayer field-effect transistors for flexible organic electronics

In this chapter a novel approach is presented in order to improve n-type SAMFET device performance. The molecule PBI-PA, which is used in chapter 7 as semiconductor in n-type SAMFETs, bears a branched alkyl tail at one side. Computer simulations revealed an orthogonal orientation of the tail to the aromatic chromophore. Steric repulsion between the branched alkyl tails resulted in a relatively low phosphorous coverage of 1.8×10^{18} molecules per cm^2 . Furthermore, a twisted arrangement of the molecules was assumed, also due to steric repulsion of the branched tails. As a result, transistor characteristics with relatively large hysteresis were observed. The origin of this hysteresis was believed to be due to hydroxide groups at the dielectric surface. To reduce hysteresis a new molecule was designed to get a more complete surface coverage. The chemical structures of PBI-PA and the new molecule PBIF-PA are shown in figure 23.

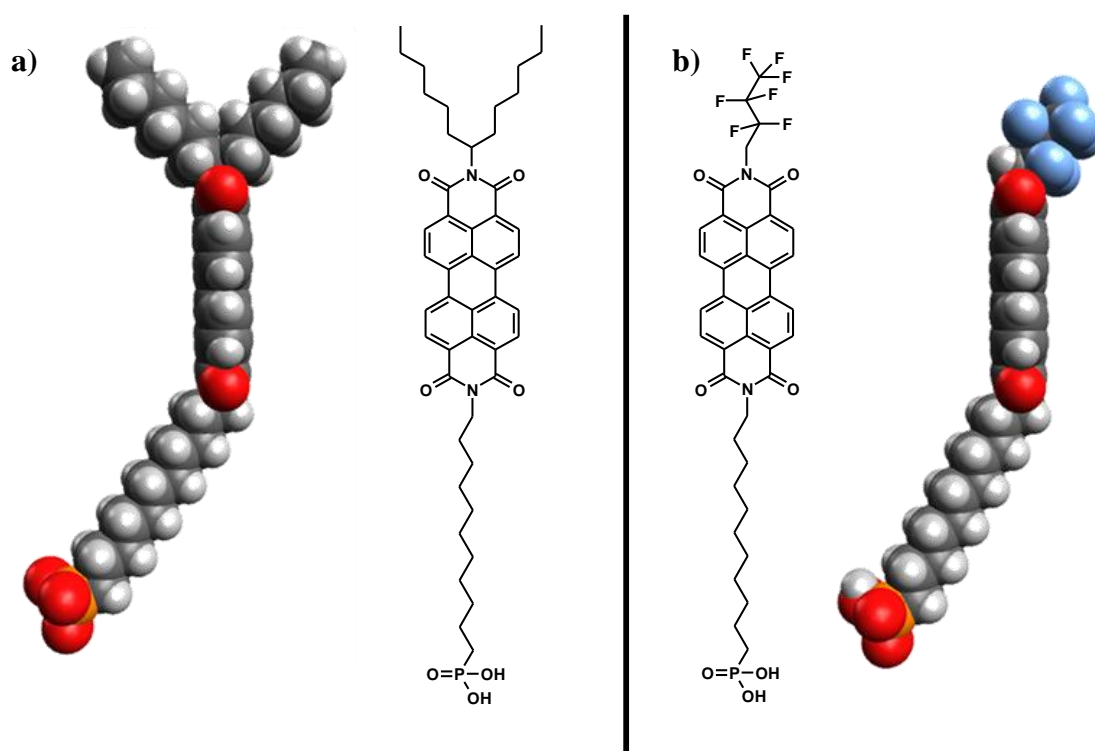


Figure 23: **a)** Side view on PBI-PA (left). Chemical structure of PBI-PA (middle) and a top view onto the corresponding calculated structure (right). **b)** Top view onto PBIF-PA (left), its chemical structure (middle), and side view (right). The top views clarify the slimmer shape of PBIF-PA in contrast to PBI-PA. The two black eyes indicate the viewing direction onto the calculated structures.

As shown in figure 23, PBI-PA claims more space, due to the bulky alkyl tail. In contrast, PBIF-PA bears a short, linear fluorinated alkyl tail with less space demand, so that a better surface coverage is expected.

Field-effect transistors were fabricated by submerging pre-structured substrates into a dilute solution of PBIF-PA. During the immersion the phosphonic acid group binds covalently to the aluminium oxide dielectric to form a dense monolayer. The monolayer was investigated using XPS, XRR, and GIXD. Surface coverage was determined by XPS. It was found that the coverage of PBIF-PA was around 20% higher compared to PBI-PA. XPS also shows that fluorine is located mainly at the outer layer, whereas phosphorous is present almost exclusively at the bottom, close to the dielectric.

The out of plane order was underpinned by XRR measurements. A monolayer was found which can be divided into three different segments. The lengths of the individual segments were in good agreement with computer calculations, which gave a thickness of 2.69 nm of the SAM. It was remarkable that the electron density of the top of the SAM was enhanced. This observation was indicative for a high concentration of fluorine at the top. The electron densities of the middle and the bottom layer were comparable to the densities which were found for PBI-PA SAMs.

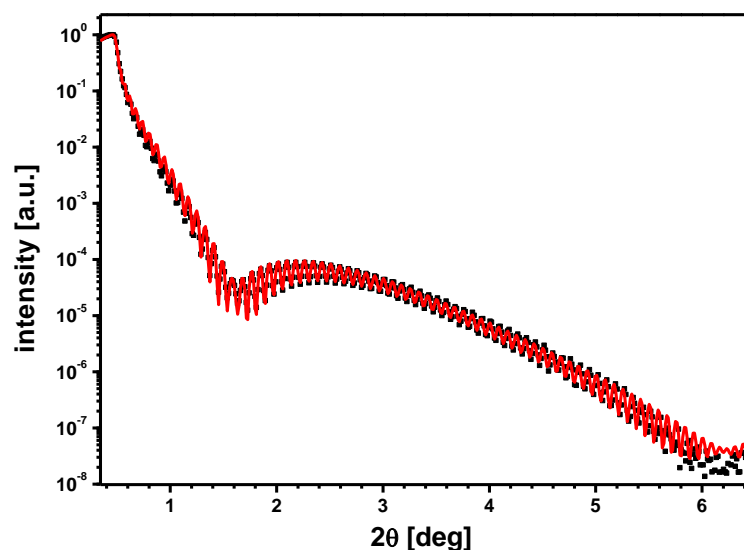


Figure 24: XRR investigations of PBIF-PA monolayers. The black curve shows the experimentally obtained data. The red curve shows a simulation using a three layer model.

In plane order was examined by grazing incidence X-ray diffraction studies. The absence of any reflection signals proved an amorphous organic layer on top of aluminium

oxide. This observation suggests a growth mechanism which is different from the island growth mechanism, known for thiophene based SAMs. In this case the SAM is formed by the driving force to create a phosphonic ester bond to aluminium oxide and predominantly not by interactions between the perylene bisimide cores.

The resulting PBIF-PA SAMFETs showed electron mobilities up to $10^{-3} \text{ cm}^2/\text{Vs}$ and high on/off-ratios up to 10^6 . In addition, forward and backward measurements showed only small hysteresis. This is attributed to better aluminium oxide coverage with PBIF-PA. Furthermore, the fact that the phosphonic acid was located completely at the dielectric enabled a more efficient passivation of hydroxide groups at the Al_2O_3 -surface.

Besides SAMFETs on non flexible devices, transistors were fabricated by using polymer based substrates. Similar results, as with non-flexible substrates, were received. Furthermore, a unipolar bias-inverter on a flexible substrate proved the capability of n-type SAMFETs with flexible electronics (see figure 25).

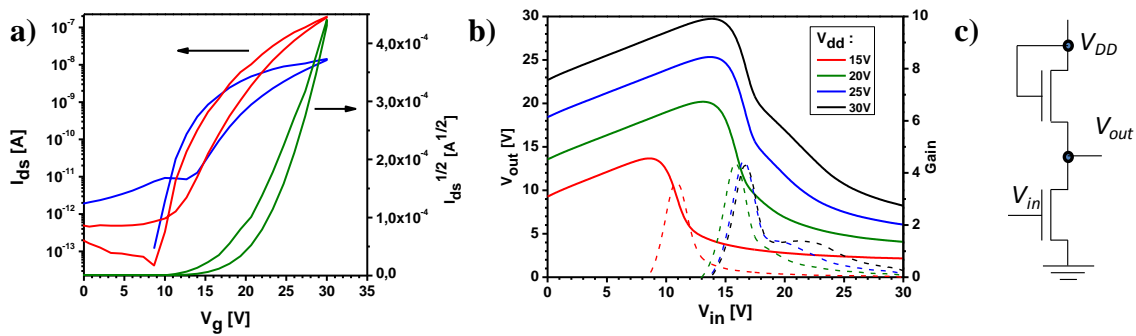


Figure 25: PBIF-PA SAMFET characteristics on a flexible polymer based substrates. **a)** Output characteristics of PBIF-PA SAMFET with a channel length of $2.5 \mu\text{m}$ and a channel width of $500 \mu\text{m}$. The drain voltage was varied from 5 V (blue) to 30 V (red). **b)** Characteristics of a unipolar NMOS bias inverter based on two n-type PBIF-PA SAMFETs. **c)** Diagram of the bias inverter.

Individual contribution to joint publications:

In the following the contributions of the individual authors to the papers are specified.

Chapter 6:

“N-Type Perylene To Fill Voids In Solution Processed Nanoparticulate Zinc Oxide Thin Films”

Published in: *Physica E* 44, **2012**, 2124–212; DOI: 10.1016/j.physe.2012.06.027

by *Simon Bubel, Andreas Ringk, Peter Strohmriegl, Roland Schmechel*

I designed, synthesized, and characterized the organic materials for this publication and I wrote the corresponding sections for this paper. Simon Bubel prepared and measured the transistor devices and wrote the paper. Prof. Peter Strohmriegl and Prof. Roland Schmechel supervised the project and corrected the manuscript.

Chapter 7:

“N-Type Self-Assembled Monolayer Field-Effect Transistors and Complementary Inverters”

Published in: *Advanced Functional Materials* **2012**, DOI: 10.1002/adfm.201202888

by *Andreas Ringk, Xiaoran Li, Fatemeh Gholamrezaie, Edsger C. P. Smits, Alfred Neuhold, Armin Moser, Cees Van der Marel, Gerwin H. Gelinck, Roland Resel, Dago M. de Leeuw, Peter Strohmriegl*

I designed, synthesized, and characterized the organic semiconductor for this publication. Transistor devices were fabricated, optimized, and characterized during my stay at the Holst Centre in the Netherlands in Eindhoven together with Xiaoran Li. Fatemeh Gholamrezaie provided the p-type SAMFET for the COMS-circuit, which was measured by Edsger Smits. Alfred Neuhold and Armin Moser performed XRR and GIXD measurements under the supervision of Prof. Dr. Roland Resel. Cees Van der Marel made XPS investigations. Dr. Gerwin Gelinck and Prof. Dago de Leeuw gave fruitful input during several discussions. I wrote the publication and jointly finalized it with the help of all co-authors. The complete work was supervised by Dr. Edsger Smits and Prof. Dr. Peter Strohmriegl.

Chapter 8:

“N-Type self-assembled monolayer field-effect transistors for Flexible Organic Electronics”

Intended for submission to *Organic Electronics*

by Andreas Ringk, Christian W. S. Roelofs, Edsger C. P. Smits, Cees van der Marel, Ingo Salzmann, Alfred Neuhold, Gerwin H. Gelinck, Roland Resel, Dago M. de Leeuw, Peter Strohrriegl

I designed, synthesized, and characterized the organic material for this publication. Transistor devices were fabricated, optimized, and characterized during my stay at the Holst Centre in the Netherlands in Eindhoven together with Christian W. S. Roelofs. Alfred Neuhold and Ingo Salzmann performed XRR and GIXD measurements under the supervision of Prof. Dr. Roland Resel. Cees Van der Marel did XPS investigations. Dr. Gerwin Gelinck and Prof. Dago de Leeuw gave fruitful input during several discussions. I wrote the publication and jointly finalized with the help of all co-authors. The complete work was supervised by Dr. Edsger Smits and Prof. Dr. Peter Strohrriegl.

Appendix:

“N-type self-assembled monolayer field-effect transistors”

Published in: *Proceedings of SPIE*, 8478, 847813, **2012**; DOI: 10.1117/12.929535

by Andreas Ringk, Xiaoran Li, Fatemeh Gholamrezaie, Edsger C. P. Smits, Alfred Neuhold, Armin Moser, Gerwin H. Gelinck, Roland Resel, Dago M. de Leeuw, Peter Strohrriegl

I designed, synthesized, and characterized the organic material for this publication. Transistor devices were fabricated and characterized during my stay at the Holst Centre in the Netherlands in Eindhoven together with Xiaoran Li. Fatemeh Gholamrezaie provided the p-type SAMFET for the COMS-circuit which was measured by Edsger Smits. Alfred Neuhold and Armin Moser performed XRR and GIXD measurements under the supervision of Prof. Dr. Roland Resel. Dr. Gerwin Gelinck and Prof. Dago de Leeuw gave fruitful input during several discussions. I wrote the publication which was corrected by Prof. Dr. Peter Strohrriegl. The complete work was supervised by Dr. Edsger Smits and Prof. Dr. Peter Strohrriegl.

- [1] Lilienfeld, J. E. A method and apparatus for controlling electric currents. US patent 1745175, **1930**.
- [2] Pierce, J. R. The naming of the transistor. *IEEE*, *86*, **1998**, 37-45.
- [3] Shockley, W. The theory of p-n junctions in semiconductors and p-n junction transistors. *14*, **1949**, 435-489.
- [4] Kilby, J. S. Integrated semiconductive circuit structure. US patent 3340406, **1928**.
- [5] Wanlass, F. M., Low stand-by power complementary field-effect circuitry. US patent 3356858, 1967.
- [6] Moore, G. E. Cramming more components onto integrated circuits. *Electronics*, *38*, **1965**, 114-117.
- [7] Fuechsle, M.; Miwa, J. A.; Mahapatra, S.; Ryu, H.; Lee, S.; Warschkow, O.; Hollenberg, L. C. L.; Klimeck, G.; Simmons, M. Y. A single-atom transistor. *Nat. Nanotech.* *4*, **2012**, 242–246.
- [8] <http://www.itproportal.com/2012/04/24/intel-ivy-bridge-architecture-breakdown> 15.07. **2012**.
- [9] <http://www.etherealisation.com>, 19.06.**2012**.
- [10] <http://www.intel.com>, 15.09.**2012**.
- [11] Klasens, H. A.; Koelmans, H. A tin oxide field-effect transistor. *Solid-State Electr.* *9*, **1964**, 701–702.
- [12] Boesen, G. F.; Jacobs, J. E. ZnO field-effect transistor. *Proc. of the IEEE*. *11*, **1968**, 2094–2095.
- [13] Nomura, K.; Ohta, H.; Ueda, K.; Kamiya, T.; Hirano, M.; Hosono, H. Thin-Film Transistor Fabricated in Single-Crystalline Transparent Oxide Semiconductor. *Science*. *5623*, **2003**, 1269–1272.
- [14] Adamopoulos, G.; Bashir, A.; Thomas, S.; Gillin, W. P.; Georgakopoulos, S.; Shkunov, M.; Baklar, M. A.; Stingelin, N.; Maher, R. C.; Cohen, L. F.; Bradley, D. D. C.; Anthopoulos, T. D. Spray-Deposited Li-Doped ZnO Transistors with Electron Mobility Exceeding 50 cm²/Vs. *Adv. Mater.* *42*, **2010**, 4764–4769.

- [15] Chang, Y.-J.; Lee, D.-H.; Herman, G. S.; Chang, C.-H. High-Performance, Spin-Coated Zinc Tin Oxide Thin-Film Transistors. *Electrochem. and Solid-State Lett.* **5**, **2007**, H135-H138.
- [16] Meyers, S. T.; Anderson, J. T.; Hung, C. M.; Thompson, J.; Wager, J. F.; Keszler, D. A. Aqueous Inorganic Inks for Low-Temperature Fabrication of ZnO TFTs. *J. Am. Chem. Soc.* **51**, **2008**, 17603–17609.
- [17] Lee, D.-H.; Chang, Y.-J.; Herman, G. S.; Chang, C.-H. A General Route to Printable High-Mobility Transparent Amorphous Oxide Semiconductors. *Adv. Mater.* **6**, **2007**, 843–847.
- [18] Fortunato, E.; Barquinha, P.; Martins, R. Oxide Semiconductor Thin-Film Transistors: A Review of Recent Advances. *Adv. Mater.* **22**, **2012**, 2945–2986.
- [19] Kim, M.-G.; Kanatzidis, M. G.; Facchetti, A.; Marks, T. J. Low-temperature fabrication of high-performance metal oxide thin-film electronics via combustion processing. *Nat. Mater.* **5**, **2011**, 382–388.
- [20] Shirakawa, H.; Louis, E. J.; MacDiarmid, A. G.; Chiang, C. K.; Heeger, A. J. Synthesis of electrically conducting organic polymers: halogen derivatives of polyacetylene. *J. Chem. Soc., Chem. Commun.* **16**, **1977**, 578–580.
- [21] C. W. Tang, Two-layer organic photovoltaic cell. *Appl. Phys. Lett.* **48**, **1986**, 183–185.
- [22] Tang, C. W.; van Slyke, A. S. *Appl. Phys. Lett.* **51**, **1987**, 913.
- [23] <http://www.crazyengineers.com>, 19.06.2012.
- [24] <http://www.circuitstoday.com>, 19.06.2012.
- [25] <http://t3n.de>, 19.06.2012.
- [26] Green, M. A.; Emery, K.; Hishikawa, Y.; Warta, W.; Dunlop, E. D. Solar cell efficiency tables. *Prog. Photovolt: Res. Appl.* **20**, **2012**, 606–614.
- [27] H. B. Michaelson, Work Functions of the Elements, *Handbook of Chemistry and Physics*, R. C. Weast, ed., CRC Press, Cleveland, Ohio, 58th ed., 1977-1978, p. E-81.
- [28] Brown, A. R.; Jarrett, C. P.; de Leeuw, D. M. Field-effect transistors made from solution-processed organic semiconductors. *Synth. Met.* **88**, **1997**, 37-55.
- [29] Newman, C. R.; Frisbie, C. D.; da Silva Filho, D. A.; Brédas, J.-L.; Ewbank, P. C.; Mann, K. R. Introduction to Organic Thin Film Transistors and Design of n-Channel Organic Semiconductors. *Chem. Mater.* **23**, **2004**, 4436–4451.
- [30] Jabbour, G. E.; Kawabe, Y.; Shaheen, S. E.; Wang, J. F.; Morrell, M. M.; Kippelen, B.; Peyghambarian, N. Highly efficient and bright organic electroluminescent devices with an aluminum cathode. *Appl. Phys. Lett.* **13**, **1997**, 1762–1764.
- [31] Shen, Y.; Li, K.; Majumdar, N.; Campbell, J. C.; Gupta, M. C. Bulk and contact resistance in P3HT:PCBM heterojunction solar cells. *Solar Energy Materials and Solar Cells.* **8**, **2011**, 2314–2317.
- [32] Chua, L.-L.; Zaumseil, J.; Chang, J.-F.; Ou, E. C.-W.; Ho, P. K.-H.; Sirringhaus, H.; Friend, R. H. General observation of n-type field-effect behaviour in organic semiconductors. *Nature.* **7030**, **2005**, 194–199.

- [33] Schwoerer, M., Wolf, H. C. *Organische Molekulare Festkörper*, Wiley-VCH, **2005**, Weinheim.
- [34] Sirringhaus, H. Device Physics of Solution-Processed Organic Field-Effect Transistors. *Adv. Mater.* *20*, **2005**, 2411–2425.
- [35] Bürgi, L.; Richards, T. J.; Friend, R. H.; Sirringhaus, H. Close look at charge carrier injection in polymer field-effect transistors. *J. Appl. Phys.* *94*, **2003**, 6129.
- [36] Marinkovic, M.; Belaine, D.; Wagner, V.; Knipp, D. On the Origin of Contact Resistances of Organic Thin Film Transistors. *Adv. Mater.* *29*, **2012**, 4005–4009.
- [37] Hoppe, A.; Knipp, D.; Gburek, B.; Benor, A.; Marinkovic, M.; Wagner, V. Scaling limits of organic thin film transistors. *Organic Electronics.* *4*, **2010**, 626–631.
- [38] Wagner, V.; Wobkenberg, P.; Hoppe, A.; Seekamp, J. Megahertz operation of organic field-effect transistors based on poly(3-hexylthiophene). *Appl. Phys. Lett.* *24*, **2006**, 243515.
- [39] Cheng, X.; Noh, Y.-Y.; Wang, J.; Tello, M.; Frisch, J.; Blum, R.-P.; Vollmer, A.; Rabe, J. P.; Koch, N.; Sirringhaus, H. Controlling Electron and Hole Charge Injection in Ambipolar Organic Field-Effect Transistors by Self-Assembled Monolayers. *Adv. Funct. Mater.* *15*, **2009**, 2407–2415.
- [40] Baeg, K.-J.; Khim, D.; Jung, S.-W.; Kang, M.; You, I.-K.; Kim, D.-Y.; Facchetti, A.; Noh, Y.-Y. Remarkable Enhancement of Hole Transport in Top-Gated N-Type Polymer Field-Effect Transistors by a High-k Dielectric for Ambipolar Electronic Circuits. *Adv. Mater.* *40*, **2012**, 5433–5439.
- [41] Nicolai, H. T.; Kuik, M.; Wetzelaer, G. A. H.; Boer, B. de; Campbell, C.; Risko, C.; Brédas, J. L.; Blom, P. W. M. Unification of trap-limited electron transport in semiconducting polymers. *Nat Mater.* *10*, **2012**, 882–887.
- [42] Kalb, W. L.; Haas, S.; Krellner, C.; Mathis, T.; Batlogg, B. Trap density of states in small-molecule organic semiconductors: A quantitative comparison of thin-film transistors with single crystals. *Physical Review B.* *15*, **2010**, 155315.
- [43] de Leeuw, D. M.; Simenon, M.M.J.; Brown, A. R.; Einerhand, R.E.F. Stability of n-type doped conducting polymers and consequences for polymeric microelectronic devices. *Synt. Met.* *87*, **1997**, 53–59.
- [44] Gill, W. D. Drift mobilities in amorphous charge-transfer complexes of trinitrofluorenone and poly-n-vinylcarbazole. *J. App. Phy.* *12*, **1972**, 5033–5040.
- [45] Scher, H.; Montroll, E. W. Anomalous transit-time dispersion in amorphous solids. *Phys. Rev. B.* *6*, **1975**, 2455–2477.
- [46] Bäessler, H. Charge Transport in Disordered Organic Photoconductors a Monte Carlo Simulation Study. *Phys. Stat. Sol. (b).* *1*, **1993**, 15–56.
- [47] Sirringhaus, H.; Brown, P. J.; Friend, R. H.; Nielsen, M. M.; Bechgaard, K.; Langeveld-Voss, B. M. W.; Spiering, A. J. H.; Janssen, R. A. J.; Meijer, E. W.; Herwig, P.; Leeuw, D. M. de. Two-dimensional charge transport in self-organized, high-mobility conjugated polymers. *Nature.* *6754*, **1999**, 685–688.
- [48] Podzorov, V.; Menard, E.; Borissov, A.; Kiryukhin, V.; Rogers, J. A.; Gershenson, M. E. Intrinsic Charge Transport on the Surface of Organic Semiconductors. *Phys. Rev. Lett.* *8*, **2004**, 86602.

- [49] Sakanoue, T.; Sirringhaus, H. Band-like temperature dependence of mobility in a solution-processed organic semiconductor. *Nat Mater.* **9**, **2010**, 736–740.
- [50] Yan, H.; Zheng, Y.; Blache, R.; Newman, C.; Lu, S.; Woerle, J.; Facchetti, A. Solution Processed Top-Gate n-Channel Transistors and Complementary Circuits on Plastics Operating in Ambient Conditions. *Adv. Mater.* **18**, **2008**, 3393–3398.
- [51] Baeg, K.-J.; Noh, Y.-Y.; Sirringhaus, H.; Kim, D.-Y. Controllable Shifts in Threshold Voltage of Top-Gate Polymer Field-Effect Transistors for Applications in Organic Nano Floating Gate Memory. *Adv. Func. Mater.* **2**, **2010**, 224–230.
- [52] Richards, T. J.; Sirringhaus, H. Analysis of the contact resistance in staggered, top-gate organic field-effect transistors. *J. Appl. Phys.* **9**, **2007**, 94510.
- [53] Li, C.; Wonneberger, H. Perylene Imides for Organic Photovoltaics: Yesterday, Today, and Tomorrow. *Adv. Mater.* **24**, **2012**, 613–636.
- [54] Ego, C.; Marsitzky, D.; Becker, S.; Zhang, J.; Grimsdale, A. C.; Müllen, K.; MacKenzie, J. D.; Silva, C.; Friend, R. H. Attaching Perylene Dyes to Polyfluorene: Three Simple, Efficient Methods for Facile Color Tuning of Light-Emitting Polymers. *J. Am. Chem. Soc.* **2**, **2002**, 437–443.
- [55] Sadrai, M.; Hadel, L.; Sauers, R. R.; Husain, S.; Krogh-Jespersen, K.; Westbrook, J. D.; Bird, G. R. Lasing action in a family of perylene derivatives: singlet absorption and emission spectra, triplet absorption and oxygen quenching constants, and molecular mechanics and semiempirical molecular orbital calculations. *J. Phys. Chem.* **20**, **1992**, 7988–7996.
- [56] Jones, B. A.; Facchetti, A.; Wasielewski, M. R.; Marks, T. J. Tuning Orbital Energetics in Arylene Diimide Semiconductors. *Materials Design for Ambient Stability of n-Type Charge Transport.* *J. Am. Chem. Soc.* **49**, **2007**, 15259–15278.
- [57] Jones, B. A.; Facchetti, A.; Marks, T. J.; Wasielewski, M. R. Cyanonaphthalene Diimide Semiconductors for Air-Stable, Flexible, and Optically Transparent n-Channel Field-Effect Transistors. *Chem. Mater.* **11**, **2007**, 2703–2705.
- [58] Molinari, A. S.; Alves, H.; Chen, Z.; Facchetti, A.; Morpurgo, A. F. High Electron Mobility in Vacuum and Ambient for PDIF-CN₂ Single-Crystal Transistors. *J. Am. Chem. Soc.* **7**, **2009**, 2462–2463.
- [59] An, Z.; Yu, J.; Jones, S. C.; Barlow, S.; Yoo, S.; Domercq, B.; Prins, P.; Siebbeles, L. D. A.; Kippelen, B.; Marder, S. R. High Electron Mobility in Room-Temperature Discotic Liquid-Crystalline Perylene Diimides. *Adv. Mater.* **21**, **2005**, 2580–2583.
- [60] Matthieu, P.; Ryoma, H.; Yasuhiro, S.; Yutaka, W.; Jonathan, P. H.; Katsuhiko, A.; Toyohiro, C. Growth and electrical properties of N,N[prime]-bis(n-pentyl)terrylene-3,4:11,12-tetracarboximide thin films. *Appl. Phys. Lett.* **16**, **2008**, 163301.
- [61] Oh, J. H.; Lee, W.-Y.; Noe, T.; Chen, W.-C.; Könnemann, M.; Bao, Z. Solution-Shear-Processed Quaterylene Diimide Thin-Film Transistors Prepared by Pressure-Assisted Thermal Cleavage of Swallow Tails. *J. Am. Chem. Soc.* **12**, **2011**, 4204–4207.

- [62] An, Z.; Yu, J.; Domercq, B.; Jones, S. C.; Barlow, S.; Kippelen, B.; Marder, S. R. Room-temperature discotic liquid-crystalline coronene diimides exhibiting high charge-carrier mobility in air. *J. Mater. Chem.* **37**, **2009**, 6688–6698.
- [63] Yan, H.; Chen, Z.; Zheng, Y.; Newman, C.; Quinn, J. R.; Dötz, F.; Kastler, M.; Facchetti, A. A high-mobility electron-transporting polymer for printed transistors. *Nature*. **7230**, **2009**, 679–686.
- [64] Babel, A.; Jenekhe, S. A. High Electron Mobility in Ladder Polymer Field-Effect Transistors. *J. Am. Chem. Soc.* **45**, **2003**, 13656–13657.
- [65] Zhan, X.; Facchetti, A.; Barlow, S.; Marks, T. J.; Ratner, M. A.; Wasielewski, M. R.; Marder, S. R. Rylene and Related Diimides for Organic Electronics. *Adv. Mater.* **2**, **2011**, 268–284.
- [66] Lang, A. S.; Neubig, A.; Sommer, M.; Thelakkat, M. NMRP versus “Click” Chemistry for the Synthesis of Semiconductor Polymers Carrying Pendant Perylene Bisimides. *Macromolecules*. **17**, **2010**, 7001–7010.
- [67] Greene, M. In *High performance pigments*; Faulkner, E. B., Schwartz, R. J., Eds.; Wiley-VCH: Weinheim, **2009**.
- [68] Kaiser, H.; Lindner, J.; Langhals, H. Synthese von nichtsymmetrisch substituierten Perylen-Fluoreszenzfarbstoffen. *Chem. Ber.* **124**, **1991**, 529-535.
- [69] Tröster, H. Untersuchungen zur Protonierung von Perylen-3,4,9,10-tetracarbonsäurealkalisalzen. *Dyes Pigm.* **4**, **1983**, 171-177.
- [70] Kaiser, H.; Lindner, J.; Langhals, H. Synthese von nichtsymmetrisch substituierten Perylen-Fluoreszenzfarbstoffen. *Chem. Ber.* **124**, **1991**, 529-535.
- [71] Yukinori, N.; Tadashi, N.; Yoshimoto, A.; Takahisa, M. Synthesis and Properties of Long and Branched Alkyl Chain Substituted Perylenetetracarboxylic Monoanhydride thesis and Properties of Long and Branched Alkyl Ch Substituted Perylenetetracarboxylic Monoanhydride Monoimides etetracarbox Monoimides. *Dyes Pigm.* **32**, **1996**, 71-84.
- [72] Wicklein, A.; Lang, A.; Muth, M.; Thelakkat, M. Swallow-Tail Substituted Liquid Crystalline Perylene Bisimides: Synthesis and Thermotropic Properties. *J. Am. Chem. Soc.* **40**, **2009**, 14442–14453.
- [73] Whitesides, G. M. Self-Assembly at All Scales. *Science*. **5564**, **2002**, 2418–2421.
- [74] Philp, D.; Stoddart, J. F. Self-Assembly in Natural and Unnatural Systems. *Angew. Chem. Inter. Ed.* **11**, **1996**, 1154–1196.
- [75] Loudet, J.-C.; Barois, P.; Poulin, P. Colloidal ordering from phase separation in a liquid-crystalline continuous phase. *Nature*. **6804**, **2000**, 611–613.
- [76] Love, J. C.; Estroff, L. A.; Kriebel, J. K.; Nuzzo, R. G.; Whitesides, G. M. Self-Assembled Monolayers of Thiolates on Metals as a Form of Nanotechnology. *Chem. Rev.* **4**, **2005**, 1103–1170.
- [77] Laibinis, P. E.; Whitesides, G. M.; Allara, D. L.; Tao, Y. T.; Parikh, A. N.; Nuzzo, R. G. Comparison of the structures and wetting properties of self-assembled monolayers of n-alkanethiols on the coinage metal surfaces, copper, silver, and gold. *J. Am. Chem. Soc.* **19**, **1991**, 7152–7167.

- [78] Campbell, I. H.; Kress, J. D.; Martin, R. L.; Smith, D. L.; Barashkov, N. N.; Ferraris, J.P. Controlling charge injection in organic electronic devices using self-assembled monolayers. *Appl. Phys. Lett.* **71**, **1997**, 3528-3531.
- [79] Ramachandran, S.; Tsai, B.-L.; Blanco, M.; Chen, H.; Tang, Y.; Goddard, W. A. Self-Assembled Monolayer Mechanism for Corrosion Inhibition of Iron by Imidazolines. *Langmuir*. **26**, **1996**, 6419-6428.
- [80] Aizenberg, J.; Black, A. J.; Whitesides, G. M. Control of crystal nucleation by patterned self-assembled monolayers. *Nature*. **6727**, **1999**, 495-498.
- [81] Dhagat, P.; Haverinen, H. M.; Kline, R. J.; Jung, Y.; Fischer, D. A.; DeLongchamp, D. M.; Jabbour, G. E. Influence of Dielectric Surface Chemistry on the Microstructure and Carrier Mobility of an n-Type Organic Semiconductor. *Adv. Func. Mater.* **5**, **2009**, 2365-2372.
- [82] Lenz, T.; Schmaltz, T.; Novak, M.; Halik, M. Self-Assembled Monolayer Exchange Reactions as a Tool for Channel Interface Engineering in Low-Voltage Organic Thin-Film Transistors. *Langmuir*. **28**, **2012**, 13900-13904.
- [83] Crivillers, N.; Orgiu, E.; Reinders, F.; Mayor, M.; Samorì, P. Optical Modulation of the Charge Injection in an Organic Field-Effect Transistor Based on Photochromic Self-Assembled-Monolayer-Functionalized Electrodes. *Adv. Mater.* **12**, **2011**, 1447-1452.
- [84] Dhagat, P.; Haverinen, H. M.; Kline, R. J.; Jung, Y.; Fischer, D. A.; DeLongchamp, D. M.; Jabbour, G. E. Influence of Dielectric Surface Chemistry on the Microstructure and Carrier Mobility of an n-Type Organic Semiconductor. *Adv. Funct. Mater.* **15**, **2009**, 2365-2372.
- [85] Dodabalapur, A.; Torsi, L.; Katz, H. E. Organic Transistors: Two-Dimensional Transport and Improved Electrical Characteristics. *Science*. **5208**, **1995**, 270-271.
- [86] Dinelli, F.; Murgia, M.; Levy, P.; Cavallini, M.; Biscarini, F.; Leeuw, D. de. Spatially Correlated Charge Transport in Organic Thin Film Transistors. *Phys. Rev. Lett.* **11**, **2004**, 116802.
- [87] Liu, S. W.; Lee, C.-C.; Wen, J.-M.; Chen, C.-T. C. In situ vacuum measurement of the thickness dependence of electron mobility in naphthalenetetracarboxylic diimide-based field-effect transistors. *Appl. Phys. Lett.* **98**, **2011**, 023306.
- [88] Wen, Y.; Chen, J.; Zhang, L.; Sun, X.; Zhao, Y.; Guo, Y.; Yu, G.; Liu, Y. Quantitative Analysis of the Role of the First Layer in p- and n-Type Organic Field-Effect Transistors with Graphene Electrodes. *Adv. Mater.* **24**, **2012**, 1471-1475.
- [89] Defaux, M.; Gholamrezaie, F.; Wang, J.; Kreyes, A.; Ziener, U.; Anokhin, D. V.; Ivanov, D. A.; Moser, A.; Neuhold, A.; Salzmann, I.; Resel, R.; Leeuw, D. M. de; Meskers, S. C. J.; Moeller, M.; Mourran, A. Solution-Processable Septithiophene Monolayer Transistor. *Adv. Mater.* **7**, **2012**, 973-978.
- [90] Wei, Z.; Cao, Y.; Ma, W.; Wang, C.; Xu, W.; Guo, X.; Hu, W.; Zhu, D. Langmuir-Blogett monolayer transistors of copper phthalocyanine. *App. Phys. Lett.* **3**, **2009**, 33304.
- [91] Fabiano, S.; Musumeci, C.; Chen, Z.; Scandurra, A.; Wang, H.; Loo, Y.-L.; Facchetti, A.; Pignataro, B. From Monolayer to Multilayer N-Channel Polymeric

- Field-Effect Transistors with Precise Conformational Order. *Adv. Mater.* **7**, **2012**, 951–956.
- [92] Scott, J. C.; Samuel, J. D. J.; Hou, J. H.; Rettner, C. T.; Miller, R. D. Monolayer Transistor Using a Highly Ordered Conjugated Polymer as the Channel. *Nano Lett.* **12**, **2006**, 2916–2919.
- [93] Tulevski, G. S.; Miao, Q.; Fukuto, M.; Abram, R.; Ocko, B.; Pindak, R.; Steigerwald, M. L.; Kagan, C. R.; Nuckolls, C. Attaching Organic Semiconductors to Gate Oxides: In Situ Assembly of Monolayer Field Effect Transistors. *J. Am. Chem. Soc.* **126**, **2004**, 15048–15050.
- [94] Guo, X.; Myers, M.; Xiao, S.; Lefenfeld, M.; Steiner, R.; Tulevski, G.S.; Tang, J.; Baumert, J.; Leibfarth, F.; Yardley, J.T.; Steigerwald, M.L.; Kim, P.; Nuckolls, C. Chemoresponsive monolayer transistors. *PNAS.* **103**, **2006**, 11452–11456.
- [95] Mottaghi, M.; Lang, P.; Rodriguez, F.; Rumyantseva, A.; Yassar, A.; Horowitz, G.; Lenfant, S.; Tondelier, D.; Vuillaume, D. Low-Operating-Voltage Organic Transistors Made of Bifunctional Self-Assembled Monolayers. *Adv. Funct. Mater.* **4**, **2007**, 597–604.
- [96] Hutchins, D. O.; Acton, O.; Weidner, T.; Cernetic, N.; Baio, J. E.; Ting, G.; Castner, D. G.; Ma, H.; Jen, A. K.-Y. Spin cast self-assembled monolayer field effect transistors. *Org. Electr.* **3**, **2012**, 464–468.
- [97] Smits, E. C. P.; Mathijssen, S. G. J.; van Hal, P. A.; Setayesh, S.; Geuns, T. C. T.; Mutsaers, K. A. H. A.; Cantatore, E.; Wondergem, H. J.; Werzer, O.; Resel, R.; Kemerink, M.; Kirchmeyer, S.; Muzafarov, A. M.; Ponomarenko, S. A.; Boer, B. de; Blom, P. W. M.; Leeuw, D. M. de. Bottom-up organic integrated circuits. *Nature.* **455**, **2008**, 956–959.
- [98] Flesch, H.-G.; Mathijssen, S. G. J.; Gholamrezaie, F.; Moser, A.; Neuhold, A.; Novák, J.; Ponomarenko, S. A.; Shen, Q.; Teichert, C.; Hlawacek, G.; Puschnig, P.; Ambrosch-Draxl, C.; Resel, R.; Leeuw, D. M. de. Microstructure and Phase Behavior of a Quinquethiophene-Based Self-Assembled Monolayer as a Function of Temperature. *J. Phys. Chem. C.* **115**, **2011**, 22925–22930.
- [99] Melucci, M.; Gazzano, M.; Barbarella, G.; Cavallini, M.; Biscarini, F.; Maccagnani, P.; Ostojica, P. Multiscale Self-Organization of the Organic Semiconductor α -Quinquethiophene. *J. Am. Chem. Soc.* **125**, **2003**, 10266–10274.
- [100] Gholamrezaie, F.; Mathijssen, S. G. J.; Smits, E. C. P.; Geuns, T. C. T.; van Hal, P. A.; Ponomarenko, S. A.; Flesch, H.-G.; Resel, R.; Cantatore, E.; Blom, P. W. M.; Leeuw, D. M. de. Ordered Semiconducting Self-Assembled Monolayers on Polymeric Surfaces Utilized in Organic Integrated Circuits. *Nano Lett.* **10**, **2010**, 1998–2002.
- [101] Brondijk, J. J.; Roelofs, W. S. C.; Mathijssen, S. G. J.; Shehu, A.; Cramer, T.; Biscarini, F.; Blom, P. W. M.; Leeuw, D. M. de. Two-Dimensional Charge Transport in Disordered Organic Semiconductors. *Phys. Rev. Lett.* **107**, **2012**, 56601.
- [102] Roelofs, W. S. C.; Mathijssen, S. G. J.; Janssen, R. A. J.; Leeuw, D. M. de; Kemerink, M. Accurate description of charge transport in organic field effect transistors using an experimentally extracted density of states. *Phys. Rev. B.* **85**, **2012**, 85202.

- [103] Gholamrezaie, F.; Kirkus, M.; Mathijssen, S. G. J.; Leeuw, D. M. de; Meskers, S. C. J. Photophysics of Self-Assembled Monolayers of a π -Conjugated Quinquethiophene Derivative. *J. Phys. Chem. A*, **2012**, *116*, 7645–7650.
- [104] Novak, M.; Ebel, A.; Meyer-Friedrichsen, T.; Jedaa, A.; Vieweg, B. F.; Yang, G.; Voitchovsky, K.; Stellacci, F.; Spiecker, E.; Hirsch, A.; Halik, M. Low-Voltage p- and n-Type Organic Self-Assembled Monolayer Field Effect Transistors. *Nano Lett.* **2011**, *11*, 156–159.

N-TYPE PERYLENE TO FILL VOIDS IN SOLUTION PROCESSED
NANOPARTICULATE ZINC OXIDE THIN FILMS

Simon Bubel,^{a,b,*} Andreas Ringk,^{c,b} Peter Strohrig,^c Roland Schmechel^a

^a Faculty of Engineering and Center for Nanointegration Duisburg-Essen (CeNIDE),
University of Duisburg-Essen, 47057 Duisburg, Germany

^b Dutch Polymer Institute (DPI), P.O. Box 902, 5600 AX Eindhoven, The Netherlands

^c Macromolecular Chemistry I, University of Bayreuth, 95440 Bayreuth, Germany

Published in *Physica E*, **2012**

Volume 44, Issue 10, pages 2124–2127

DOI: 10.1016/j.physe.2012.06.027

Reprinted with permission; Copyright © 2012 by Elsevier B.V.

1. Introduction

Recent development in zinc oxide (ZnO) semiconductor research has led to simple, low cost, low temperature processes capable of building thin functional ZnO films on silicon, glass, and flexible polymer substrates. These thin films have been used as electrodes in photovoltaics,^[1,2,3] electroluminescent devices,^[4,5,6] and as the active channel material in thin film transistors (TFT).^[7,8,9] In such devices, the density of thermal charge carriers, and hence the work function of ZnO, is difficult to control and has proven to be sensitive to ambient conditions.^[7,10,11] Even the bulk or crystal morphology of ZnO has been shown to be affected by the surrounding media.^[12,13] Therefore, it has turned out to be essential to manage the sensitive electrical properties of ZnO in a reproducible manner. In surface governed systems, including exceedingly thin or porous films of any ZnO morphology or nanostructure, the key to the electrical properties is the ZnO surface. Using organic adsorbates at the ZnO surface has been demonstrated to improve the atmospheric durability of ZnO TFTs^[10,11,14,15,16] and the adhesion of additional functional organics in ZnO/organic ambipolar devices.^[17] Organic adsorbates have even been used to tune the ZnO work function,^[11,18,19] e.g. in dye sensitized solar cells to establish a good energetic alignment^[3] or to improve the exciton dissociation.^[20] In general, it can be stated that the study of ZnO and its heterostructures and interfaces with organic semiconductors is enjoying the increasing popularity, bearing a growing number in publications, e.g. ZnO/pentacene ambipolar devices.^[21,22,23,24] Looking at the use of dispersions in classic print products, the pigments or nanoparticles are usually synthesized first rather than transformed to the desired pigment after printing. Semiconducting nanoparticle dispersions seem to be the consequent further development in terms of printing because the semiconductor synthesis can likewise be separated from low temperature thin film deposition and patterning, which is not the case for printing precursor solutions. However, only a couple of publications deal with dispersion processed nanoparticulate thin films due to two major drawbacks: On the one hand, if organic adsorbates are used in order to passivate perturbing surface effects or to stabilize the ZnO nanoparticles in the dispersion, the presence of organics disrupts the interparticle charge transfer^[25,26,27] or their removal requires high temperatures which are incompatible with flexible polymer substrates.^[28] On the other hand, very small ZnO nanoparticles (np-ZnO) around 5 nm^[29] have been used to avoid the need for organic stabilizing agents in the dispersion and in order to establish thin films with smoother

interfaces to the gate dielectric. However, np-ZnO of such size will not form long term stable dispersions due to nanoparticle degradation as was shown by Ali and Winterer.^[12] In this work we show a way to surmount the drawbacks of nanoparticulate thin films, by using sufficiently large ZnO nano- particles to prevent ZnO degradation, qualified surface adsorbates to passivate the ZnO surface, and an n-type conducting organic to bridge the insulating voids between the nanoparticles. In our approach we build a ZnO organic composite using an electron conducting perylene diimide (PDI) with pyrrolidone moieties as the linker to the ZnO surface. Judging from TFTs with np-ZnO polyvinylpyrrolidone (PVP) composites^[11,30] we deploy the pyrrolidone group because it was suspected to adsorb to the ZnO nanoparticles during ultrasonic treatment in 2-methoxyethanol and should serve as a np-ZnO surface passivating agent. We countercheck our findings with ZnO PDI composites without the linker group.

2. Experimental

As the organic base molecule we used the well known airstable n-type conducting perylene diimide (PDI)^[31] derivatives with two different moieties. The functionalized PDI molecule (PDI-Pyr) displayed in Fig. 1, exhibits two N-propyl-pyrrolidone side groups which are to act as a linker to the np-ZnO surface. The first molecule in Fig. 1 (PDI-F) was used as a reference additive without a linker to ZnO. It possesses perfluorinated alkyl moieties, which are known to enhance the atmospheric stability by exhibiting a higher work function (lower lowest unoccupied molecular orbital) compared to PDI with alkyl substituents.^[31,32,33] The PDI derivatives were synthesized according to a slightly modified literature procedure.^[34] The detailed process description, nuclear magnetic resonance (NMR) spectra, and transistor characteristics of the organic compounds can be found in the supplementary material.

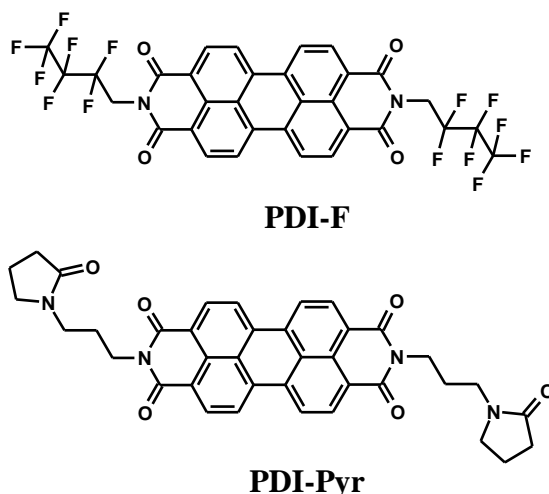


Figure 1: Molecular structure of the perylenediimide with heptafluorobutyl or N-propyl pyrrolidone moieties.

For the nanoparticulate ZnO dispersion, a suspension of 10 wt% of ZnO nanoparticles (Evonik Industries, AdNano VP20, ca. 25 nm, log normal 15–50 nm^[26]) and 1 ml of a 1:1 mixture of 2-methoxyethanol (2-MeEtOH) (anhydrous 99.8%, Sigma-Aldrich) and chloroform (anhydrous 99%, Sigma-Aldrich) was dispersed using an air cooled ultrasonic bar sonotrode (Hielscher Ultraschall, VialTweeter) at 200W for 10 min. Nanoparticulate thin films were made by spin-coating the dispersion at 3000 rpm followed by an annealing step at 125°C for 30 min in ambient atmosphere.

In order to build thin film transistors, n-doped silicon substrates (Si:P $3 \times 10^{17} \text{ cm}^{-3}$) with 200 nm of thermally grown silicon dioxide (SiO₂) as gate dielectric were used (Fraunhofer IPMS Dresden). Source and drain aluminum top electrodes were processed using a shadow mask in a physical vapor deposition system. The electrodes geometry was 0.74 cm and 100 mm for channel width and length, respectively. Electrical transistor characterization was carried out in a nitrogen filled glove box under exclusion of ambient light and using a parameter analyzer (Keithley 4200 SCS) in combination with a probe station. All TFT output- and transfer characteristics were measured in forward and backward sweeps with an incremental bias delay of 100 ms/V. The scanning electron microscope (SEM) analysis was done using a Jeol JSM 7500F.

3. Results and discussion

As seen in Fig. 1 PDI-F does not possess a linker group to attach to the ZnO surface. The application of PDI-F in a ZnO organics composite leads to organic precipitates in the thin film which can be identified as red spots in the microscope image in Fig. 2. The

image shows the top view on the film and the transistor channel with the two aluminum electrodes as depicted in the transistor device sketch at the lower left hand side of Fig. 2. In all likelihood, the PDI-F precipitates reduce the number of conducting percolation pathways, as the organic displaces parts of the np-ZnO film and lowers the homogeneity of the thin film. Looking at Fig. 2, it can be seen that the conductivity of the composite films decreases with increasing PDI-F content. As the PDI-F ionization energy (6.4 eV)^[31] is deeper than the work function of the ZnO nanoparticles (ca. 4.6 eV),^[11] a charge transfer, if at all, will only occur from ZnO to PDI-F.^[35] Ergo, the precipitates could act as trapping centers which contribute to the decrease in conductivity.

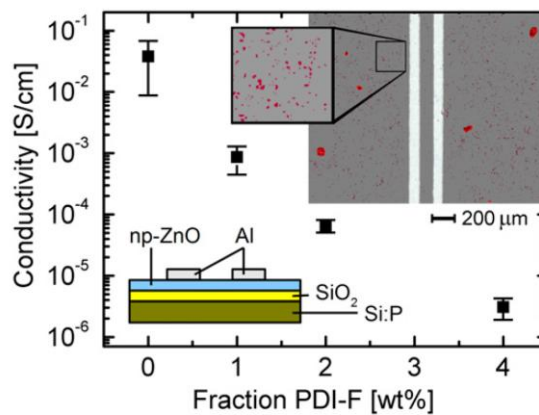


Figure 2: Conductivity of the ZnO PDI-F composite as a function of PDI-F fraction. Inset: (Bottom left) Sideview of the TFT device layout. (Top right) Topview microscope image of the np-ZnO thin film with 4wt% of PDI-F. The two vertical lines are the aluminum source and drain electrodes. (For interpretation of the references to color in this figure caption, the reader is referred to the web version of this article.)

Additionally, due to the missing adequate linker group, the high density of donor states at the ZnO nanoparticle surface stays unaltered. The unperturbed high surface donor density gives rise to a metal like surface conduction as seen by Allen et al.^[36] Looking at the TFT transfer characteristics of the np-ZnO PDI-F composites in Fig. 3, no gate bias dependence of the drain current can be observed. The PDI-F containing thin films exhibit ohmic rather than semiconducting properties.

In contrast to PDI-F without a linker group to ZnO, PDI-Pyr may attach to the np-ZnO surface. Looking at the transistor transfer characteristics of the PDI-Pyr functionalized np-ZnO transistors in Fig. 4, a distinct field effect can be seen for 4 wt% of PDI-Pyr. If only 2 wt% of the organic was added to the dispersion, the TFT shows depletion-type transistor behavior as known from thin films with thermally active charge carriers.^[37] If no organic was added, the thin film shows ohmic conduction and no field effect

whatsoever, whereas if 8 wt% of the organic was added, the film renders insulating. Looking at the dark field microscope image in Fig. 4 at 8 wt%, this amount of PDI-Pyr decreases the film forming properties of the dispersion dramatically and uncovered areas show up in the transistor channel.

Figure 5(a) and (b) shows the output and transfer characteristic of the 4 wt% TFT more in detail. The saturation mobility of this device reaches $7.5 \times 10^{-5} \text{ cm}^2/\text{Vs}$ and the on/off ratio is slightly below 10^3 . These poor device parameters originate from a simple fact: Adding an organic compound with more than one linker group to np-ZnO immediately cross-links the ZnO nanoparticles and transforms the dispersion into a suspension which exhibits very poor film forming properties as the 8 wt% layer demonstrates convincingly (cf. Fig. 4).

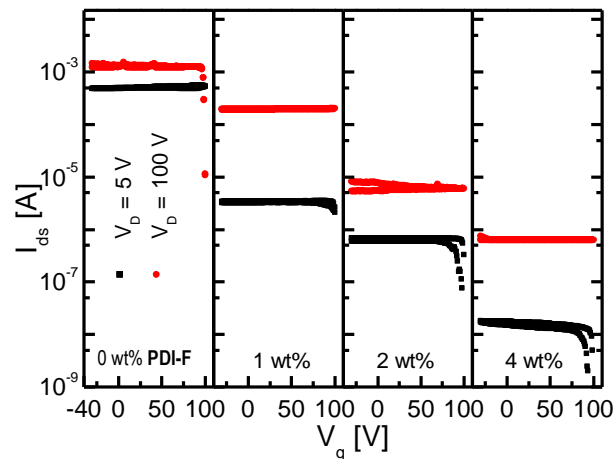


Figure 3: Transfer characteristics of np-ZnO TFTs with 0–4 wt% of PDI-F.

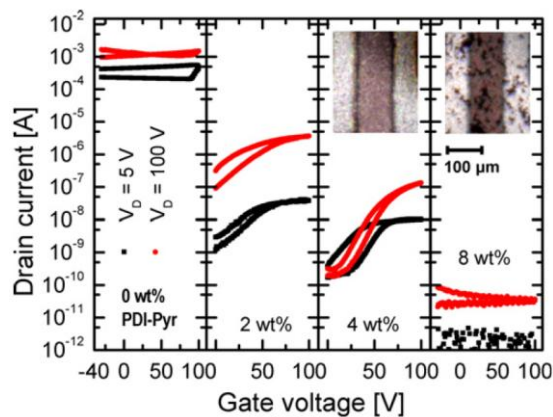


Figure 4: Transfer characteristics of np-ZnO TFTs with 0–8wt% of PDI-Pyr. Inset: Dark field microscope image of the transistor channel area for 4 and 8 wt%. The dark areas in the 8wt% picture originate from the substrate shining through.

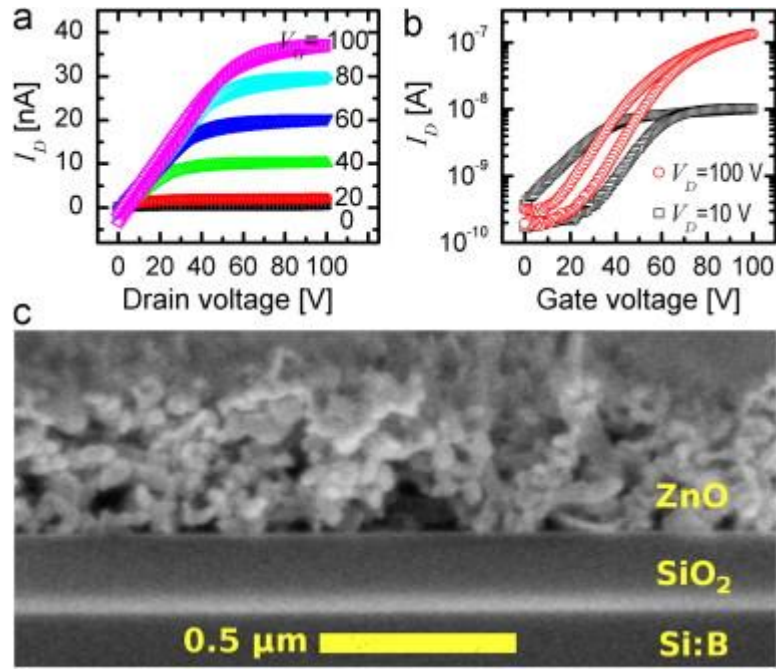


Figure 5: (a) Output and (b) transfer characteristic of np-ZnO TFTs with 4wt% PDI- Pyr. (c) Scanning electron micrograph of the cross-section of the TFT.

The resulting thin film morphology for the 4 wt% dispersion is shown by the cross section image of the thin film in Fig. 5(c). Usually, transistors with such porous semiconductors and rough gate dielectric interfaces will not perform much better than the presented device [25,30]. Due to the flocculation of the dispersion, there are organic molecules between the individual ZnO nanoparticles in the thin film and it can be assumed that charge is transported through the organic junctions between the particles. However, such transport would require an energetic match of the work function of ZnO and the ionization energy of the organic^[35] (<6.4 eV). Judging from the transition from depletion-type to enhancement-type TFT for 2 and 4 wt% in Fig. 4, the PDI-Pyr lowers the density of thermally active charge carriers. Consequently, the adsorbates increase the work function of the np-ZnO as likewise shown for polyvinylpyrrolidone adsorbates where the work function of np-ZnO was increased from 4.6 eV for unpassivated particles to 4.9 eV for PVP passivated np-ZnO.^[11] In addition, the ionization energy of PDI-Pyr is certainly smaller than that of PDI-F (ca. 6.4 eV), as the fluorination is known to increase the HOMO energy level.^[31] Both effects will improve the energetic alignment between the n-type organic and the ZnO surface but might not be enough to facilitate barrier free charge movement. Besides removing the perturbing surface conductivity of the ZnO nanoparticles, the PDI- Pyr acts as a shallow trap level causing trap and release behavior as can be seen in the hysteresis in Fig. 5(b).

4. Conclusion

We built two different composite thin films from ZnO nano- particles and n-type organics by using a low temperature dispersion process. While one composite used a well known air stable perylene diimide the other contained a newly synthesized PDI with a pyrrolidone linker group. The compound without the pyrrolidone linker did not inhibit the high conductivity of the used ZnO nanoparticles, it rather formed precipitates in the thin film. Eventually that composite film turned out to be ohmic conducting with decreasing conductivity at increasing PDI-F fraction. In contrast to PDI-F, the pyrrolidone functionalized compound turned the np-ZnO films into a semiconductor which showed n-type field effect behavior in TFT devices. However, due to the two linker groups per PDI-Pyr molecule the colloids in the dispersion were cross-linking and flocculating. The herewith formed thin films were accordingly porous and of minor performance in transistor devices. In summary, our functionalized n-type organic succeeded in passivating the ZnO surface by removing the perturbing surface conduction and enabled inter particle charge transfer. Unfortunately, our new functionalization failed as a stabilizing agent in the dispersion and only very porous thin films were obtained. In order to print np-ZnO transistors using n-type organic additives in np-ZnO dispersions, the additives should act as a surfactant rather than as a flocculation agent. Such a surfactant should exhibit a linker group to np-ZnO, e.g. pyrrolidone or organic acids, and a solubility group according to the solvent most suitable for the printing process. Consequently, the experiments conducted here can be understood as preliminary work pointing out a practicable way and the main problems in order to develop an additive for printable np-ZnO dispersions, yielding air stable semiconducting thin films. In this regard it is particularly helpful to not only think about the most relevant parameters of a dispersion additive for the printing process itself, like rheology and stability, but also to think about how to improve the electrical properties by choosing the right surfactant.

5. Acknowledgments

We gratefully acknowledge financial support from the Dutch Polymer Institute (DPI), project 627, and from the Deutsche Forschungsgemeinschaft (DFG). The work of Andreas Ringk forms part of the research programme of the Dutch Polymer Institute (DPI), project 624.

6. References

- [1] Olson, D. C.; Shaheen, S. E.; Collins, R. T.; Ginley, D. S. The Effect of Atmosphere and ZnO Morphology on the Performance of Hybrid Poly(3-hexylthiophene)/ZnO Nanofiber Photovoltaic Devices. *J. Phys. Chem. C*, **2007**, *111*, 16670–16678.
- [2] Krebs, F. C. All solution roll-to-roll processed polymer solar cells free from indium-tin-oxide and vacuum coating steps. *Org. Electr.* **2009**, *5*, 761–768.
- [3] Bulliard, X.; Ihn, S.-G.; Yun, S.; Kim, Y.; Choi, D.; Choi, J.-Y.; Kim, M.; Sim, M.; Park, J.-H.; Choi, W.; Cho, K. Enhanced Performance in Polymer Solar Cells by Surface Energy Control. *Adv. Funct. Mater.* **2010**, *24*, 4381–4387.
- [4] Wadeasa, A.; Tzamalis, G.; Sehati, P.; Nur, O.; Fahlman, M.; Willander, M.; Berggren, M.; Crispin, X. Solution processed ZnO nanowires/polyfluorene heterojunctions for large area lightening. *Chem. Phys. Lett.* **2010**, *486*, 200–204.
- [5] Kim, T. W.; Choo, D. C.; No, Y. S.; Choi, W. K.; Choi, E. H. High work function of Al-doped zinc-oxide thin films as transparent conductive anodes in organic light-emitting devices. *Appl. Surf. Sci.* **2006**, *212*, 1917–1920.
- [6] Yuto, T.; Christian, M.; Michael, T.; Joerg, A.; Michael, E.; Frank, L.; Claus, L.; Karl, L.; Karsten, W.; Karsten, F.; Qiang, H. Highly efficient p-i-n-type organic light emitting diodes on ZnO:Al substrates. *Appl. Phys. Lett.* **2007**, *91*, 63510.
- [7] Theissmann, R.; Bubel, S.; Sanlialp, M.; Busch, C.; Schierning, G.; Schmechel, R. High performance low temperature solution-processed zinc oxide thin film transistor. *Thin Solid Films*. **2011**, *519*, 5623–5628.
- [8] Tellier, J.; Kuščer, D.; Malič, B.; Cilenšek, J.; Škarabot, M.; Kovač, J.; Gonçalves, G.; Mušević, I.; Kosec, M. Transparent, amorphous and organics-free ZnO thin films produced by chemical solution deposition at 150°C. *Thin Solid Films*. **2010**, *518*, 5134–5139.
- [9] Meyers, S. T.; Anderson, J. T.; Hung, C. M.; Thompson, J.; Wager, J. F.; Keszler, D. A. Aqueous Inorganic Inks for Low-Temperature Fabrication of ZnO TFTs. *J. Am. Chem. Soc.* **2008**, *130*, 17603–17609.
- [10] S., B.; N., M.; H., H.; R., S. Trap states and space charge limited current in dispersion processed zinc oxide thin films. *J. Appl. Phys.* **2010**, *108*, 124502.
- [11] Bubel, S.; Mechau, N.; Schmechel, R. Electronic properties of polyvinylpyrrolidone at the zinc oxide nanoparticle surface. *J. Mater. Sci.* **2011**, *46*, 7776–7783.
- [12] Ali, M.; Winterer, M. ZnO Nanocrystals: Surprisingly ‘Alive’. *Chem. Mater.* **2009**, *21*, 85–91.
- [13] Claflin, B. B. Zinc oxide has developed a case of acne (A perspective on the article, “Nanostructure Growth-Induced Defect Formation and Band Bending at ZnO Surfaces”, by T. A. Merz, D. R. Dutt, T. Bolton, Y. Dong, and L. J. Brillson). *Surf. Sci.* **2011**, *263*, 859–860.

- [14] Faber, H.; Burkhardt, M.; Jedaa, A.; Kälblein, D.; Klauk, H.; Halik, M. Low-Temperature Solution-Processed Memory Transistors Based on Zinc Oxide Nanoparticles. *Adv. Mater.* **30**, **2009**, 3099–3104.
- [15] Sohn, J. I.; Hong, W. K.; Lee, M. J.; Lee, T.; Siringhaus, H.; Kang, D. J.; Welland, M. E. The influence of surface chemical dynamics on electrical and optical properties of ZnO nanowire field effect transistors. *Nanotech.* **20**, **2012**, 505202.
- [16] Won, I. P.; Jin, S. K.; Gyu-Chul, Y.; M., H. B.; H.-J., L. Fabrication and electrical characteristics of high-performance ZnO nanorod field-effect transistors. *Appl. Phys. Lett.* **21**, **2004**, 5052–5054.
- [17] Yang, C.; Kwack, Y.; Kim, S. H.; An, T. K.; Hong, K.; Nam, S.; Park, M.; Choi, W.-S.; Park, C. E. Ambipolar thin-film transistors and an inverter based on pentacene/self-assembled monolayer modified ZnO hybrid structures for balanced hole and electron mobilities. *Org. Electr.* **3**, **2011**, 411–418.
- [18] Komolov, A. S.; Møller, P. J.; Mortensen, J.; Komolov, S. A.; Lazneva, E. F. Electronic properties of a zinc oxide surface modified by ultra-thin layers of conjugated organic molecules. *Surf. Sci.* **1–3**, **2005**, 129–136.
- [19] Aguilar, C. A.; Haight, R.; Mavrokefalos, A.; Korgel, B. A.; Chen, S. Probing Electronic Properties of Molecular Engineered Zinc Oxide Nanowires with Photoelectron Spectroscopy. *ACS Nano.* **10**, **2009**, 3057–3062.
- [20] Prades, J. D.; Hernandez-Ramirez, F.; Jimenez-Diaz, R.; Manzanares, M.; Andreu, T.; Cirera, A.; Romano-Rodriguez, A.; Morante, J.R. The effects of electron–hole separation on the photoconductivity of individual metal oxide nanowires. *Nanotech.* **19**, **2008**, 465501.
- [21] Hajime, N.; Masayuki, Y.; Chihaya, A.; Koki, Y. Ambipolar field-effect transistor based on organic-inorganic hybrid structure. *Appl. Phys. Lett.* **26**, **2007**, 262104.
- [22] Pal, B. N.; Trottman, P.; Sun, J.; Katz, H. E. Solution-Deposited Zinc Oxide and Zinc Oxide/Pentacene Bilayer Transistors: High Mobility n-Channel, Ambipolar, and Nonvolatile Devices. *Adv. Funct. Mater.* **12**, **2008**, 1832–1839.
- [23] Soumya, D.; Shannon, D. L.; Ananth, D. Hybrid organic/inorganic ambipolar thin film transistor chemical sensor. *Appl. Phys. Lett.* **21**, **2011**, 213504.
- [24] Samarendra, P. S.; Zi-En, O.; Serene Ng Lay Geok; Gregory K. L. Goh; Ananth, D. Electrical characteristics of zinc oxide-organic semiconductor lateral heterostructure based hybrid field-effect bipolar transistors. *Appl. Phys. Lett.* **7**, **2011**, 73302.
- [25] Simon, B.; Donna, N.; Norman, M.; Horst, H. Influence of stabilizers in ZnO nanodispersions on field-effect transistor device performance. *J. Appl. Phys.* **6**, **2009**, 64514.
- [26] Mechau, N.; Bubel, S.; Nikolova, D.; Hahn, H. Influence of stabilizers in ZnO nano-dispersions on the performance of solution-processed FETs. *Physica Status Solidi (a)*. **7**, **2010**, 1684–1688.

- [27] Hirschmann, J.; Faber, H.; Halik, M. Concept of a thin film memory transistor based on ZnO nanoparticles insulated by a ligand shell. *Nanoscale*. **2**, **2012**, 444–447.
- [28] Walther, S.; Schäfer, S.; Jank, M. P. M.; Thiem, H.; Peukert, W.; Frey, L.; Ryssel, H. Influence of annealing temperature and measurement ambient on TFTs based on gas phase synthesized ZnO nanoparticles. *Microelectr. Engin.* **11**, **2010**, 2312–2316.
- [29] Faber, H.; Klaumunzer, M.; Voigt, M.; Galli, D.; Vieweg, B. F.; Peukert, W.; Spiecker, E.; Halik, M. Morphological impact of zinc oxide layers on the device performance in thin-film transistors. *Nanoscale*. **3**, **2011**, 897–899.
- [30] Bubel, S.; Schmechel, R. Mechanical layer compaction for dispersion processed nanoparticulate zinc oxide thin film transistors. *Microelectr Engin.* **96**, **2012**, 36–39.
- [31] Jones, B. A.; Facchetti, A.; Wasielewski, M. R.; Marks, T. J. Tuning Orbital Energetics in Arylene Diimide Semiconductors. Materials Design for Ambient Stability of n-Type Charge Transport. *J. Am. Chem. Soc.* **49**, **2007**, 15259–15278.
- [32] Chen, H. Z.; Ling, M. M.; Mo, X.; Shi, M. M.; Wang, M.; Bao, Z. Air Stable n-Channel Organic Semiconductors for Thin Film Transistors Based on Fluorinated Derivatives of Perylene Diimides. *Chem. Mater.* **4**, **2007**, 816–824.
- [33] Li, Y.; Tan, L.; Wang, Z.; Qian, H.; Shi, Y.; Hu, W. Air-Stable n-Type Semiconductor: Core-Perfluoroalkylated Perylene Bisimides. *Org. Lett.* **4**, **2008**, 529–532.
- [34] Demmig, S.; Langhals, H. Leichtlösliche, lichtechte Perylen-Fluoreszenzfarbstoffe. *Chemi. Ber.* **2**, **1988**, 225–230.
- [35] Greiner, M. T.; Helander, M. G.; Tang, W.-M.; Wang, Z.-B.; Qiu, J.; Lu, Z.-H. Universal energy-level alignment of molecules on metal oxides. *Nat Mater.* **1**, **2012**, 76–81.
- [36] Allen, M. W.; Swartz, C. H.; Myers, T. H.; Veal, T. D.; McConville, C. F.; Durbin, S. M. Bulk transport measurements in ZnO: The effect of surface electron layers. *Phys. Rev. B.* **7**, **2010**, 75211.
- [37] Hsing-Hung, H.; Toshio, K.; Kenji, N.; Hideo, H.; Chung-Chih, W. Modeling of amorphous InGaZnO₄ thin film transistors and their subgap density of states. *Appl. Phys. Lett.* **13**, **2008**, 133503.

Supporting information for:

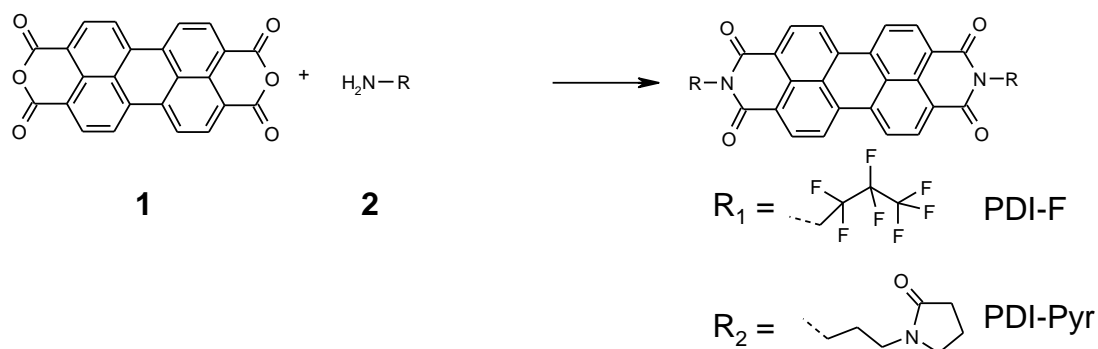
N-Type Perylene to fill Voids in Solution Processed
Nanoparticulate Zinc Oxide Thin Films

Content:

Synthesis of PDI-F and PDI-Pyr

PBI-F thin film characterization

SYNTHESIS OF PDI-F AND PDI-Pyr



Perylene-3,4,9,10-tetracarboxylic dianhydride **1** and Imidazole were purchased from Aldrich. 2,2,3,3,4,4,4-Heptafluorobuthylamine was purchased from Alfa Aesar and N-(3'-Aminopropyl)-2-pyrrolidone from Across Organics. All chemicals were used as received. NMR spectra were recorded on a Bruker AC 250 spectrometer (250 MHz) in a CHCl_3 /trifluoroacetic acid (TFA) mixture as solvent.

General procedure:

A mixture of 15 g imidazole, 1 g (2.5 mmol) Perylene-3,4,9,10-tetracarboxylic dianhydride **1** and 6.4 mmol of the corresponding amine **2** was stirred under argon at 165°C . After 22 h the reaction mixture were cooled to rt, poured into 400 ml of EtOH/2N HCl 1:3 and stirred for 2 h. The dispersion was filtered, the residue washed with water and dried for 12 h at 60°C in vacuum. After soxhlet extraction with toluene and drying in vacuum a red solid is obtained.

N,N'-1H,1H-Perfluorobutyl Perylene Diimide (PDI-F)

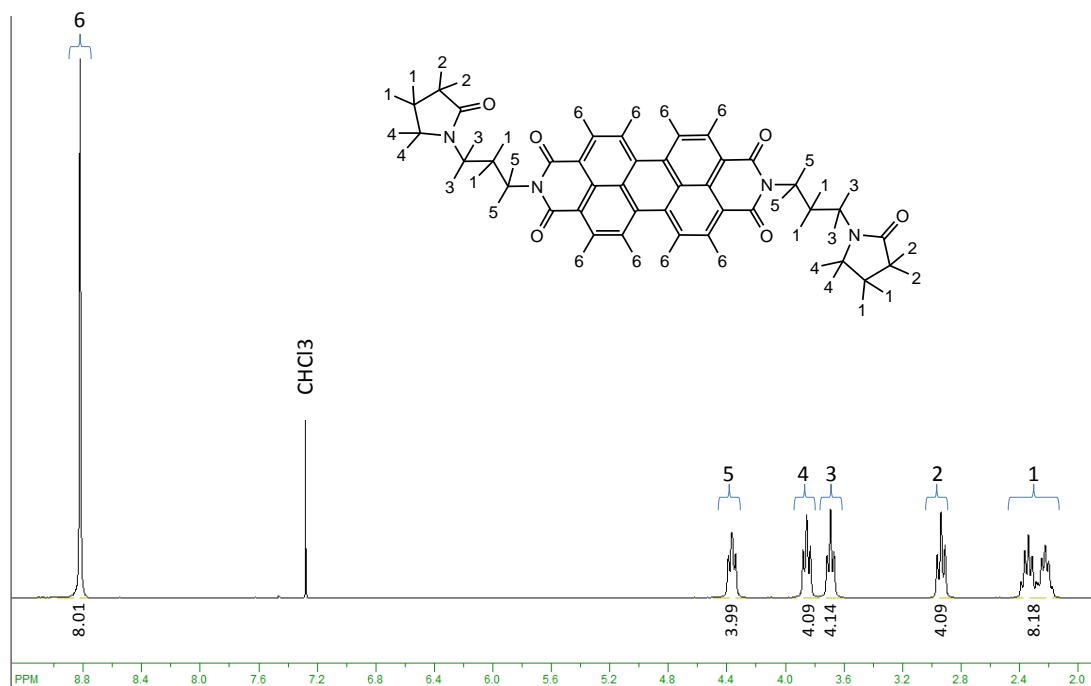
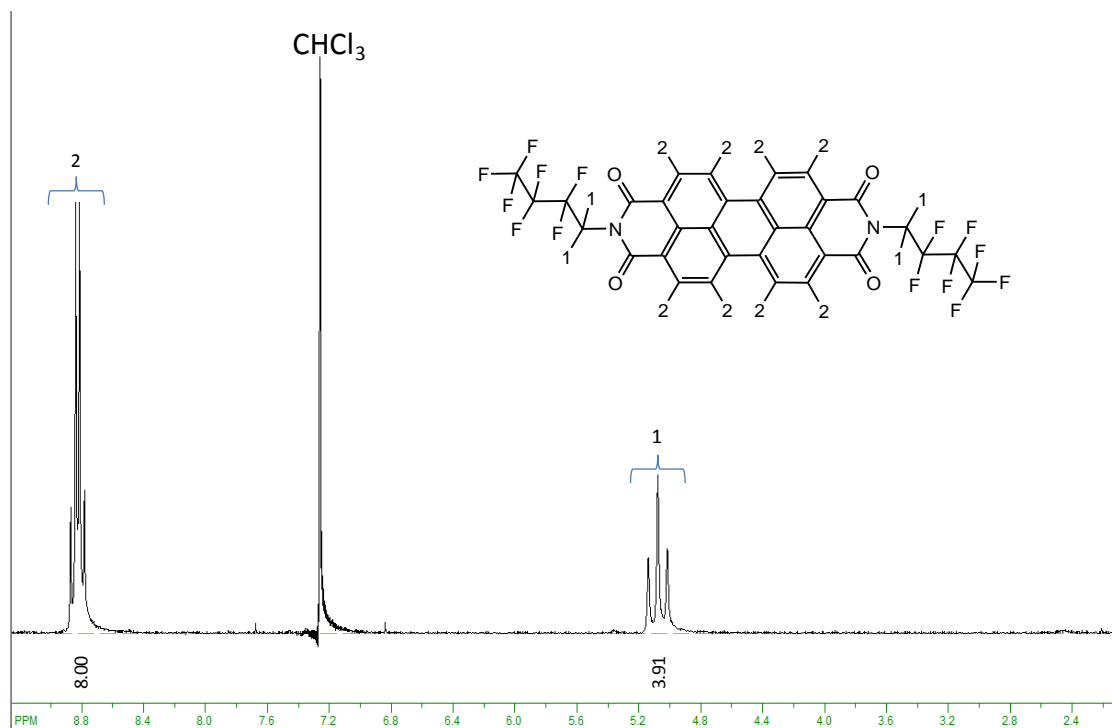
Perylene-3,4,9,10-tetracarboxylic dianhydride (1 g 2.6 mmol) and 2,2,3,3,4,4,4-heptafluorobuthylamine (0.8 ml, 6 mmol) were reacted according to the general procedure. After soxhlet extraction 1.48 g (78%) of a red solid were obtained.

^1H NMR (250 MHz, CDCl_3 /TFA, 298K): δ [ppm]= 5.08 (t, 4H), 8.83 (m, 8H).

N,N'-3-(2,2,2,2-tetrafluoropropyl)perylene diimide (PDI-Pyr)

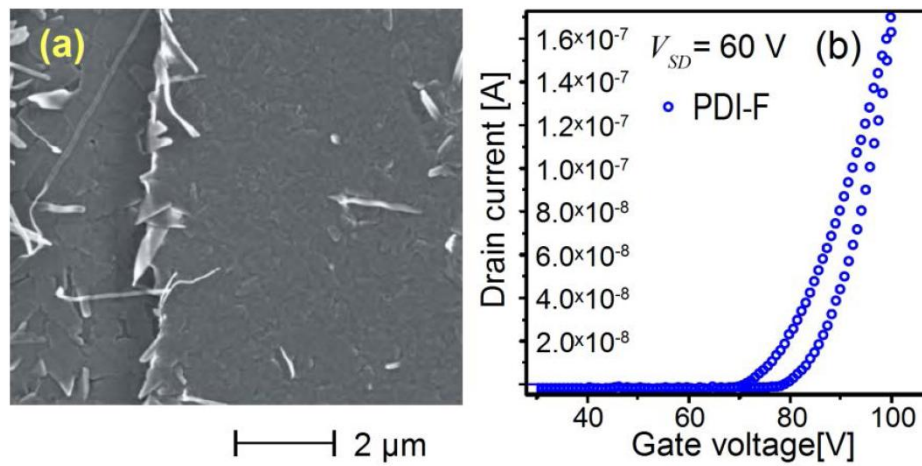
Perylene-3,4,9,10-tetracarboxylic dianhydride (1 g 2.6 mmol) and N-(3'-Aminopropyl)-2-pyrrolidone (0.9 ml, 6.4 mmol) were reacted according to the general procedure. After soxhlet extraction 1.54 g (2.5 mmol; 98 %) of a red solid were obtained.

$^1\text{H NMR}$ (250 MHz, $\text{CDCl}_3 + \text{TFA}$, 298K): $\delta = 2.16 - 2.37$ (m, 8 H), 2.91 (t, 4 H), 3.67 (t, 4 H), 3.83 (t, 4 H), 4.34 (t, 4 H), 8.80 (m, 8 H).



THIN FILM CHARACTERIZATION

The PDI-F film is semiconducting after evaporation.



(a) Scanning electron micrograph of the evaporated PDI-F thin film. The vertical displacement indicates the end of the underlying gold source electrode. (b) TFT transfer characteristic of the thin film, measured in dual sweep mode at $V_{SD} = 60$ V, $\mu_{sat} = 10^{-4}$ cm²/Vs.

N-TYPE SELF-ASSEMBLED MONOLAYER FIELD-EFFECT TRANSISTORS AND COMPLEMENTARY INVERTERS

Andreas Ringk,^{a,b} Xiaoran Li,^{c,d} Fatemeh Gholamrezaie,^{b,e,f} Edsger C. P. Smits,^{c,*}
Alfred Neuhold,^g Armin Moser,^g Cees Van der Marel,^h Gerwin H. Gelinck,^c
Roland Resel,^g Dago M. de Leeuw,^{e,f} Peter Strohriegel^{a,*}

^aMacromolecular Chemistry I, University of Bayreuth, 95440 Bayreuth, Germany

^bDutch Polymer Institute (DPI), P.O. Box 902, 5600 AX Eindhoven, The Netherlands

^cHolst Centre/TNO, High Tech Campus 31, 5656 AE Eindhoven, The Netherlands

^dDepartment of Chemical Engineering and Chemistry, Eindhoven University of Technology P.O. Box 513, 5600 MB Eindhoven, The Netherlands,

^ePhilips Research Laboratories, High Tech Campus 4, 5656 AE Eindhoven, The Netherlands

^fMolecular Electronics, Zernike Institute for Advanced Materials, University of Groningen, Nijenborgh 4, 9747 AG Groningen, The Netherlands

^gInstitute of Solid State Physics, Graz University of Technology, Petersgasse 16, A-8010 Graz, Austria

^hPhilips Innovation Services – Materials Analysis, High Tech Campus 11, 5656 AE Eindhoven, The Netherlands

Published in *Advanced Functional Materials*, **2012**

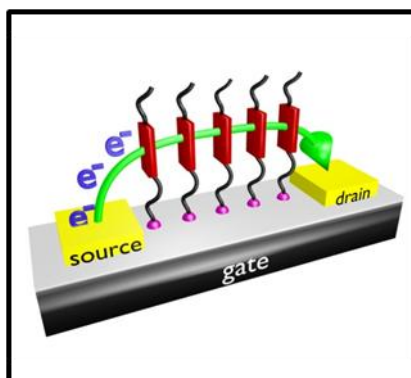
Volume 23, Issue 16, pages 2016–2023

DOI: 10.1002/adfm.201202888

Reprinted with permission; Copyright © 2012 by John Wiley & Sons, Inc.

Table of content: We report highly reproducible n-type self-assembled monolayer field-effect transistors (SAMFETs) based on a perylene derivative. Electron mobilities of $1.5 \times 10^{-3} \text{ cm}^2/\text{Vs}$ and on/off current ratios up to 10^5 were obtained. By implementing n-type and p-type transistors in one device a complimentary inverter based solely on SAMFETs is demonstrated for the first time.

Keywords: self-assembled monolayer, n-type field-effect transistor, perylene bisimide, organic circuits, complementary inverter



Abstract: We report n-type self-assembled monolayer field-effect transistors (SAMFETs) based on a perylene derivative which is covalently fixed to an aluminum oxide dielectric via a phosphonic acid linker. The n-type SAMFETs spontaneously formed by a single layer of active molecules were demonstrated for transistor channel length up to 100 μm . Highly reproducible transistors with electron mobilities of $1.5 \times 10^{-3} \text{ cm}^2/\text{Vs}$ and on/off current ratios up to 10^5 were obtained. By implementing n-type and p-type transistors in one device a complimentary inverter based solely on SAMFETs is demonstrated for the first time.

1. Introduction

Self-assembled monolayers (SAMs) are dense organic layers spontaneously formed on a surface.^[1] The autonomous and selective organization of molecules without human intervention is a promising technology for mass production of organic electronics. Self-assembled monolayer field-effect transistors (SAMFETs) where the organic semiconductor consists of only one monolayer covalently anchored onto the dielectric have been reported.^[2,3] The covalent fixation of the active material to the dielectric allows the fabrication of flexible and transparent devices^[4] with reduced delamination of the semiconductor during bending. The absence of bulk material eliminates bulk currents to give high on/off current ratios. Recent publications have shown that truly two dimensional semiconducting systems are exhibiting confinements effects with new charge transport^[5] and are well suitable for analysing charge transport without interferences from the bulk.^[6,7] A dense packing of the chromophores, full coverage, and strong π - π coupling over long distances are required for reliable devices^[8] and enable a two dimensional charge transport between the source and drain electrodes.

So far the most promising SAMFETs have been demonstrated using a quinquethiophene derivative attached to silicon dioxide.^[9] Hole mobilities up to $10^{-2} \text{ cm}^2/\text{Vs}$ were achieved and the first unipolar integrated circuits as for example a 15-bit code generator based on SAMFETs, were made. State of the art integrated circuits however are mostly based on the well-established complementary metal oxide semiconductor (CMOS) technique, where pairs of p- and n-type transistors are combined in one device. This circuit design results in high noise immunity and low power consumption. To realize complementary organic circuits based on self-assembled

monolayers, suitable n-type materials for the preparation of SAMFETs are required. Compared to p-type materials it is difficult to find n-type transistor materials, because of their high reactivity towards oxygen and moisture.^[10,11] Only recently have stable n-type semiconducting materials been demonstrated with mobilities matching those of p-type semiconductors.^[12,13]

Progress on fabricating n-type SAMFETs has been reported.^[14] A semiconducting fullerene based monolayer (C60C18-PA) on aluminum oxide was shown to exhibit electron mobilities up to 10^{-4} cm²/Vs. A major issue in this work is that the C60C18-PA monolayers tend to form disordered layers with poor electrical properties as a result. A possible suggested solution is to use mixed monolayers. By the combination of C60C18-PA together with a C12 fluorinated phosphonic acid the out of plane order in the SAMs could be improved. The result – a mixed monolayer of both species – will however always be a necessary trade-off between interfacial order and surface coverage.^[15] The lack of reliable n-type SAMFET materials hampers the realization of self-assembled CMOS circuits. High performance and reliable n-type SAMFETs will enable a huge step forward in a bottom-up approach towards robust self-assembled complementary organic circuits.

Here we present reproducible n-type SAMFETs based on heterosubstituted perylene bisimides with mobilities up to 1.5×10^{-3} cm²/Vs. By implementing p- and n-type transistors, complementary inverters based solely on SAMFETs with large noise margin of 7 volts and a gain up to 15 are demonstrated.

2. Results and Discussion

2.1. SAMFET device preparation

The perylene bisimide derivative N-(1-hexylheptyl)-N'-(undecyl-11-phosphonic acid) perylene-3,4,9,10-tetracarboxylic bisimide, (PBI-PA), was synthesized as the n-type active material in our SAMFETs. The molecule belongs to a class of semiconductors well-known for their high performance in n-type organic transistors.^[11] The chemical structure of PBI-PA is shown in **Figure 1**. The active molecule PBI-PA consists of a heterosubstituted perylene bisimide core bearing a branched alkyl tail to increase the solubility on one side, and a linear undecyl alkyl chain with a phosphonic acid anchor group on the other side. The phosphonic acid allows a covalent fixation of PBI-PA to aluminum oxide. Major benefits of phosphonic acid terminated molecules compared to

the chlorosilanes previously reported^[9] are easier handling, storage and device fabrication as they are environmentally stable.

The substrates for the SAMFET preparation consist of a silicon monitor wafer with patterned gold gate electrodes on which a 100 nm thick aluminum oxide layer is deposited by atomic layer deposition (ALD). Gold source and drain electrodes and vertical interconnections are made by conventional photolithography.^[16]

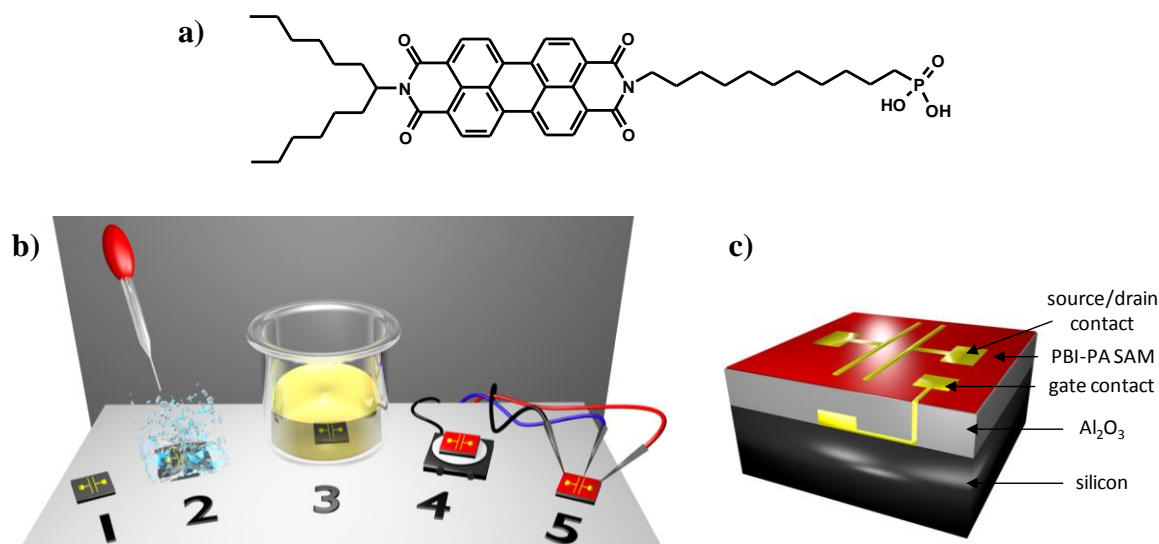


Figure 1: a) Chemical structure of PBI-PA b) Illustration of the n-type SAMFET fabrication process. c) Scheme of SAMFET layout.

To facilitate the anchoring of the phosphonic acid to the dielectric, the substrate was cleaned with acetone and isopropanol and activated by UV-ozone treatment.

A high tendency to form aggregates in solution is well known for perylene bisimides. However, the formation of large aggregates is undesirable for depositing smooth and dense monolayers on surfaces. Spectroscopic investigations revealed that at low concentrations of about 10^{-5} mol l⁻¹, aggregation of perylenes is suppressed.^[17] Therefore bottom-gate/bottom-contact PBI-PA SAMFETs were prepared by immersing the transistor substrate into a dilute solution of PBI-PA in tetrahydrofuran (1.5×10^{-5} mol/l). During the immersion the phosphonic acid reacts in a condensation reaction with the OH-groups on the oxide surface to form a covalent bond.^[18] In comparison to thiols, which form relatively weak bonds to gold, phosphonic acids bind more strongly to aluminium oxide.^[19]

After immersion for 24 hours under ambient atmosphere and room temperature, the devices were dipped into tetrahydrofuran and annealed at 120°C under N₂ atmosphere for 20 minutes. Subsequently the SAMFETs were analyzed and measured.

2.2. Monolayer analysis

To characterize the SAMs, atomic force microscopy (AFM), X-ray photoelectron spectroscopy (XPS), X-ray reflectivity (XRR), and grazing incidence X-ray diffraction (GIXD) investigations were carried out. AFM measurements revealed a smooth and uniform surface, typical for a monolayer (**Figure 2**). The apparent lack of structures confirms the presence of a smooth conformal monolayer similar to other semiconducting monolayers on SiO_2 .^[9] Only a few particles of 100 nm in diameter are present. Presumably they are aggregates of PBI-PA molecules. As they are so sparsely distributed electrical conduction through the aggregates can be ruled out.

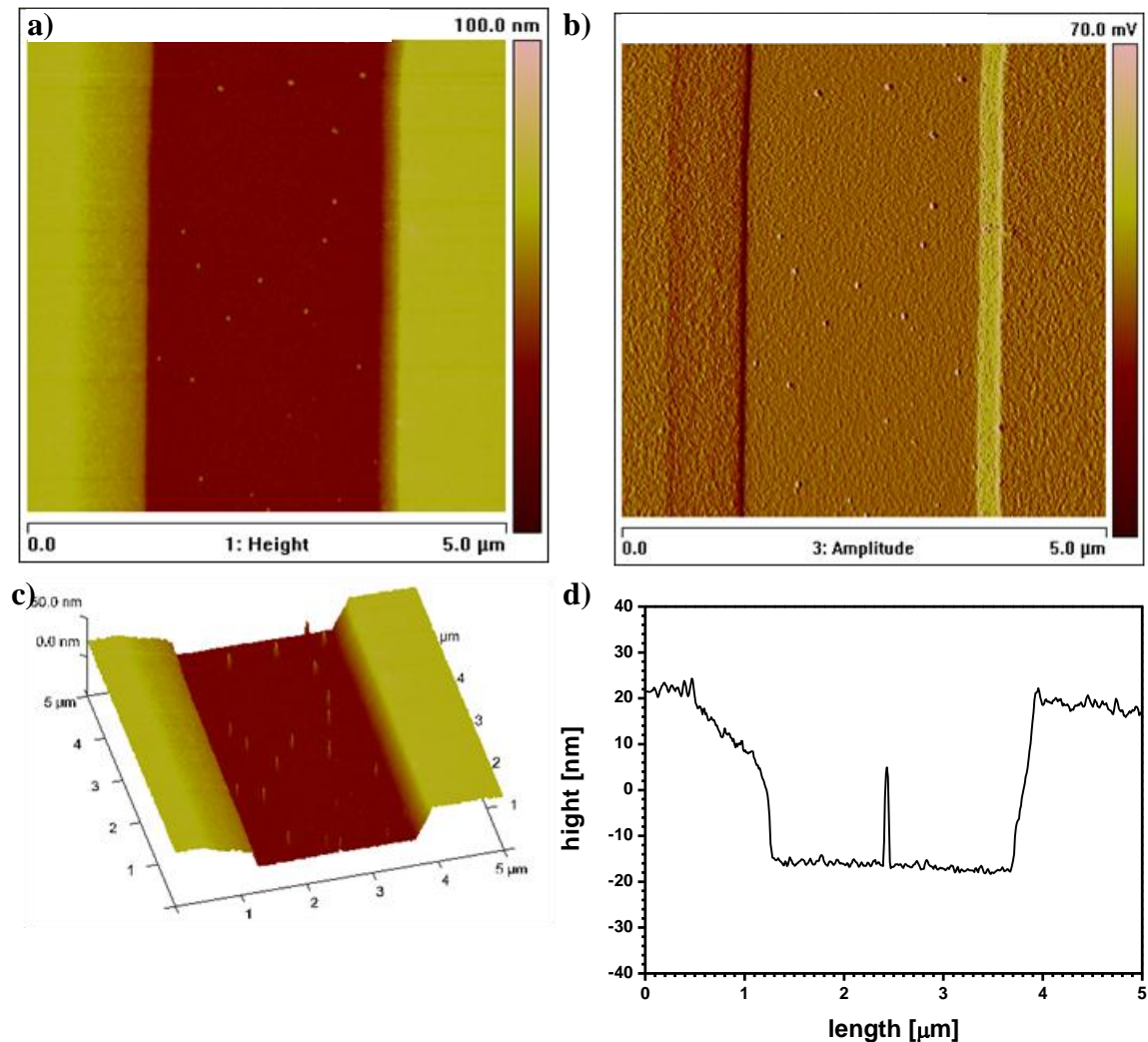


Figure 2: 5 by 5 μm AFM images of a transistor substrate with a PBI-PA monolayer. **a)** Height image of a transistor channel with a PBI-PA monolayer. **b)** Phase amplitude image of the transistor channel. **c)** 3-dimensional illustration of panel a. **d)** Cross section through the transistor channel.

The chemical composition of the same layer was investigated by angle dependent XPS measurements. The results revealed a thin organic layer on the Al_2O_3 surface with an

estimated thickness of $3.1 \text{ nm} \pm 0.2$ which is in line with the calculated molecular length of 2.9 nm . This confirms the proper formation of the monolayer on the surface. To determine the extent of surface coverage by XPS analysis, phosphorus was chosen as a marker because each molecule has only one phosphorus atom and no other source of phosphorus is present in the system. A number of $1.8 \times 10^{14} \pm 0.2 \times 10^{14}$ phosphorus atoms per cm^2 was measured which corresponds to a complete coverage, estimated by the unit cell dimensions of a known perylene bisimide derivative with branched alkyl tails.^[20]

The out of plane order of the pristine PBI-PA SAMs prepared on Al_2O_3 substrates was analyzed by X – ray reflectivity measurements. The experimental data were simulated with a model containing the Al_2O_3 substrate and the monolayer separated into three layers with different thicknesses, r.m.s roughness and densities (**Table 1**). The bottom layer of the SAM is formed by the spacer and anchor groups of the molecule, the middle layer consists of the aromatic cores and the top layer is assembled by the terminal alkyl group of the molecule. Alternatively, a two layer fitting model and a fitting model comprising the SAM as a single layer with constant density were performed (not shown). However, the three layer model presented here gives the physically most realistic description of the measured XRR data. **Figure 3** illustrates the different separated parts of the SAM used in the fitting model and the experimental XRR data (black line) with the associated fit (red line). The thicknesses of the end group layer, the aromatic core layer and the spacer with anchor group layer are found to be 0.71 nm , 0.98 nm and 1.32 nm , respectively. The numbers are in good agreement with the estimated lengths of the individual molecular units which were found to be 0.63 nm , 1.13 nm and 1.17 nm by molecular modeling. The numerical fit reveals that the density of the middle layer is considerably enhanced in comparison with the other two layers, which supports the presence of aromatic carbon, nitrogen and oxygen. In the XRR simulation the anchor group was coupled with the spacer group and due to the presence of phosphorus and oxygen the density is increased, compared to the density of the top alkyl group. Next to the molecular parameters, the XRR graph additionally comprises the substrate information. The rapid oscillations in the graph originate from the 165 nm thick Al_2O_3 layer (Table 1), of the plain Al_2O_3 substrates, which is emphasized in the insert of Figure 3.

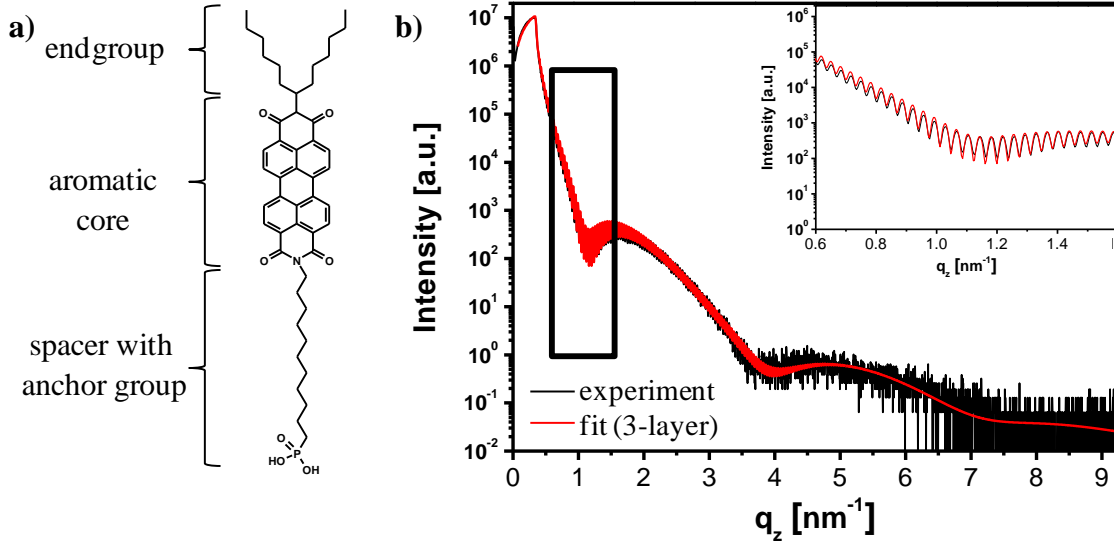


Figure 3: X-ray reflectivity (XRR) investigation of PBI-PA monolayers. **a)** The sketch shows the three separated molecule parts, which were used for the XRR simulation. **b)** The graph illustrates the XRR of the PBI-PA monolayer on aluminum oxide. The red solid line gives the simulation to the experimental data (black line). The insert of the graph illustrates the thickness oscillations of the Al₂O₃ substrate around the first minimum.

Table 1: Layer thickness d , r.m.s. roughness σ , mass density ρ_m and electron density ρ_{el} of the individual parts of the investigated PBI-PA SAM on the Al₂O₃ substrate extracted from the XRR data shown in Figure 3.

layer	d [nm]	σ [nm]	ρ_m [g/cm ³]	ρ_{el} [nm ⁻³]
alkyl groups	0.71±0.05	0.28±0.05	0.48±0.07	157±5
aromatic core	0.98±0.06	0.45±0.05	1.23±0.02	391±6
spacer with anchor group	1.32±0.10	0.12±0.03	0.81±0.03	259±4
Al ₂ O ₃ substrate	165.23±4.31	0.85±0.08	2.89±0.10	862±6

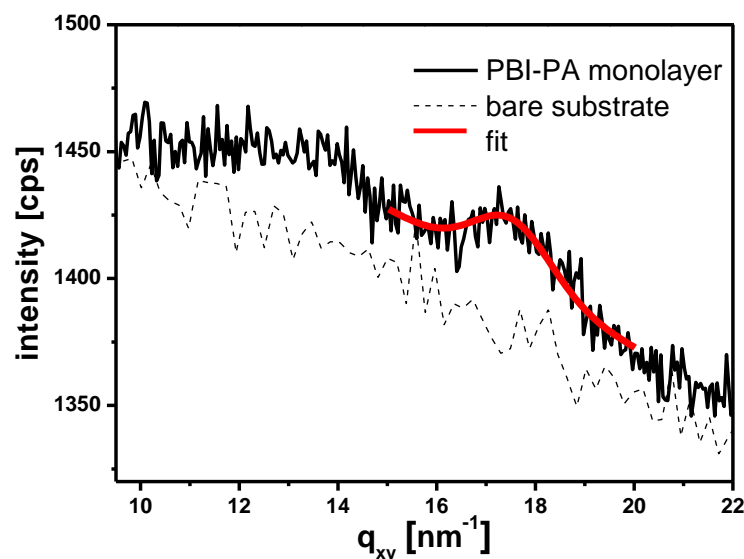


Figure 4: Grazing incidence X-ray diffraction (GIXD) of a PBI-PA monolayer together with the scattering signal of the bare aluminum oxide substrate. The intensity was measured with a one-dimensional detector and integrated in the q_z range between 0 nm^{-1} and 3 nm^{-1} . A Gaussian fitting curve to the peak at 17.5 nm^{-1} is plotted in red color.

The XPS, AFM and XRR measurements show that PBI-PA forms a densely packed monolayer. To investigate the in-plane order we performed grazing incidence X-ray diffraction measurements. Due to the absence of periodicity perpendicular to the SAM layer, any long-range in-plane order is manifested as Bragg rods. A typical example is chloro[11-(5''-ethyl-2,2':5',2'':5'',2''':5''',2''''-quinquethien-5-yl)undecyl]dimethylsilane self-assembled on SiO_2 .^[9] The diffracted intensity as a function of in-plane scattering vector, q_{xy} , is presented in **Figure 4**. Bragg rods are not found. Only a broad diffraction peak (q_{xy}) at 17.5 nm^{-1} corresponding to an intermolecular distance of 0.36 nm is observed. From the width of the diffraction peak (Δq_{xy}) of 2 nm^{-1} , the correlation length, or crystal size, was estimated to be 3.1 nm . The extracted length corresponds to only 9 repeated conjugated units. The PBI-PA SAM forms a nano-crystalline layer. We note that the weak crystallinity can be inferred from X-ray diffraction studies on bulk branched perylene derivatives.^[20-22] The packing of alkyl terminated PBI-PA based molecules is dominated by the interaction between the conjugated PBI-PA cores. The π - π stacking of the aromatic cores leads to parallel stacks with a typical distance of 0.36 nm .^[23-25], where the aromatic chains are arranged perpendicular to the substrate surface. However, the stacks arrange themselves in twisted columns without long range order. The

nano-crystallinity along the columns is confirmed by XRD measurement on bulk PBI-PA material, which also shows a very broad diffraction peak at the same distance (Supporting Figure S2). The interplay between steric repulsion of branched alkyl tails, π - π packing effects, and self-assembly of the phosphonic acid groups ultimately results in nano-crystalline self-assembled monolayers of PBI-PA.^[24]

2.3 Electrical characterization

The output and transfer characteristics of an n-type PBI-PA SAMFET with a channel length of 40 μm and a channel width of 1000 μm are shown in **Figure 5a** and **5b**.

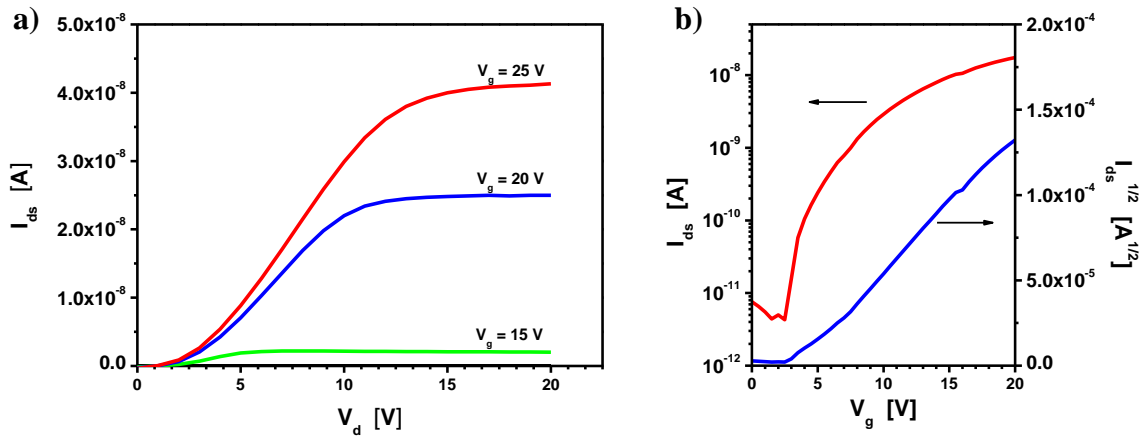


Figure 5. Transistor measurements of PBI-PA SAMFETs. **a)** Output characteristics of a SAMFET having a channel length of 40 μm and a channel width of 1000 μm . The drain voltage is swept from 0 V to 20 V, the gate voltage is varied starting from 0 V to 25 V in 5 V per step. **b)** Transfer characteristics of the same device in the saturation regime with a drain voltage of 20 V.

The saturation mobility of the transistor is $1.5 \times 10^{-3} \text{ cm}^2 \text{ V}^{-1} \text{ s}^{-1}$, with an on/off-current ratio on the order of 10^4 and a threshold voltage close to zero. We note that properly functioning device characteristics were obtained for short as well as long channel length devices up to 100 μm , for the first time.^[14,15] Field-effect behaviour was obtained for all measured transistors, i.e. device yield of 100%, which is indicative of a high reproducibility over large areas. The transistors were contact limited as confirmed by the nonlinear ‘s’ shaped behaviour at the low drain bias in the output characteristics (Figure 5a). We have used Au source and drain electrodes with a work function of $\sim 5 \text{ eV}$. The LUMO of the PBI-PA is estimated at around 3.8 eV.^[26] Despite the injection barrier of more than 1 eV, electrons can still be injected. Comparable contact limited injection has been reported for thin-film transistors of semiconducting PBI derivatives.^[27]

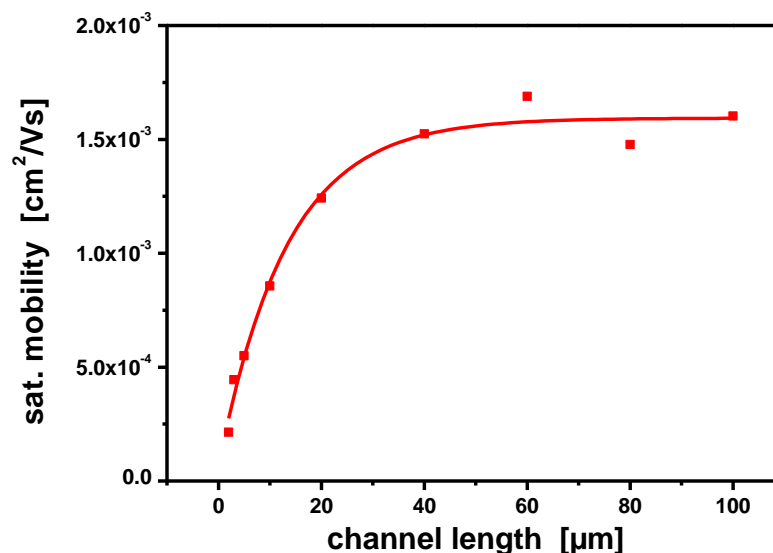


Figure 6. Scaling of mobility. The saturation mobility of PBI-PA SAMFETs as a function of channel length (ranging from 2 to 100 μm). For channel lengths smaller than 40 μm the mobility is dominated by the contact resistance. For larger channels the mobility becomes independent of the channel length. The red line is a guide for the eye.

The saturation mobility as a function of channel length is presented in **Figure 6**. In short channel transistors the transport is limited by the contact resistance which lowers the mobility.^[28] For long channels the mobility is constant up to a channel length of 100 μm . The constant mobility is remarkable. Traditionally, as reported previously for p-type SAMFETs,^[8] the mobility of self-assembled monolayer field-effect transistors decreases dramatically with increasing channel length. This dependence is a direct consequence of incomplete coverage. Here the mobility remains constant for channel lengths up to 100 μm , which is a fingerprint of complete coverage with long-range connectivity within the SAM. The constant mobility for long channel length, as shown in Figure 6, reflects the homogeneous long-range charge transport through a densely packed monolayer without conduction barriers from e.g. grain boundaries or from incomplete coverage. The channel-length dependence of the carrier mobility, XPS investigations, XRR, and XRD data confirm that a fully covered and conductive self-assembled monolayer of PBI-PA was formed on the aluminum oxide surface.

A crucial step towards realizing robust and low power circuits is the use of complementary logic. For SAMFET based complementary circuits reliable n-type as well as p-type SAMFETs are essential. For this purpose p-type and n-type SAMFETs were fabricated on two substrates and connected in a complementary inverter configuration. The p-type transistors were fabricated as described previously,^[9] and consist of a quinquethiophene derivative grafted to a silicon dioxide dielectric via a

dimethylchlorosilane anchor group. As the n-type material PBI-PA anchored to an aluminum oxide dielectric via a phosphonic acid group was taken. Due to the difference in mobility, the currents from both transistors were matched by adjusting the channel length. For the p-type SAMFET a channel length of 40 μm was chosen and a 2 μm channel length was taken for the n-type SAMFET. Both transistors had a channel width of 1000 μm . Prior electrical measurements confirmed that both SAMFETs showed a proper conductivity typical for dense organic monolayers on top of oxides. The resulting inverter characteristics are shown in **Figure 7**. When the supply voltage (V_{dd}) was set at 30 V and the input voltage (V_{in}) was swept from 30 V to 0 V with a typical scan speed of 1 V s^{-1} (red curve in Figure 7a), a high gain value of ~ 15 with the “trip-point” at around 23 V of V_{in} was obtained. Here, gain is defined as $dV_{\text{out}}/dV_{\text{in}}$. The so-called ‘maximal equal criterion’ noise margin^[29] of 7 volts (for $V_{\text{dd}} = 30$ V) was substantially larger than values reported for PMOS inverters used in complex circuitry,^[29,30] also higher than the previous unipolar p-type SAMFET inverters (Supporting Figure S10a), and on par with conventional organic CMOS.^[29]

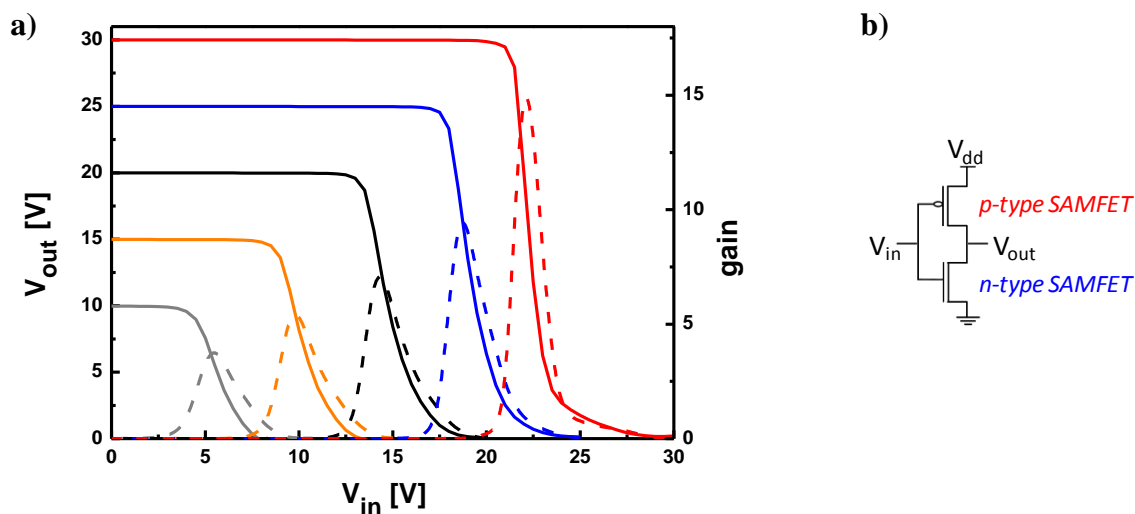


Figure 7. SAMFET based complementary inverter. a) Device characteristics: The supply voltage (V_{dd}) was varied starting from 10 V to 30 V in 5 V per step. The dashed lines present the gains. b) Diagram of the SAMFET CMOS inverter.

3. Conclusion

In summary, we present n-type SAMFETs based on a perylene derivative with a phosphonic acid anchor group which enables an efficient fixation to aluminum oxide. Simple device fabrication under ambient conditions leads to a complete surface coverage of the monolayer and to transistors with electron mobilities up to $10^{-3} \text{ cm}^2 \text{ V}^{-1} \text{ s}^{-1}$ for channel length as long as 100 μm . By implementing p- and n-type SAMFETs in one circuit, a complementary inverter based solely on SAMFETs with a large noise margin

and a high gain is demonstrated for the first time, paving the way to robust and low power self-assembled monolayer based complementary circuits.

4. Experimental Section

Further informations on molecular modeling, atomic force microscopy (AFM), X-ray diffraction studies, transistor substrate manufacture, and electrical characterization are given in the supporting informations available from the Wiley Online Library or from the authors.

Synthesis of PBI-PA 6 N-(1-hexylheptyl)-N'-(undecyl-11-phosphonic acid) perylene-3,4,9,10-tetracarboxylic bisimide.

Materials and methods: The starting materials perylene-3,4,9,10-tetracarboxylic-3,4,9,10-dianhydrid, potassium hydroxide, ammonia, 1,11-dibromoundecane, sodium hydride, triethyl phosphite, bromotrimethylsilane, and solvents were purchased from Aldrich, Acros Organics and VWR. Solvents used for precipitation and column chromatography were distilled once before use. ^1H - and ^{13}C -NMR spectra were recorded on a Bruker AC 250 spectrometer (250 MHz). Chemical shifts are reported in ppm at room temperature using CDCl_3 as solvent and internal standard. Mass spectroscopic data were obtained from a FINNIGAN MAT 8500 instrument.

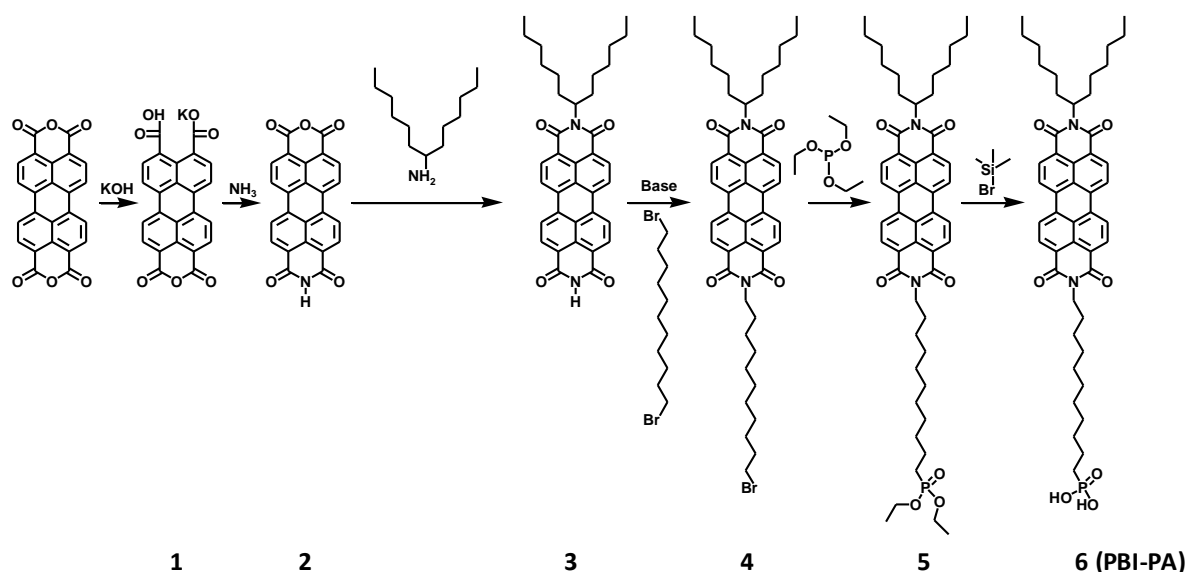


Figure 8. Overview of the synthetic strategy towards the target molecule PBI-PA. Compounds 1-3 were synthesized according to literature procedure.^[31]

Synthesis of N-(1-hexylheptyl)-N'-(undecylbromide) perylene-3,4,9,10-tetracarboxylic bisimide 4.

Perylenebisimide 3 (530 mg, 0.93 mmol) and sodium hydride (46 mg, 65% dispersed in mineral oil, 1.24 mmol) were dissolved in 45 ml dry DMF and stirred at room temperature. After 24 h the solution was heated to 90°C and 1,11-dibromoundecane (5 g, 15.9 mmol) were added. After 60 h the reaction mixture was poured into water and extracted with CHCl₃. The solvent was evaporated, the crude product redissolved in CHCl₃ and poured into hexane. The precipitate was filtered off and purified by flash chromatography (solvent gradient hexane→CHCl₃). The resulting red solid was freeze dried with dioxane to yield 365 mg (0.453 mmol, 49%) of bromide 4.

TLC (CHCl₃): R_f = 0.65

EIMS(m/z): [M]⁺ calculated for C₄₈H₅₇BrN₂O₄, 805.90; found, 806

¹H-NMR (300 MHz, CDCl₃, δ): 0.82 (t, *J* = 6.9 Hz, 6H; CH₃), 1.20 – 1.45 (m, 30H; CH₂), 1.70 – 1.80 (m, 2H; CH₂), 1.80 – 1.93 (m, 4H; CH₂), 2.18 – 2.32 (m, 2H; CH₂), 3.36 – 3.44 (t, *J* = 3.7 Hz, 2H; CH₂), 4.18 (t, *J* = 7.6 Hz, 2H; CH₂), 5.13 – 5.24 (m, 1H; CH), 8.58 – 8.78 (m, 8H; Ar-H).

¹³C-NMR (75 MHz, CDCl₃, δ): 14.38, 22.93, 27.31, 27.48, 28.54, 29.10, 29.58, 29.67, 29.74, 29.80, 29.81, 30.05, 32.12, 32.76 (alkyl C), 33.22 (C-Br), 34.33 (alkyl C), 41.03, 55.18 (N-C), 123.29, 123.39, 123.60, 126.69, 126.80, 129.70, 129.89, 131.68, 134.97, 163.67 (aromatic C).

Synthesis of N-(1-hexylheptyl)-N'-(undecylphosphonic acid diethylester) perylene-3,4,9,10-tetracarboxylic bisimide 5.

Perylenebisimide 4 (759 mg, 0.942 mmol) was dissolved in 200 ml triethyl phosphite and heated to 150°C for 24 h. The excess of triethyl phosphite was removed by vacuum distillation and the remaining solid purified by flash chromatography (THF/Hexane 1:1) to yield 800 mg (0.927 mmol, 98%) of 5 as red solid.

TLC (THF : Hexane / 1:1): R_f = 0.5

EIMS(m/z): [M]⁺ calculated for C₅₂H₆₇N₂O₇P, 863.10; found, 863

¹H-NMR (300 MHz, CDCl₃, δ): 0.83 (t, *J* = 6.7 Hz, 6H; CH₃), 1.20 – 1.40 (m, 38H; CH₂), 1.51 – 1.60 (m, 2H; CH₂), 1.73 – 1.78 (m, 2H; CH₂), 1.80 – 1.94 (m, 2H; CH₂), 2.18 –

2.33 (m, 2H; CH₂), 4.03 – 4.12 (m, 4H; CH₂), 4.14 – 4.21 (m, 2H), 5.12 – 5.24 (m, 1H; CH), 8.43 – 8.73 (m, 8H; Ar-H).

¹³C-NMR (75 MHz, CDCl₃, δ): 14.20, 22.51, 22.51, 22.58, 22.73, 24.88, 26.74, 27.08, 27.28, 28.24, 29.22, 29.37, 29.50, 29.66, 30.66, 30.89, 31.90, 32.50 (alkyl C), 54.94 (C-N), 61.54 (C-P), 123.08, 123.17, 123.29, 126.39, 126.49, 129.41, 129.63, 131.44, 134.69, 163.44 (aromatic C).

³¹P-NMR (120 MHz, CDCl₃, δ): 32.60.

Synthesis of N-(1-hexylheptyl)-N'-(undecylphosphonic acid) perylene-3,4,9,10-tetracarboxylic bisimide 6 (PBI-PA).

Perylenebisimide 5 (400 mg, 0.46 mmol) was dissolved under argon in 40 ml dry CH₂Cl₂, cooled to 0°C and bromotrimethylsilane (1 ml, 7.58 mmol) was added dropwise through a syringe. After addition of the silane, the reaction mixture was allowed to warm up to room temperature. After 48 h stirring, 5 ml water was added. After additional 2 h, the mixture was poured into 50 ml of a mixture of methanol and water (1:1). The resulting precipitate was collected by filtration and freeze dried from dioxane to obtain 352 mg (0.44 mmol, 95%) of the phosphonic acid 6 which was used without further purification.

¹H-NMR (300 MHz, CDCl₃, δ): 0.79 – 0.87 (t, *J* = 6.6 Hz, 6H; CH₃), 1.19 – 1.49 (m, 34H; CH₂), 1.57 – 1.65 (2H, m; CH₂), 1.70 -1.75 (m, 2H; CH₂), 1.87 – 1.93 (m, 2H; CH₂), 4.08 – 4.16 (t, *J* = 6.4 Hz, 2H; CH₂), 5.09 – 5.20 (m, 1H; CH₁), 8.24 – 8.53 (m, 8H; Ar-H).

Acknowledgements

The work of Andreas Ringk and Fatemeh Gholamrezaie forms part of the research programme of the Dutch Polymer Institute (DPI), project 624 and 627. We are grateful to Bas van der Putten (Holst Centre) for technical assistance, to Ingo Salzmann (Humboldt University Berlin) for help with the X-ray measurements and the Austrian Science Foundation FWF:[P21094].

Supporting Information is available online from Wiley InterScience or from the author.

References

- [1] Whitesides, G. M. Self-Assembly at All Scales. *Science* **2002**, *295*, 2418.
- [2] Tulevski, G. S.; Miao, Q.; Fukuto, M.; Abram, R.; Ocko, B.; Pindak, R.; Steigerwald, M. L.; Kagan, C. R.; Nuckolls, C. Attaching Organic Semiconductors to Gate Oxides: In Situ Assembly of Monolayer Field Effect Transistors. *J. Am. Chem. Soc.* *126*, **2004**, 15048.
- [3] Hutchins, D. O.; Acton, O.; Weidner, T.; Cernetic, N.; Baio, J. E.; Ting, G.; Castner, D. G.; Ma, H.; Jen, A. K.-Y. Spin cast self-assembled monolayer field effect transistors. *Org. Electron.* *13*, **2012**, 464.
- [4] Gholamrezaie, F.; Mathijssen, S. G. J.; Smits, E. C. P.; Geuns, T. C. T.; van Hal, P. A.; Ponomarenko, S. A.; Flesch, H. G.; Resel, R.; Cantatore, E.; Blom, P. W. M.; de Leeuw, D. M. Ordered Semiconducting Self-Assembled Monolayers on Polymeric Surfaces Utilized in Organic Integrated Circuits. *Nano Lett.* *10*, **2010**, 1998.
- [5] Brondijk, J. J.; Roelofs, W. S. C.; Mathijssen, S. G. J.; Shehu, A.; Cramer, T.; Biscarini, F.; Blom, P. W. M.; de Leeuw, D. M. Two-Dimensional Charge Transport in Disordered Organic Semiconductors. *Phys. Rev. Lett.* *109*, **2012**, 056601.
- [6] Roelofs, W. S. C.; Mathijssen, S. G. J.; Janssen, R. A. J.; de Leeuw, D. M.; Kemerink, M. Accurate description of charge transport in organic field effect transistors using an experimentally extracted density of states. *Physical Review B.* *8*, **2012**, 85202.
- [7] Gholamrezaie, F.; Kirkus, M.; Mathijssen, S. G. J.; Leeuw, D. M. de; Meskers, S. C. J. Photophysics of Self-Assembled Monolayers of a π -Conjugated Quinque thiophene Derivative. *J. Phys. Chem. A.* *29*, **2012**, 7645–7650.
- [8] Mathijssen, S. G. J.; Smits, E. C. P.; van Hal, P. A.; Wondergem, H. J.; Ponomarenko, S. A.; Moser, A.; Resel, R.; Bobbert, P. A.; Kemerink, M.; Janssen, R. A. J.; de Leeuw, D. M. Monolayer coverage and channel length set the mobility in self-assembled monolayer field-effect transistors. *Nature Nanotech.* *4*, **2009**, 674.
- [9] Smits, E. C. P.; Mathijssen, S. G. J.; van Hal, P. A.; Setayesh, S.; Geuns, T. C. T.; Mutsaers, K. A. H. A.; Cantatore, E.; Wondergem, H. J.; Werzer, O.; Resel, R.; Kemerink, M.; Kirchmeyer, S.; Muzafarov, A. M.; Ponomarenko, S. A.; de Boer, B.; Blom, P. W. M.; de Leeuw, D. M. Bottom-up organic integrated circuits. *Nature* *455*, **2008**, 956.
- [10] de Leeuw, D. M.; Simenon, M. M. J.; Brown, A. R.; Einerhand, R. E. F. Stability of n-type doped conducting polymers and consequences for polymeric microelectronic devices. *Synt. Met.* *87*, **1997**, 53.
- [11] Jones, B. A.; Facchetti, A.; Wasielewski, M. R.; Marks, T. J. Tuning Orbital Energetics in Arylene Diimide Semiconductors. Materials Design for Ambient Stability of n-Type charge Transport. *J. Am. Chem. Soc.* *129*, **2007**, 15259.

- [12] Yan, H.; Chen, Z.; Zheng, Y.; Newman, C.; Quinn, J. R.; Dötz, F.; Kastler, M.; Facchetti, A. A high-mobility electron-transporting polymer for printed transistors. *Nature* *457*, **2009**, 679.
- [13] Soeda, J.; Uemura, T.; Mizuno, Y.; Nakao, A.; Nakazawa, Y.; Facchetti, A.; Takeya, J. High Electron Mobility in Air for N,N'-1H,1H-Perfluorobutyldicyanoperylene Carboxydi-imide Solution-Crystallized Thin-Film Transistors on Hydrophobic Surfaces. *Adv. Mater.* *23*, **2011**, 3681.
- [14] Novak, M.; Ebel, A.; Meyer-Friedrichsen, T.; Jedaa, A.; Vieweg, B. F.; Yang, G.; Voitchovsky, K.; Stellacci, F.; Spiecker, E.; Hirsch, A.; Halik, M. Low-Voltage p- and n-Type Organic Self-Assembled Monolayer Field Effect Transistors. *Nano Lett.* *11*, **2011**, 156.
- [15] Rumpel, A.; Novak, M.; Walter, J.; Braunschweig, B.; Halik, M.; Peukert, W. Tuning the Molecular Order of C60 Functionalized Phosphonic Acid Monolayers. *Langmuir* *27*, **2011**, 15016.
- [16] Tripathi, A. K.; Smits, E. C. P.; van der Putten, J. B. P. H.; van Neer, M.; Myny, K.; Nag, M.; Steudel, S.; Vicca, P.; O'Neill, K.; van Veenendaal, E.; Genoe, J.; Heremans, P.; Gelinck, G. H. Low-voltage gallium-indium-zinc-oxide thin film transistors based logic circuits on thin plastic foil: Building blocks for radio frequency identification application. *Appl. Phys. Lett.* *98*, **2011**, 162102.
- [17] Chen, Z.; Stepanenko, V.; Dehm, V.; Prins, P.; Siebbeles, L. D. A.; Seibt, J.; Marquetand, P.; Engel, V.; Würthner, F. Photoluminescence and Conductivity of Self-Assembled π - π Stacks of Perylene Bisimide Dyes. *Chem. Eur. J.* *13*, **2007**, 436.
- [18] Thissen, P.; Valtiner, M.; Grundmeier, G. Stability of Phosphonic Acid Self-Assembled Monolayers on Amorphous and Single-Crystalline Aluminum Oxide Surfaces in Aqueous Solution. *Langmuir* *26*, **2010**, 156.
- [19] Levine, I.; Weber, S. M.; Feldman, Y.; Bendikov, T.; Cohen, H.; Cahen, D.; Vilan, A. Molecular Length, Monolayer Density, and Charge Transport: Lessons from Al-AlOx/Alkyl-Phosphonate/Hg Junctions. *Langmuir* *28*, **2012**, 404.
- [20] Marcon, V.; Breiby, D. W.; Pisula, W.; Dahl, J.; Kirkpatrick, J.; Patwardhan, S.; Grozema, F.; Andrienko, D. Understanding Structure-Mobility Relations for Perylene Tetracarboxydiimide Derivatives. *J. Am. Chem. Soc.* *131*, **2009**, 11426.
- [21] Nolde, F.; Pisula, W.; Müller, S.; Kohl, C.; Müllen, K. Synthesis and Self-Organization of Core-Extended Perylene Tetracarboxdiimides with Branched Alkyl Substituents. *Chem. Mater.* *18*, **2006**, 3715.
- [22] Kohn, P.; Ghazaryan, L.; Gupta, G.; Sommer, M.; Wicklein, A.; Thelakkat, M.; Thurn-Albrecht, T. Thermotropic Behavior, Packing, and Thin Film Structure of an Electron Accepting Side-Chain Polymer. *Macromolecules* *45*, **2012**, 5676-5683.
- [23] Klebe, G.; Graser, F.; Hadicke, E.; Berndt, J. Crystallochromy as a solid-state effect: correlation of molecular conformation, crystal packing and colour in perylene-3,4:9,10-bis(dicarboximide) pigments. *Acta Cryst.* *B45*, **1989**, 69.

- [24] Hansen, M. R.; Graf, R.; Sekharan, S.; Sebastiani, D. Columnar Packing Motifs of Functionalized Perylene Derivatives: Local Molecular Order Despite Long-Range Disorder. *J. Am. Chem. Soc.* *131*, **2009**, 5251.
- [25] Guillermet, O.; Mossoyan-Déneux, M.; Giorgi, M.; Glachant, A.; Mossoyan, J. C. Structural study of vapour phase deposited 3,4,9,10-perylene tetracarboxylic acid diimide: Comparison between single crystal and ultra thin films grown on Pt(100). *Thin Solid Films* *514*, **2006**, 25.
- [26] Wicklein, A.; Lang, A.; Muth, M.; Thelakkat, M. Swallow-Tail Substituted Liquid Crystalline Perylene Bisimides: Synthesis and Thermotropic Properties. *J. Am. Chem. Soc.* *131*, **2009**, 14442.
- [27] Fabiano, S.; Wang, H.; Piliego, C.; Jaye, C.; Fischer, D.A.; Chen, Z.; Pignataro, B.; Facchetti, A.; Loo, Y. L.; Loi, M. A. Organic Transistors: Supramolecular Order of Solution-Processed Perylenediimide Thin Films: High-Performance Small-Channel n-Type Organic Transistors. *Adv. Funct. Mater.* *21*, **2011**, 4478.
- [28] Meijer, E. J.; Gelinck, G. H.; van Veenendaal, E.; Huisman, B. H.; de Leeuw, D. M.; Klapwijk, T. M. Scaling behavior and parasitic series resistance in disordered organic field-effect transistors. *Appl. Phys. Lett.* *82*, **2003**, 4576.
- [29] Gelinck, G. H.; Heremans, P.; Nomoto, K.; Anthopoulos, T. D. Organic Transistors in Optical Displays and Microelectronic Applications. *Adv. Mater.* *22*, **2010**, 3778.
- [30] Spijkman, M.; Smits, E. C. P.; Blom, P. W. M.; de Leeuw, D. M., Bon Saint Come, Y.; Setayesh, S.; Cantatore, E. Increasing the noise margin in organic circuits using dual gate field-effect transistors. *Appl Phys. Lett.* *92*, **2008**, 143304.
- [31] Wicklein, A.; Lang, A.; Muth, M.; Thelakkat, M. Swallow-Tail Substituted Liquid Crystalline Perylene Bisimides: Synthesis and Thermotropic Properties. *J. Am. Chem. Soc.* *131*, **2009**, 14442.

Supporting information for:

N-Type Self-Assembled Monolayer Field-Effect Transistors and Complementary Inverters

Content:

Molecular modelling

XPS measurements

X-ray diffraction studies

Transistor substrates

Electrical characterizations

SAMFET-CMOS measurement

References

MOLECULAR MODELLING

The length of the PBI-PA molecule was calculated using Avogadro 1.0.3 software with the united force-field (UFF). The molecule can be classified into three different segments: the end capping alkyl tail (0.63 nm), the aromatic core (1.13 nm) and an aliphatic spacer (1.17 nm) (**Figure S1**). All three layers and the calculated molecular length of 2.93 nm matches well with the lengths obtained from the XPS and X-ray reflectivity measurements.

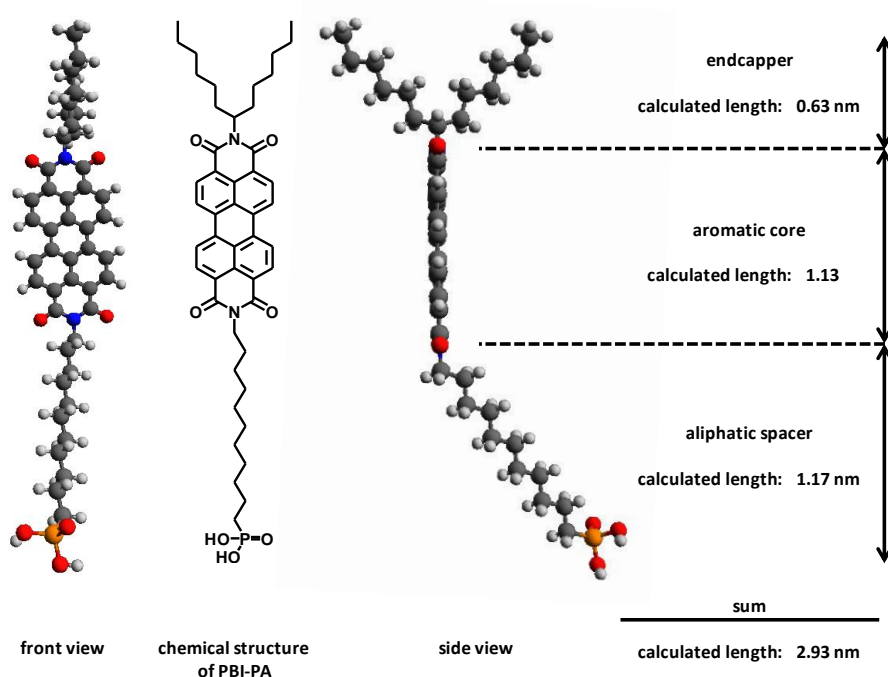


Figure S1. Illustration of the calculated intramolecular distances of PBI-PA.

XPS MEASUREMENTS

Experimental details

The measurements have been carried out in a Quantera SXMtm from Ulvac-PHI. The measurements have been performed using monochromatic AlK α -radiation and a rectangular measurement spot of approximately 500 x 250 μm . By means of wide-scan measurements the elements present at the surface have been identified. The chemical state and the apparent atomic concentrations of the detected elements are determined from accurate narrow-scan measurements. Standard PHI sensitivity factors^[1,2] were used to convert peak areas to apparent concentrations. As a result of this, it is possible that the

concentrations deviate from reality in the absolute sense (generally not more than 20% relative).

Results and discussion

XPS measurements were performed on the PBI-PA SAMFETs to verify the presence of a monolayer reasonable for the electrical characteristics. First, measurements were done at two positions using a take-off angle Θ of 45° ; at this measurement angle the information depth is approximately 7 nm. The elements that are present at the surface according to survey scans and the apparent concentrations obtained from narrow-scan measurements are summarised in **Table S1**. In this table is also shown which XPS line was measured, the peak position and the most likely chemical assignment.

Table S1. Apparent atomic concentrations (at%) measured at the surface ($\Theta = 45^\circ$). Peak positions in eV are given in the second row. The most likely chemical assignment is given in the third row.

Position	Al 2p	C 1s				F 1s	N 1s	O 1s	P 2s	Si 2p
	74.7	284.8	286.5	288.0	289.0	685.8	400.1		191.4	102.6
	Al ₂ O ₃	C-H	-C-O	-C=O	O-C=O	F ⁻	N-C=O		-PO ₃	org.?
position 1	15	44	2.4	2.9	0.8	1.7	2.1	29	0.9	1.1
position 2	15	44	2.4	3.1	0.8	1.7	2.1	29	0.9	1.1

Table S2. Apparent concentrations (at%) measured at position 2 for two values of the take-off angle Θ . In the lower row, the concentration ratios $c_{\Theta = 80^\circ} / c_{\Theta = 20^\circ}$ are given. A large value of this ratio corresponds to a relatively large distance of the component from the outer surface.

Position	Θ	Al 2p	C 1s				F 1s	N 1s	O 1s	P 2s	Si 2p
	($^\circ$)	Al ₂ O ₃	C-H	-C-O	-C=O	O-C=O	F ⁻	N-C=O		-PO ₃	org.?
pos 2	80	19	33	2.2	2.0	1.0	2.1	1.5	37	0.8	0.8
pos 2	20	8	59	4.4	3.4	1.6	1.0	2.7	17	1.4	0.9

pos 2	80	20	32	2.6	1.9	0.9	2.1	1.6	38	0.8	0.9
ratio 80 / 20		2.3	0.5	0.5	0.6	0.6	2.1	0.6	2.2	0.6	1.0

To determine the position of the detected elements relative to the outer surface (the “layer structure” of the sample), additional measurements were done at one position for $\Theta = 80^\circ$, $\Theta = 20^\circ$ and again for $\Theta = 80^\circ$. The results of these measurements are given in **Table S2**.

The first and the second measurement for $\Theta = 80^\circ$ are in good agreement with each other; hence we conclude that the SAMs are not sensitive for irradiation with X-rays.

Based on the concentration ratios we conclude that the “layer structure” of the sample is as follows:

Al_2O_3 and F / Si (org?) / organic layer containing C, O, N and P

We notice that a contamination with Si is present at the interface Al / organic layer (possibly as silicones) as well as a contamination of Fluor, chemically bound as aluminium oxifluoride. According to the analysis the element P is not only positioned at the interface Al_2O_3 / organic layer but can also be found within the organic layer. This suggests that possibly not all molecules are anchored to the substrate. Similar results were observed for quinquethiophene SAMs on SiO_2 and organic dielectrics where π - π stacking plays an important role in the monolayer formation.^[3,4] To obtain insight into the thickness and the real concentrations of the organic layer, model calculations have been performed.^[5,6] Important for these calculations is the assumption that the sample consists of a homogeneous substrate on which a homogeneous thin film is present (thickness D_{org}). In [5] relations are derived between the real concentrations in the substrate and the thin film on the one hand and the apparent concentrations on the other hand, with the layer thickness D_{org} as a parameter. During the model calculations the value of D_{org} is adjusted in such a way that the sum of the real concentrations in the thin film is 100 at%; mathematically can be shown [30] that at this condition also the sum of the real concentrations in the substrate is 100 at%.

Calculations have been performed using the data in table 1 (measured for $\Theta = 45^\circ$) and the data obtained for $\Theta = 20^\circ$ in table S2. To estimate values for the apparent concentration of organic O, the components of the C1s-peak were calculated assuming:

$$C_{\text{O-org}} = 0.5 * C_{\text{C in C-O}} + C_{\text{C in C=O}} + 2 * C_{\text{C in O-C=O}}$$

Values of the Inelastic Mean Free Path in the organic layer were taken from Cumpson; to take into account the lower atomic density of the present molecules relative to C-H polymers the IMFP-values of Cumpson were multiplied with a factor of 1.19.^[7]

The results of the model calculations are given in **Table S3**. The uncertainty in the obtained values of the thickness D_{org} is determined mainly by the uncertainties in the IMFP-values. The uncertainty is estimated at $\pm 5\%$ ^[7]; by consequence the possible error in D_{org} is estimated at ± 0.2 nm. The uncertainty in the coverage N_{p} is determined predominantly by the limited accuracy of the concentration of P and is estimated at $\pm 0.2 \times 10^{14}$ at/cm².

Table S3. Results of model calculations: values are given for the thickness of the organic layer, D_{org} , the coverage with P, N_{p} , and the real atomic concentrations in the organic layer. Remark: the value of the coverage N_{p} was calculated starting from the apparent concentration of P, taking into account that P is present randomly within the entire organic layer.

Position	D_{org}	N_{p}	N 1s	C 1s	O 1s	P 2s	F 1s	O 1s	Al 2p
	(nm)	(at/cm ²)			org			inorg	
position 1 ($\Theta = 45^\circ$)	3.1	1.8×10^{14}	3.3	86	9.0	1.6	8	53	40
position 2 ($\Theta = 45^\circ$)	3.1	1.8×10^{14}	3.3	86	9.0	1.6	8	52	40
position 2 ($\Theta = 20^\circ$)	3.1	1.8×10^{14}	3.1	85	10.3	1.7	14	50	37

In conclusion XPS-analyses confirm the presence of a PO_3 alkyl-containing SAM-layer homogenously deposited on Al_2O_3 . The concentration corresponds to a coverage N_{p} of 1.8×10^{14} atoms P / cm² and an effective layer thickness d_{org} of 3.08 nm. These results coincide well with a theoretical coverage calculated from the crystal structure^[8,18] (1.6×10^{14}) and the layer thickness calculated by united force-field (UFF) of 2.93 nm.

X-RAY DIFFRACTION STUDIES ON SELF-ASSEMBLED MONOLAYERS

Specular x-ray reflectivity (XRR) measurements were performed on a Panalytical Empyrean Reflectometer set up with copper sealed tube, a $1/32^\circ$ primary slit, a 10mm beam mask and a multilayer mirror ($\lambda = 0.1542$ nm) on the primary side. A small receiving slit of 0.1 mm and a 3D Panalytical Pixcel detector were used on the secondary side. The experimental data were fitted with Parrat formalism^[9] using X'Pert Reflectivity 1.3 software (PANalytical). This software package uses a genetic fitting algorithm,^[10] which finds the vicinity of the global optimum of the fit and uses the Marquardt-Levenberg algorithm to finally optimize the parameters to the found local minimum. The error estimation of the fitting parameters is done as described in chapter 15.6 of the Numerical Recipes.^[11] The surface roughness and the interface roughness of the specimen were determined using the Nevot and Croce approach.^[12]

Grazing incidence x-ray diffraction (GIXD) measurements were performed at the beamline W1 at the synchrotron HASYLAB, Germany. A wavelength of 0.11801 nm was used. The incidence angle of the primary beam was chosen at the optimum value $\alpha_i = 0.15^\circ$ resulting in the best signal to noise ratio. The samples were investigated in an inert helium atmosphere provided by a stage with a domed x-ray window (DHS900, AntonPaar).^[13] The results of in-plane GIXD measurements are presented as line scans obtained by integrating intensities of reciprocal space maps^[14] measured by a one dimensional position sensitive detector (Mythen 1K, Dectris). The crystallite size was estimated by line broadening analysis using the Scherrer equation,^[15] the instrumental broadening in the used experimental range was about $\Delta q_{xy} = 0.2 \text{ nm}^{-1}$.^[16]

X-ray diffraction studies on drop casted films

Thick films are prepared by drop casting from tetrahydrofuran solutions on thermally oxidized silicon wafers. The films are investigated by specular X-ray diffraction (SXRD) and by grazing incidence X-ray diffraction (GIXD). The SXRD was performed by a SIEMENS D501 diffractometer using Bragg-Brentano geometry. Radiation from a sealed copper tube was used in combination with a graphite monochromator at the secondary side. Laboratory GIXD measurements were performed with a commercial four-circle Bruker D8 Discover diffractometer upgraded with the Bruker Ultra GID add-on using a sealed copper tube ($\lambda = 0.1542 \text{ \AA}$).^[16] The incidence angle ($\alpha_i = 0.17^\circ$) of the primary beam was optimized to maximize the scattering intensity from the parabolic graded

multilayer mirror,^[17] the beam size was defined by a 0.6 mm primary slit. Both the incidence X-ray path as well as the secondary path contains large Soller slits and the scattered beam was detected with a one-dimensional position sensitive detector (Vantec-1). The results of in-plane GIXD measurements are presented as line scans obtained by integrating intensities of reciprocal space maps.^[14] The crystallite size was estimated by line broadening analysis using the Scherrer equation;^[15] the instrumental broadening in the used experimental range was about $\Delta q_{xy} = 0.2 \text{ nm}^{-1}$.^[16]

Figure S2 shows the SXRD pattern and the GIXD pattern of a drop casted film, plotted as a function of q_z and q_{xy} , respectively. In case of SXRD two dominating peaks are observed at $q_z = 2.2 \text{ nm}^{-1}$ and 2.8 nm^{-1} , a peak at 7.1 nm^{-1} and a broad feature at 14 nm^{-1} . GIXD reveals a strong peak at $q_{xy} = 2.9 \text{ nm}^{-1}$ a peak at 18.0 nm^{-1} and broad feature at 14 nm^{-1} . The diffraction pattern are in qualitative good agreement with X-ray diffraction studies on comparable molecules which are formed by a conjugated core of PBI and branched side chains.^[8,18] The peak at $q_{xy} = 18.0 \text{ nm}^{-1}$ represents the stacking distance of the conjugated cores of 0.35 nm . The large peak width of $\Delta q_{xy} = 1.4 \text{ nm}^{-1}$ can be referred to a rather small crystalline correlation length of 4.6 nm which corresponds to 13 repeating units of stacked PBI cores. The peaks at $q_z = 2.2 \text{ nm}^{-1}$ and 2.9 nm^{-1} are representative for the two-dimensional lateral packing of the columns formed by the stacked PBI units. The broad features at $q = 14 \text{ nm}^{-1}$ are typical for disordered alkyl chains.

Within the drop casted film the crystals of PBI-PA show a strong preferred orientation. While both peaks of the column packing ($q_z = 2.2 \text{ nm}^{-1}$ and 2.8 nm^{-1}) are present in the SXRD pattern, only one peak of the column packing ($q_{xy} = 2.9 \text{ nm}^{-1}$) is present together with the peak of the stacking of the conjugated PBI cores ($q_{xy} = 18 \text{ nm}^{-1}$) at the GIXD pattern. This reveals that the columns of stacked PBI cores are aligned parallel to the substrate surface.

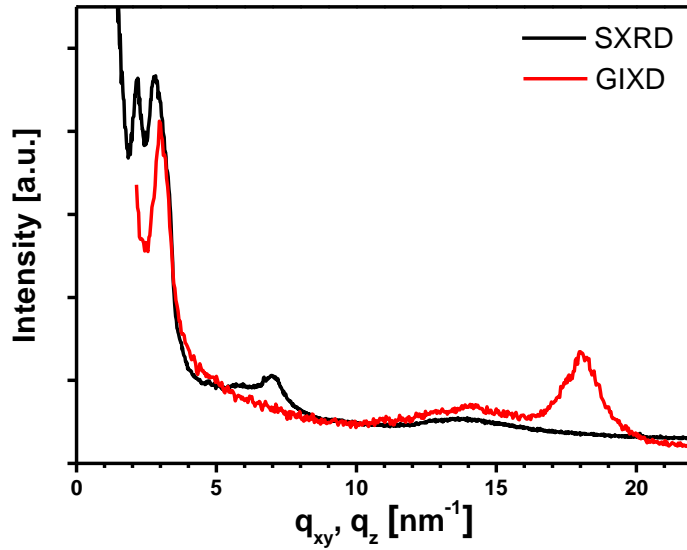


Figure S2. Specular x-ray diffraction (SXR) and grazing incidence x-ray diffraction (GIXD) of a drop casted film prepared from a tetrahydrofuran solution. The intensity of the GIXD pattern was integrated in the q_z range around the Yoneda peak ($0 \dots 0.5 \text{ nm}^{-1}$).

TRANSISTOR SUBSTRATES

Bottom-gate/bottom-contact transistor substrates with patterned gate and interconnections were fabricated on monitor silicon wafers with a native silicon dioxide layer. First the gate was created by sputtering a thin gold layer and structuring it via photolithographic processes. On top a 100 nm thick Al_2O_3 layer was grown by atomic layer deposition (ALD) at 120°C using trimethylaluminum and H_2O as precursors. Next vertical interconnections were created to enable contacting the gate. Finally the gold source and drain electrodes were deposited via sputtering and structured by conventional photolithography on top of the Al_2O_3 . The whole process was developed to remain below 150°C compatible with low temperature flexible electronic processes.^[19] An AFM image of a typical transistor substrate is shown in **Figure S3**.

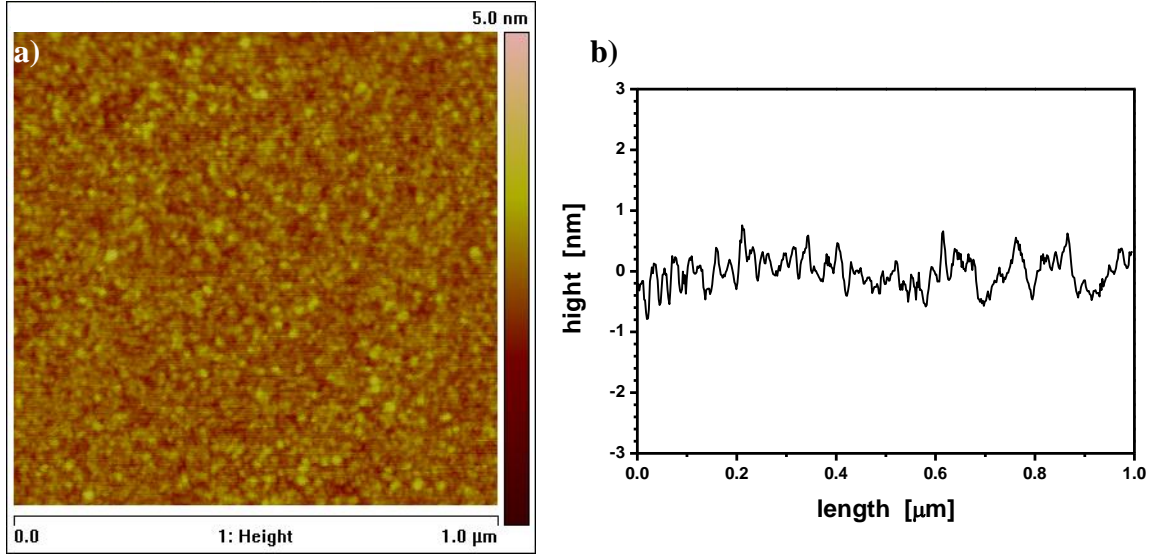


Figure S3: AFM image of a bare Al_2O_3 substrate without SAM. The nanocrystalline layer exhibits a roughness of r_q of 0.3nm.

ELECTRICAL CHARACTERIZATION OF PBI-PA SAMFETS

Transistor device characteristics were measured at room temperature in inert atmosphere (N_2 glove box) using an Agilent 4155C semiconductor parameter analyzer controlled by a PC. The field-effect mobilities of the SAMFETs in saturation (μ_{sat}) regime were calculated from the equation S1 as follows, at $V_{DS} = 20$ V:

$$\mu_{sat}(V_G) = \frac{2L}{W \cdot C_i} \left(\frac{\partial \sqrt{I_{ds}(V_G)}}{\partial V_G} \right)^2 \quad (\text{S1})$$

where C_i is the capacitance per unit area of the gate dielectric layer ($70\text{nF}/\text{cm}^2$ for the Al_2O_3 used in this work), and L and W are channel length and width, respectively. The threshold voltage (V_{th}) of the devices is extracted by extrapolating the square root (SQRT) of $|I_{DS,sat}|$ vs. V_G plot to $I_{ds,sat} = 0$ (as depicted in the plots in Figure 5b).

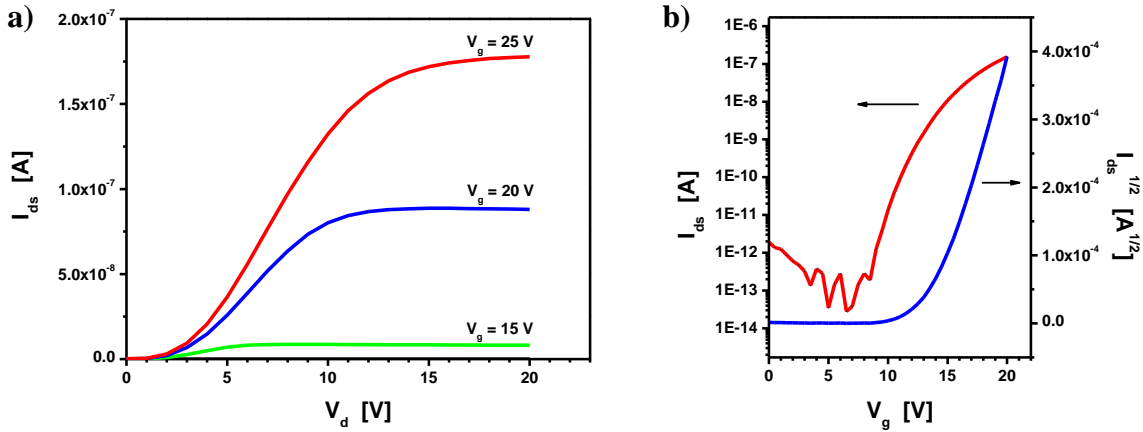


Figure S4. Characteristics of a PBI-PA based SAMFET. (a) Output characteristics of a transistor with a channel length of 5 μm and a channel width of 1000 μm . The drain voltage is swept from 0 V to 20 V, the gate voltage is varied starting from 0 V to 25 V in 5 V per step. (b) Transfer characteristics of the device, in the saturation regime with a drain voltage of 20 V.

Figure S4 shows the output and transfer characteristics of a transistor with a channel length of 5 μm and a width of 1000 μm . The mobility of this transistor is in the order of $10^{-4} \text{ cm}^2/\text{Vs}$, and showed an excellent on-off ratio of 10^5 . We note that the transistors are strongly contact limited as can be observed from the strong nonlinear “s” shaped behaviour at the low drain bias. The contact resistance is understandable considering the large mismatch between the gold work function (-4.8 eV) and the LUMO level (-3.8 eV) of the semiconductor.^[20]

Back and forth measurements

To enable the fabrication of reliable devices the hysteresis was investigated for the SAMFETs. In general the transfer measurements exhibited strong hysteresis and gate bias instabilities. A method to suppress the hysteresis was drop casting of a thin layer of polystyrene on top of the SAMFETs. The results are demonstrated in **Figure S5**.

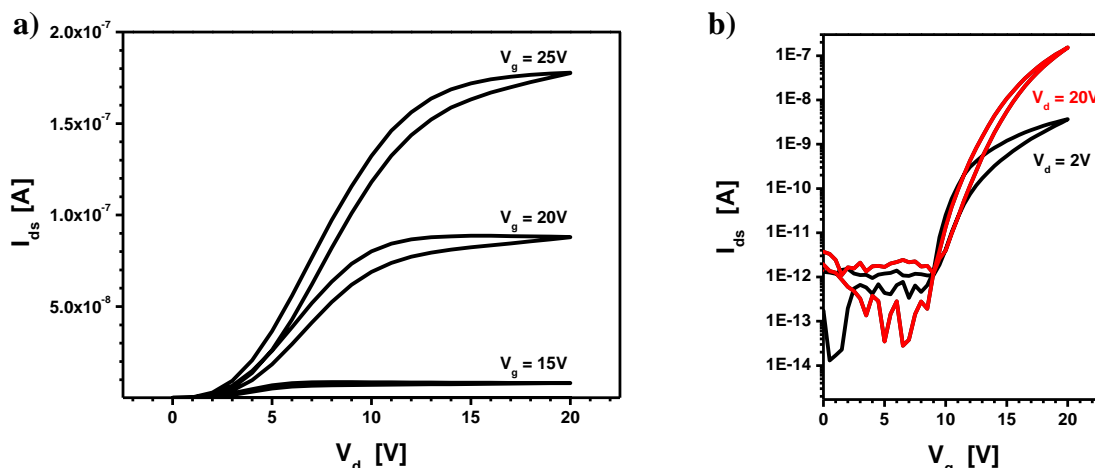


Figure S5. PBI-PA SAMFET characteristics of a device with a thin polystyrene layer on top. a) Output characteristics of a SAMFET based on PBI-PA with a channel length of $5 \mu\text{m}$ and a channel width of $1000 \mu\text{m}$. The drain voltage is swept from 0 V to 20 V , the gate voltage is varied starting from 0 V to 25 V in 5 V per step. b) Transfer characteristics of the device, in the saturation regime with a drain voltage of 2 V (black curve) and 20 V (red curve).

Electrical characteristics of the bulk layers of PBI-PA

In order to benchmark the electrical performance of the PBI-PA semiconductor, thin films were drop casted on conventional transistor substrates (**Figure S6a**). From the transfer characteristics, mobilities in the range of $1 \times 10^{-4} \text{ cm}^2/\text{Vs}$, an on/off ratio of 250 and a threshold voltage $V_t = 5 \text{ V}$ was observed. The device was also heavily contact limited. Compared to the SAMFETs the devices exhibited lower mobility and on/off ratios (Figure S6c).

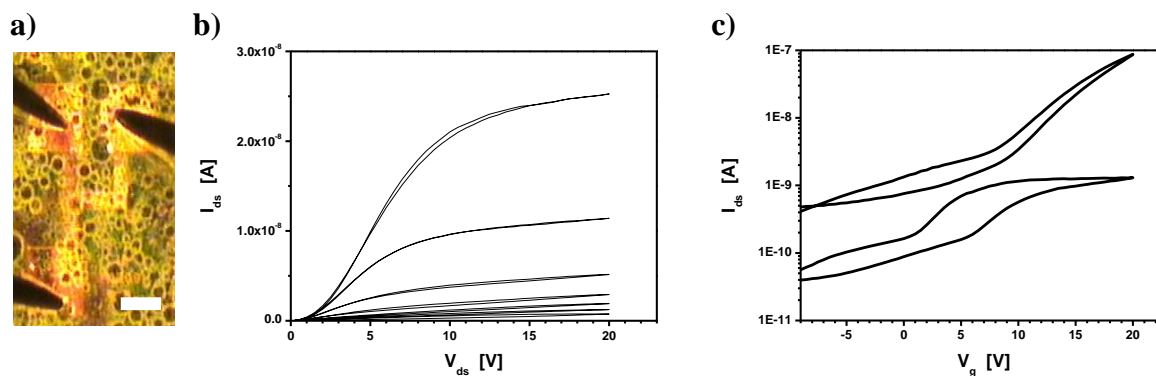


Figure S6. Investigation of a PBI-PA bulk transistor. a) Optical image of a drop casted PBI-PA transistor. b) Output characteristic and c) transfer characteristic of a drop casted PBI-PA transistor.

Results of PBI-PA on SiO₂

To verify chemical self-assembly as the driving force for the monolayer fabrication, transistor substrates with a SiO₂ gate dielectric were incubated in a PBI-PA solution according to the method described above. Whereas Al₂O₃ substrates always exhibited functional transistor characteristics, the SiO₂ based devices did not. None of all SiO₂ based devices measured showed any electrical conductivity (**Figure S7**). This result demonstrates the selectivity of the PBI-PA molecule to Al₂O₃.

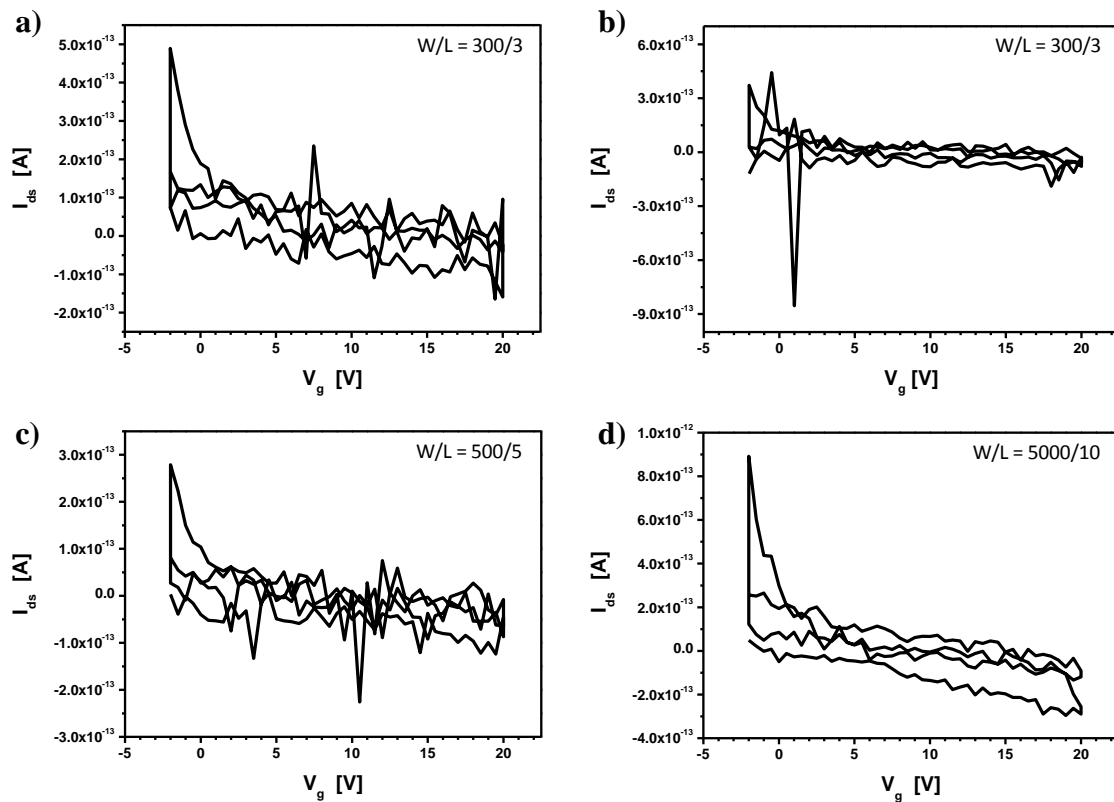


Figure S7. Current-voltage characteristics of transistors with SiO₂ dielectrics. The devices were fabricated according to the same procedure described above. The insets reflect the width (W) and length (L) ratios.

SAMFET COMPLEMENTARY INVERTERS

CMOS inverters were fabricated by integrating p-type SAMFETs with n-type SAMFETs. The use of a complementary logic design allows the development of logic which is substantially more robust and power efficient. The improvement in noise immunity from using CMOS logic warrants the current focus on stable and high mobility n-type materials.^[21] As a p-type SAMFET, a quinquethiopene derivative with a dimethylchlorosilane anchor tail was taken. The SAMFET was fabricated on an heavily doped n⁺⁺ silicon wafer with a 200 nm thermally grown SiO₂ gate dielectric and gold

electrodes according to the procedure described in literature.^[3,4] **Figure S8a** shows the p-SAMFET transfer characteristics. It exhibits mobilities in the order 10^{-2} cm²/Vs and a threshold voltage of approximately 10V. For the n-type SAMFET, PBI-PA was used as the semiconductor. The monolayers were fabricated according to procedures described above. The transfer characteristics of n-type SAMFET is given in **Figure S8b**. The device exhibits a mobility in the order of 5×10^{-4} cm/Vs, on/off ratio of 5 decades and a threshold voltage of around 7V. Due to the difference in mobility and other parameters, the currents of the p-type SAMFET were matched with that of the n-type SAMFET. This was done by adjusting the channel length only. In the case of the p-type SAMFET a 40 μ m channel length was chosen and for the n-type SAMFET a 2 μ m channel length was taken. The channel width equaled in both cases 1000 μ m.

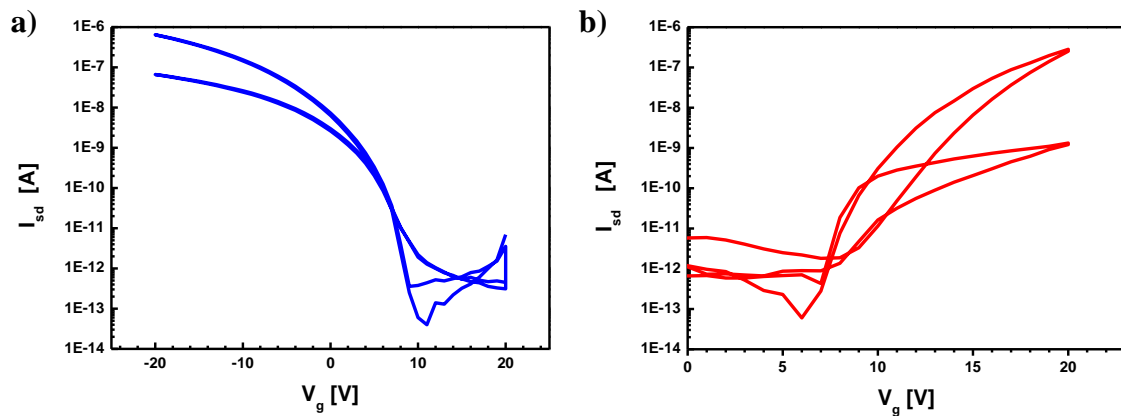


Figure S8. Transfer characteristics two SAMFETs which were implemented to the bias inverter. **a)** Transfer characteristic of the used p-type SAMFET. **b)** Transfer characteristic of the n-type SAMFET.

The inverter was realized by connecting two substrates in a complementary layout. A schematic overview of the inverter is given in **Figure S9**.

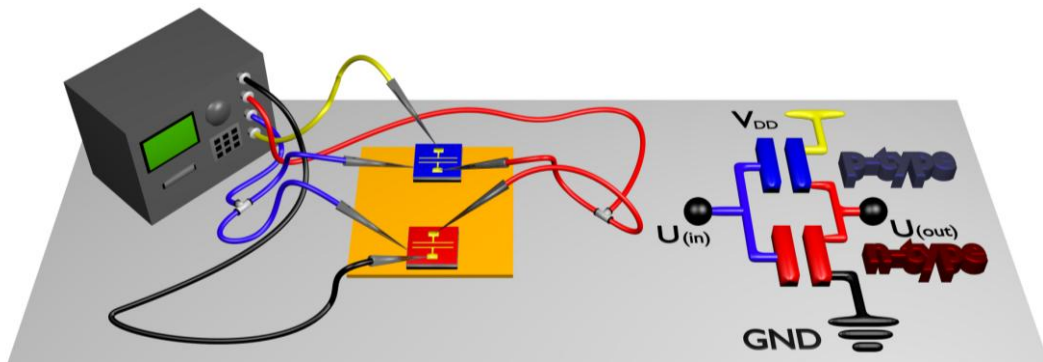


Figure S9. Schematic illustration of the measurement setup for the SAM-CMOS bias inverter.

PMOS logic was previously reported.^[3] Whereas the SAMFETs showed good electrical properties such as high on/off ratio's and high mobility, the realized logic suffered from the limitations on unipolar logic. A p-type SAMFET based inverter is shown in **Figure S10a**. The SAMFET is based on a $V_{gs}=0$ logic. The inverter exhibited a gain of 6 and a 2-3 V noise margin. In addition the inverters showed leakage of current even when the inverter was not switching. To resolve these issues, complementary logic is indicated. By combing using the CMOS design, noise margin were doubled, gain was somewhat increased and leakage currents in the switched states eliminated.

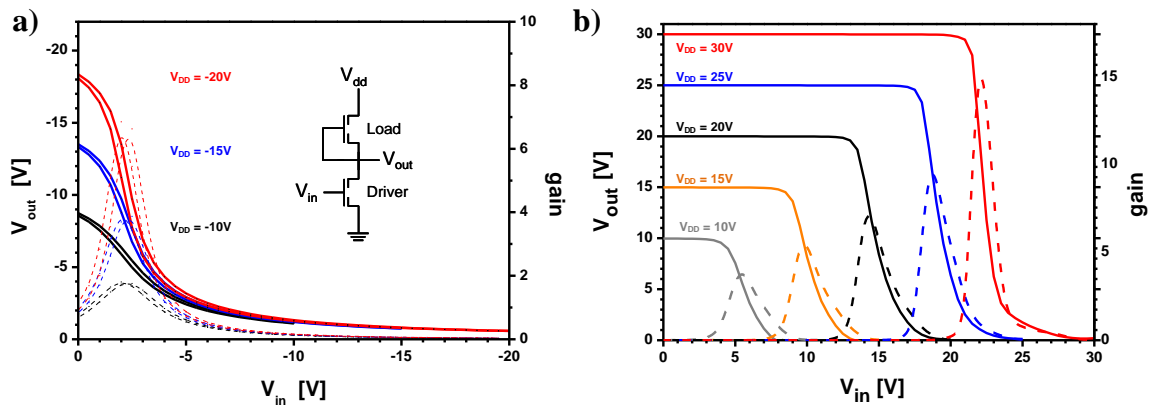


Figure S10. SAMFET based inverter characteristics. The dashed lines reflect the gain. **a)** Characteristic of a unipolar PMOS logic. The inset shows a diagram of the inverter. **b)** Characteristic of a bipolar CMOS logic.

Finally for low input and output voltages the inverters showed large hysteresis, due to the current threshold voltage positions ($V_t = 7V$) and instabilities exhibited in the devices. In additions the contact resistance also play a dominant role. However at higher V_{dd} and input voltage reasonable hysteresis can be obtained as demonstrated in **Figure S11**.

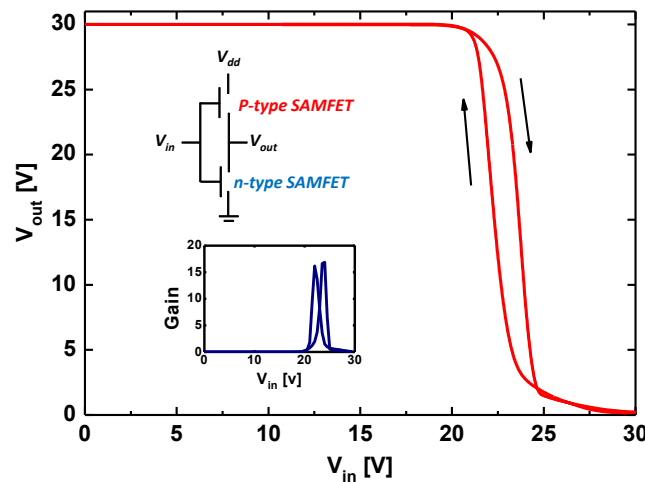


Figure S11. Characteristics of a SAMFET based complementary inverter. The supply voltage was 30 Volts. The insets show a diagram of the inverter and a plot of the measured gain.

References:

- [1] Moulder, J. F.; Stickle, W. F.; Sobol, P. E.; Bomben, K. D. in *Handbook of X-ray Photoelectron Spectroscopy*, (Ed: J. Chastain), Perkin-Elmer Corporation, Physical Electronics, Eden Prairie, **1992**.
- [2] PHI-Multipak Software Manual Version 6.0 (Physical Electronics Division, Eden Prairie, **1998**.
- [3] Smits, E. C. P.; Mathijssen, S. G. J.; van Hal, P. A.; Setayesh, S.; Geuns, T. C. T.; Mutsaers, K. A. H. A.; Cantatore, E.; Wondergem, H. J.; Werzer, O.; Resel, R.; Kemerink, M.; Kirchmeyer, S.; Muzafarov, A. M.; Ponomarenko, S. A.; de Boer, B.; Blom, P. W. M.; de Leeuw, D. M. Bottom-up organic integrated circuits. *Nature*. **455**, **2008**, 956.
- [4] Mathijssen, S. G. J.; Smits, E. C. P.; van Hal, P. A.; Wondergem, H. J.; Ponomarenko, S. A.; Moser, A.; Resel, R.; Bobbert, P. A.; Kemerink, M.; Janssen, R. A. J.; de Leeuw, D. M. Monolayer coverage and channel length set the mobility in self-assembled monolayer field-effect transistors. *Nat. Nanotech.* **4**, **2009**, 674.
- [5] van der Marel, C.; Yildirim, M.; Stapert, H. R. Multilayer approach to the quantitative analysis of x-ray photoelectron spectroscopy results: Applications to ultrathin SiO₂ on Si and to self-assembled monolayers on gold. *Journal of Vacuum Science & Technology A: Vacuum, Surfaces, and Films* **23**, **2005**, 1456.
- [6] van der Marel, C.; Verheijen, M. A.; Tamminga, Y.; Pijnenburg, R. H. W.; Tombros, N.; Cubaynes F. Thickness and composition of ultrathin SiO₂ layers on Si. *Journal of Vacuum Science & Technology A: Vacuum, Surfaces, and Films* **22**, **2004**, 1572.
- [7] Cumpson, P. J. Estimation of inelastic mean free paths for polymers and other organic materials: use of quantitative structure–property relationships. *Surface and Interface Analysis*, **31**, **2001**, 23.
- [8] Nolde, F., Pisula, W., Müller, S., Kohl, C., Müllen, K. Synthesis and Self-Organization of Core-Extended Perylene Tetracarboxdiimides with Branched Alkyl Substituents. *Chem. Mater.* **18**, **2006**, 3715.
- [9] Parratt, L. G. *Phys. Rev.* **95**, **1954**, 359.
- [10] Dane, A. D.; Veldhuis, A.; de Boer, D. K. G.; Leenaers, A. J. G.; Buydens, L. M. C. Application of genetic algorithms for characterization of thin layered materials by glancing incidence X-ray reflectometry. *Physica B: Condensed Matter* **253**, **1998**, 254.
- [11] Press, W. H.; Teukolsky, S. A.; Vetterling, W. T.; Flannery, B. P. Cambridge University Press **2007**.
- [12] Croce, P.; Névoit, L. Étude des couches minces et des surfaces par réflexion rasante, spéculaire ou diffuse, de rayons X. *Rev. Phys. Appl. (Paris)* **11**, **1976**, 113.

- [13] Resel, R.; Tamas, E.; Sonderegger, B.; Hofbauer, P.; Keckes J. A heating stage up to 1173 K for X-ray diffraction studies in the whole orientation space. *J. Appl. Cryst.* **36**, **2003**, 80.
- [14] Moser, A. PhD thesis, Graz University of Technology **2012**.
- [15] Smilgies, D. M., Scherrer grain-size analysis adapted to grazing incidence scattering with area detectors. *J. Appl. Cryst.* **42**, **2009**, 1030.
- [16] Neuschitzer, M.; Moser, A.; Neuhold, A.; Kraxner, J.; Stadlober, B.; Oehzelt, M.; Salzmann, I.; Resel, R.; Novák, J. Grazing-incidence in-plane X-ray diffraction on ultra-thin organic films using standard laboratory equipment. *J. Appl. Cryst.* **45**, **2012**, 367.
- [17] Schuster, M., Gobel, H. Parallel-beam coupling into channel-cut monochromators using curved graded multilayers. *J. Phy. D: App. Phy.* **28**, **1995**, A270.
- [18] Marcon, V.; Breiby, D. W.; Pisula, W.; Dahl, J.; Kirkpatrick, J.; Patwardhan, S.; Grozema, F.; Andrienko, D. Understanding Structure–Mobility Relations for Perylene Tetracarboxydiimide Derivatives. *J. Am. Chem. Soc.* **131**, **2009**, 11426.
- [19] Tripathi, A. K., Smits, E. C. P, van der Putten, J. B. P. H., van Neer, M., Myny, K., Nag, M., Steudel, S., Vicca, P., O'Neill, K., van Veenendaal, E., Genoe, J., Heremans, P., Gelinck, G. H. Low-voltage gallium-indium-zinc-oxide thin film transistors based logic circuits on thin plastic foil: Building blocks for radio frequency identification application. *Appl. Phys. Lett.* **98**, **2011**, 162102.
- [20] Wicklein, A.; Lang, A.; Muth; M., Thelakkat, M. Swallow-Tail Substituted Liquid Crystalline Perylene Bisimides: Synthesis and Thermotropic Properties. *J. Am. Chem. Soc.* **131**, **2009**, 14442.
- [21] Bode, D.; Rolin, C.; Schols, S.; Debucquoy, M.; Steudel, S.; Gelinck, G. H.; Genoe, J.; Heremans, P. Noise-Margin Analysis for Organic Thin-Film Complementary Technology Electron Devices. *IEEE Transactions* **57**, **2010**, 201.



N-TYPE SELF-ASSEMBLED-MONOLAYER FIELD-EFFECT
TRANSISTORS FOR FLEXIBLE ORGANIC ELECTRONICS

Andreas Ringk,^{a,b} W. S. Christian Roelofs,^c Edsger C. P. Smits^{d,}, Cees van der Marel,^e*

Ingo Salzmann,^f Alfred Neuhold,^g Gerwin H. Gelinck,^d Roland Resel,^g

Dago M. de Leeuw,^h Peter Strohriegl^{d,}*

^aMacromolecular Chemistry I, University of Bayreuth, 95440 Bayreuth, Germany

^bDutch Polymer Institute (DPI), P.O. Box 902, 5600 AX Eindhoven, The Netherlands

^cP.O. Box 513, 5600 MB Eindhoven, The Netherlands

^dHolst Centre/TNO, High Tech Campus 31, 5656 AE Eindhoven, The Netherlands

^ePhilips Innovation Services – Materials Analysis, High Tech Campus 11, 5656 AE Eindhoven, The Netherlands

^fDepartment of Physics – Humboldt-Universität zu Berlin, Brook-Taylor-Straße 6 D-12489 Berlin, Germany

^gInstitute of Solid State Physics, Graz University of Technology, Petersgasse 16, A-8010 Graz, Austria

^hMax Planck Institute for Polymer Research Ackermannweg 10, D-55128 Mainz, Germany

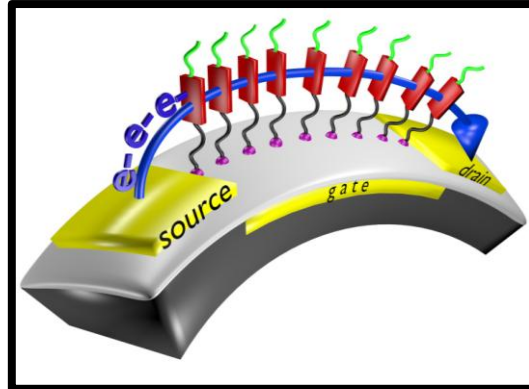
Published in a slightly modified version in *Organic Electronics*, **2013**

Volume 14, Issue 5, pages 1297–1304

DOI: [org/10.1016/j.orgel.2013.02.016](https://doi.org/10.1016/j.orgel.2013.02.016)

Reprinted with permission; Copyright © 2013 by Elsevier B.V.

Keywords: self-assembled monolayer, n-type field-effect transistor, perylene bisimide, flexible transistor, unipolar bias inverter



Abstract: Within this work we present n-type self-assembled monolayer field-effect transistors (SAMFETs) based on a novel perylene bisimide. The molecule spontaneously forms a covalently fixed monolayer on top of aluminum oxide dielectrics via a phosphonic acid anchor group. Precise studies revealed an amorphous, 2-dimensional semiconducting sheet on top the dielectric. Reliable transistors with electron mobilities on the order of $10^{-3} \text{ cm}^2/\text{Vs}$ with low hysteresis were achieved on rigid as well on flexible substrates. Furthermore, a flexible NMOS-bias inverter based on SAMFETs is demonstrated for the first time.

1. Introduction

Self-assembled monolayers (SAMs) have attracted attention due to a manifold potential of applications. SAMs enable surface modification in order to change the wetting behaviour of various materials,^[1] match work functions of metals,^[2] or tune the orientation of organic molecules on surfaces^[3] in a simple way. Since the postulation that charge transport in organic field-effect transistors can be managed by a single, two-dimensional sheet of molecules,^[4] and its experimental approval^[5,6] SAMs have become also attractive as semiconductors in organic field-effect transistors. The realization of the first chemisorbed self-assembled monolayer field-effect transistors (SAMFETs)^[7] opened a new promising field for low-cost large area organic electronics.

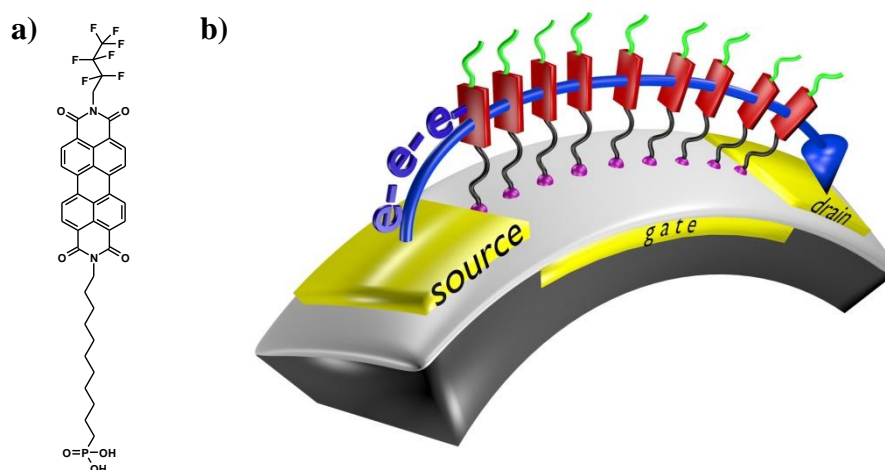


Figure 1. a) Chemical structure of PBIF-PA. b) Schematic illustration of a polymer based SAMFET.

In SAMFETs molecules spontaneously form a uniform layer on the dielectric. Dense packing of semiconducting cores over large distances allows efficient charge transport between source and drain electrode.^[8] The molecule itself consists of a semiconducting core connected via a spacer to a reactive group which anchors covalently to the dielectric. Depending on the dielectric different anchor groups, e.g. carboxylic acids or phosphonic acids, are possible.^[9,10] In comparison to common organic thin-film transistors the on/off-ratio in SAMFETs is greatly enhanced because of the absence of any bulk current. Furthermore the simple SAMFET fabrication process, low material usage, surface selectivity, and possible high device yields are promising steps forward to the mass production of organic electronics. The best SAMFETs so far are based on a quinquethiophene derivative fixed to a silicon oxide dielectric via a chlorosilane group.^[11] Hole mobilities of 10^{-2} cm²/Vs and on/off-ratios of 10^6 were obtained. The

implementation into different integrated circuits^[11] and the use as sensors^[12] point out the versatility of SAMFETs.

Most of the SAMFETs described in literature are based on hole conducting materials as for instance thiophene derivatives. However, the established integrated circuit design is based on the complementary metal oxide semiconductor (CMOS) technique. For CMOS-circuits p- and n-type transistors are combined in one device. High noise immunity and low power consumption are advantages compared to unipolar circuits. Due to their high sensitivity towards oxygen and water n-type transistors are difficult to realize.^[13] Up to now n-type publications reporting SAMFETs are lagging.^[14,15,16] The first n-type SAMFET was presented by Novak et al. They used a fullerene based molecule as semiconductor and obtained electron mobilities up to $10^{-4} \text{ cm}^2/\text{Vs}$.^[14] The performance of these SAMFETs could be further increased by using a mixed monolayer derivative.^[15] Recently, we have demonstrated an n-type SAMFETs based on a perylene bisimide derivative PBI-PA.^[16] Electron mobilities of $1.5 \times 10^{-3} \text{ cm}^2/\text{Vs}$ and on/off-ratios up to 10^5 were measured. In addition a CMOS circuit based solely on SAMFETs was presented by combining an PBI-PA n-type SAMFET with a thiophene based p-type SAMFET to a CMOS inverter.^[16]

Typical substrates for SAMFETs are doped silicon wafers. To obtain flexible devices a foil based polymeric substrate is indicated.^[17] Low temperatures during device fabrication steps are required in order to avoid damage of the flexible polymer substrate. An advantage of SAMFETs in flexible devices is that covalent fixation of the semiconducting molecules, which prevents delamination during bending procedures. P-type SAMFETs on flexible dielectric have been reported with silane based anchor groups.^[18] SAMFETs with phosphonic moiety have, however, only been made rigid silica substrates although their fabrication procedure enables low temperature fabrication.^[14,15,16]

Here we present n-type SAMFETs based on a novel heterosubstituted perylene bisimide. As anchor group phosphonic acid was chosen which is able to bind covalently to aluminium oxide dielectrics. Electron mobilities up to $10^{-3} \text{ cm}^2/\text{Vs}$, high on/off-ratios of 10^5 and a limited hysteresis were obtained for n-type SAMFETs on flexible substrates.

2. Results and Discussion

A perylene bisimide PBI-PA recently reported for n-type SAMFET applications^[16] consisted of a linear spacer with a pendant phosphonic acid unit, an electron conducting

perylene core, and a branched alkyl tail. Computer calculations revealed an orthogonal orientation of the branched alkyl tail to the perylene core. Due to steric hindrance between neighbouring PBI-PA molecules a surface coverage of only 1.8×10^{14} molecules per cm^2 on the dielectric is achieved. A high surface coverage in SAMFETs is crucial for efficient charge transport.

A second important point is the passivation of unwanted hydroxyl groups which are present at the dielectric surface.^[19] These groups are known to act as traps especially for electrons.^[20] Passivation is performed by the phosphonic acid during the self-assembly process with a condensation reaction of the hydroxide groups from the surface.^[21] Therefore a lower coverage results in a higher amount of hydroxyl groups at the dielectric. Besides relatively lower coverage of PBI-PA, in this case the phosphonic acid is also present within the organic layer such that not each acid linker can be used for passivation of the dielectric. Unreacted acid groups may even negatively affect the electron conductivity. Nevertheless reliable transistors were achieved, however, with substantial hysteresis. Such hysteresis can principally be divided into two types: “higher back sweep current” and “lower back sweep current”.^[22] The first type is attributed to mobile ions at the dielectric-semiconductor interface whereas the second type causes by charge trapping which is observed also for PBI-PA SAMFETs.

To improve n-type SAMFET device performance, the perylene bisimide N-(2,2,3,3,4,4,4-Heptafluoro-butyl)-N'-(undecyl-11-phosphonic acid) perylene-3,4,9,10-tetracarboxylic bisimide (PBIF-PA) was tailored to reduce steric repulsion which should lead to a denser packing of the perylene cores.^[23] In addition, a halogenation was employed which are known to increase electron transport stability.^[24] This was achieved by attaching a linear fluorinated alkyl tail instead of a branched alkyl tail at one side of the perylene bisimide. The chemical structure of PBIF-PA is depicted in figure 2.

The synthesis is described in the experimental section. Computer simulations of PBIF-PA already revealed a molecular length of 2.69 nm. From calculations a much smaller volume demand is expected compared to PBI-PA (see figure 2). From literature a higher surface coverage in the range of 2.4×10^{14} molecules per cm^2 is expected.^[25]

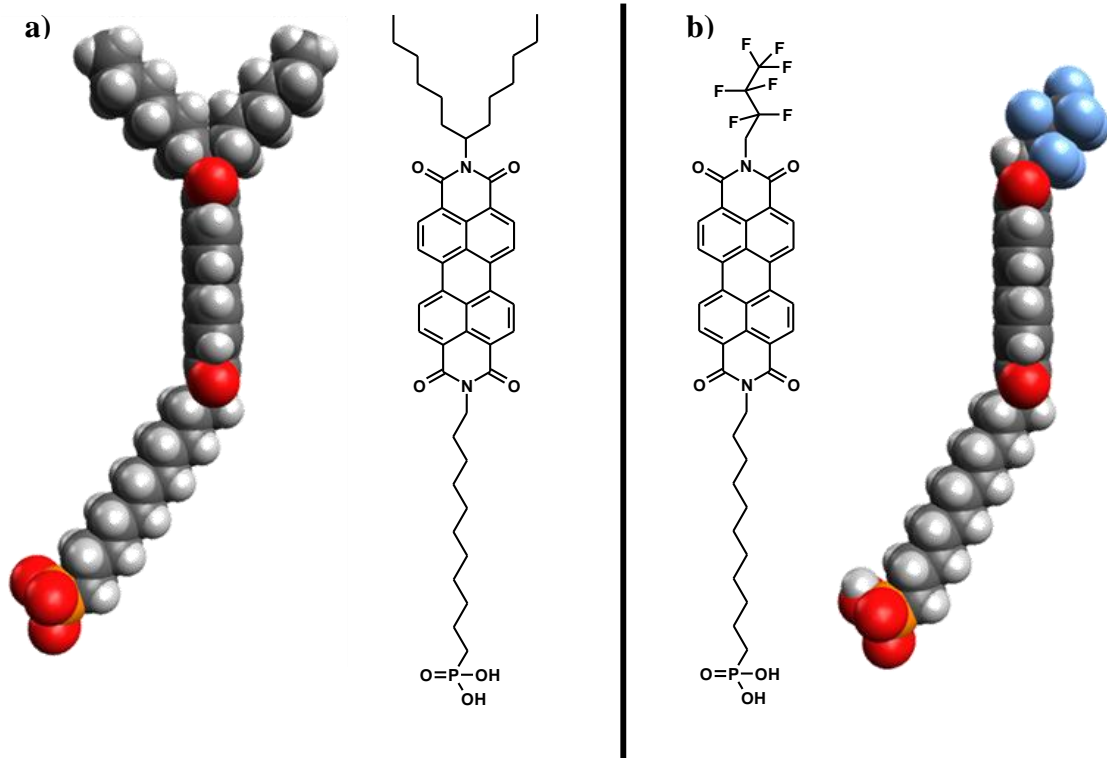


Figure 2: a) Side view on PBI-PA (left) and chemical structure of PBI-PA b) Chemical structure of PBIF-PA and its calculated structure (right).

Bottom-gate bottom-contact field-effect transistors were realized by submerging transistor structures on foil into a dilute solution of PBIF-PA in dimethylformamide (DMF). During the immersion PBIF-PA spontaneously forms a covalent phosphonic ester bond to the aluminium oxide dielectric. The substrates were immersed for 24 hours into a dilute solution of PBIF-PA ($c \approx 10^{-5}$ mol/L), rinsed with DMF to remove possible residual material, dried on a hotplate at 110°C for 20 minutes, and subsequently measured.

PBIF-PA monolayers were studied using X-ray photoelectron spectroscopy (XPS), X-ray reflectivity (XRR), grazing incident X-ray diffraction (GIXD) and via electrical characterization. XPS investigations show a monomolecular layer on top of aluminium oxide with a thickness of around 2.6 nm well in line with the calculated molecular length. A value of 2.4×10^{14} phosphorous atoms per cm^2 was found indicating a dense and complete coverage of PBIF-PA. The phosphorous density is about 30% higher compared to PBI-PA.^[16] Furthermore, angle dependent XPS measurements reveal the linear fluorinated tail present on top of the SAM. This observation points to a higher degree of out of plane order of the aluminium oxide functionalization with PBIF-PA.

Additional information on the out of plane order of the SAM was achieved by XRR-investigations. To analyse the experimental data model calculations were done using a three layer model. The results are depicted in figure 2.

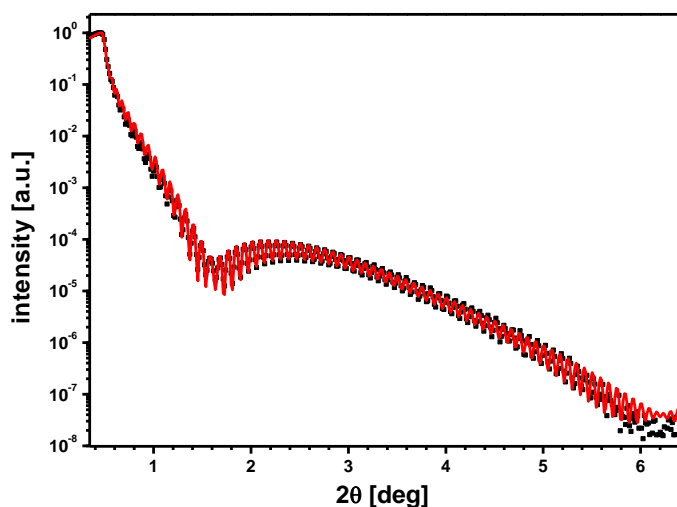


Figure 2: XRR investigations of PBIF-PA monolayers. The black dots give the experimentally obtained data, while the red curve shows a fit of the experimental data using a three layer model for the SAM.

The SAM itself can be divided into three different regions with different electron densities. As shown in figure 2 PBIF-PA consists of a linear fluorinated alkyl tail, a semiconducting perylene bisimide core, and a linear C11-alkyl spacer with a phosphonic acid anchor group. This structure was also confirmed from XRR measurements. A length of 0.60 nm for the fluorinated tail, 0.93 nm for the semiconducting core, and 1.15 nm for the linear spacer was found. All values fit with the data obtained from model calculations which are 0.39 nm, 1.13 nm, and 1.17 nm respectively. In the sum a value of 2.72 nm (calculated 2.69 nm) is obtained for the molecular length by XRR. The presence of electron rich atoms such as oxygen and nitrogen enhances the electron density of the middle layer similar to what was observed for PBI-PA SAMs before.^[16] A difference, however, is found for the outer layer of the SAM. Here the enhanced electron density originates from the high amount of fluorine, consistent with the XPS results. For perylene bisimides with branched alkyl tails, twisted perylene cores are evidenced by X-ray studies.^[26] Such a twisted arrangement is also presumed for PBI-PA monolayers.^[16] In contrast, perylene bisimides with linear tails show no twisted arrangement.^[23] The fact that fluorine and phosphorous is separated at the outer layer of the SAM and at the dielectric surface respectively, indicates also a non twisted, lamellar arrangement of PBIF-PA in the monolayer.

Grazing incidence diffraction (GIXD) measurements were done to itemize in-plane order and to get informations about the packing of the chromophores (see supporting informations). No characteristic reflection peak was found for drop casted as well as for the self-assembled monolayer. This suggests an amorphous PBIF-PA without grain boundaries onto the dielectric. In contrast, highly crystalline monolayers are reported for a quinquethiophene derivative, fixed via a chlorosilane onto silicon dioxide.^[8] We speculate, that different growth mechanism are responsible for the difference in crystallinity. Island growth mechanism, which is delegated by interactions of the aromatic core, is described for the thiophene derivative.^[8] The amorphous character of PBIF-PA suggests, that the assembly of PBIF-PA is directed by the driving force to form a covalent bond between phosphonic acid group and aluminium oxide and not by π - π -interactions of the chromophores.

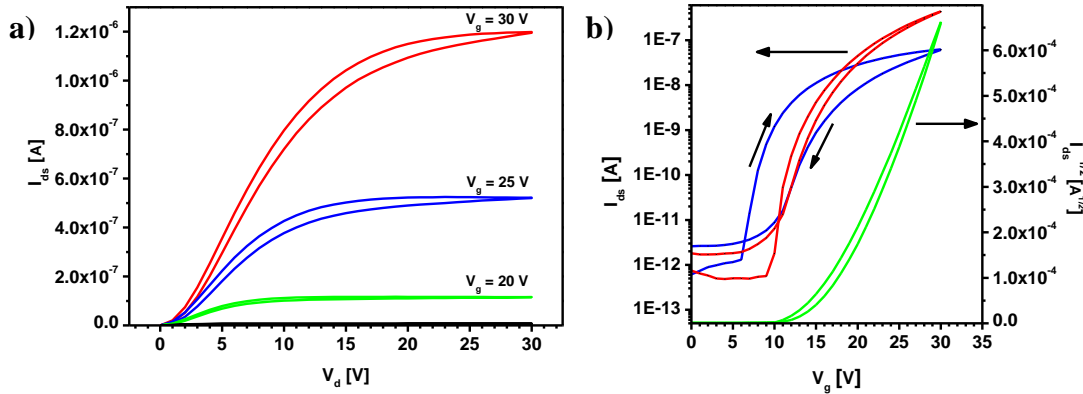


Figure 3: PBIF-PA SAMFET characteristics on a non flexible silicon substrate. **a)** Output characteristics and **b)** transfer characteristics. The channel length was 10 μm and the channel width was 1000 μm . The calculated mobility in the saturation regime is $10^{-3} \text{ cm}^2/\text{Vs}$, the on/off ratio is on the order of 10^6 , and the onset voltage is 10 V.

SAMFETs were prepared at first on rigid silicon based substrates (for details see supporting information). Typical output and transfer characteristics of a PBIF-PA SAMFET are shown in figure 3. The transistor channel dimensions are 10 μm in length and 1000 μm in width. The extracted electron mobility in the saturation regime is $10^{-3} \text{ cm}^2/\text{Vs}$, the on/off ratio is in the order of 10^6 , and the onset voltage is 10 V. It is remarkable that the PBIF-PA SAMFETs show limited hysteresis, without any additional treatments. This improvement is attributed to the high surface coverage of 2.4×10^{14} molecules per cm^2 and to the fact that the molecules are oriented upright indicating almost all phosphorous is located at the dielectric surface.

Polymer based substrates, as shown in figure 1, were used for n-type SAMFETs in order to demonstrate their applicability in flexible electronic devices. The resulting transfer characteristics are shown in figure 4. The transistor channel length was $2.5\ \mu\text{m}$ and the width $1000\ \mu\text{m}$. Electron mobilities of $5 \times 10^{-4}\ \text{cm}^2/\text{Vs}$ in the saturation regime and high on/off ratios on the order of 10^5 were obtained. By integrating two transistors, enhancement load NMOS inverters were realized. The schematic of the inverter is presented in the inset of figure 4b. The channel length of the transistors is $2.5\ \mu\text{m}$, the width of the load was $200\ \mu\text{m}$ and the width of the driver $2000\ \mu\text{m}$. Figure 4c shows the output voltage as function of the input bias for a supply bias (V_{DD}) of 15 V to 30V. The inverter shows a high output voltage for low input biases and a low output voltage for high input biases. However further design optimization should be made to improve the maximum and minimum output voltages.

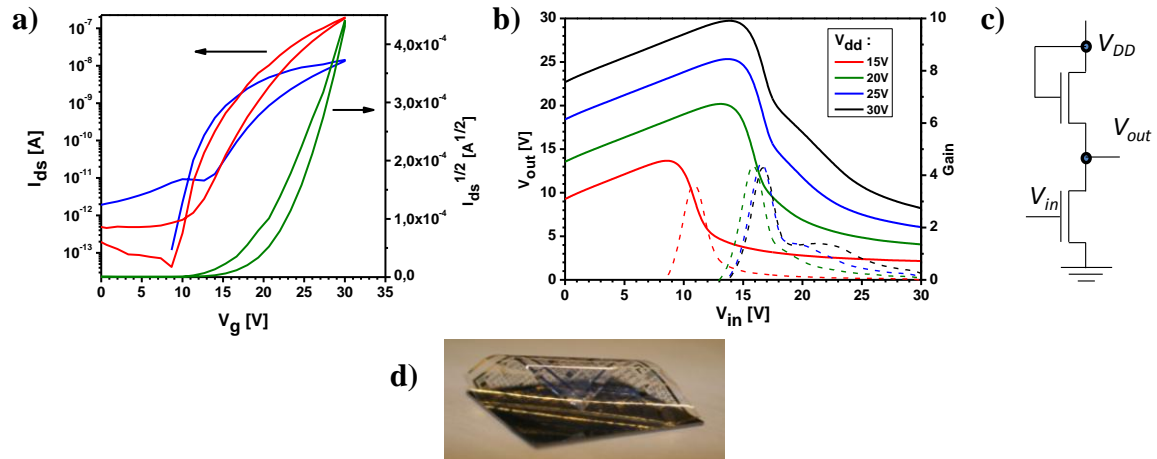


Figure 4: PBIF-PA SAMFET characteristics on a flexible polymer based substrates. **a)** Output characteristics of PBIF-PA SAMFET with a channel length of $2.5\ \mu\text{m}$ and a channel width of $500\ \mu\text{m}$. The drain voltage was varied from 5 V (blue) to 30 V (red). **b)** Characteristics of a unipolar NMOS bias inverter based on two integrated n-type PBIF-PA SAMFETs with a supply bias of 15 V to 30 V increased in steps of 5V. **c)** Schematic representation of enhancement load inverter. **d)** Optical image of a flexible substrate which was used for this paper.

3. Conclusion

A novel perylene bisimide with a phosphonic acid anchor group was tailored for application in self-assembled monolayer field-effect transistors (SAMFETs). The molecule self-assembles covalently onto aluminium oxide dielectrics. A homogeneous and dense monolayer is spontaneously formed in which the molecules stand upright to the surface. An amorphous 2-dimensional semiconducting layer allows charge transport without disturbing grain boundaries. Electron mobilities in the order of $10^{-3}\ \text{cm}^2/\text{Vs}$ were achieved on rigid as well on flexible substrates. To test the suitability of the perylene bisimide in more complex circuits, the first flexible NMOS bias inverter based on

SAMFETs was established, underpinning the capability of n-type SAMFETs for flexible organic electronics.

Acknowledgements

The work of Andreas Ringk forms part of the research programme of the Dutch Polymer Institute (DPI), project 624. The authors thank Oliver Werzer, Institute of Pharmaceutical Sciences, University Graz, Austria for his support in fitting of the X-ray reflectivity experiments.

4. Experimental Section

Preparation of PBIF-PA 6 N-(2,2,3,3,4,4,4-Heptafluoro-butyl)-N'-(undecyl-11-phosphonic acid) perylene-3,4,9,10-tetracarboxylic bisimide.

Materials and methods: The starting materials perylene-3,4,9,10-tetracarboxylic dianhydride, potassium hydroxide, ammonia, 1,11-dibromoundecane, sodium hydride, triethyl phosphite, bromotrimethylsilane, and solvents were purchased from Aldrich, Acros Organics and VWR. Solvents used for precipitation and column chromatography were distilled once before use. ^1H - and ^{13}C -NMR spectra were recorded on a Bruker AC 250 spectrometer (250 MHz). Chemical shifts are reported in ppm at room temperature using CDCl_3 as solvent and internal standard. Mass spectroscopic data were obtained from a FINNIGAN MAT 8500 instrument. An overview of the synthesis is given in figure 5.

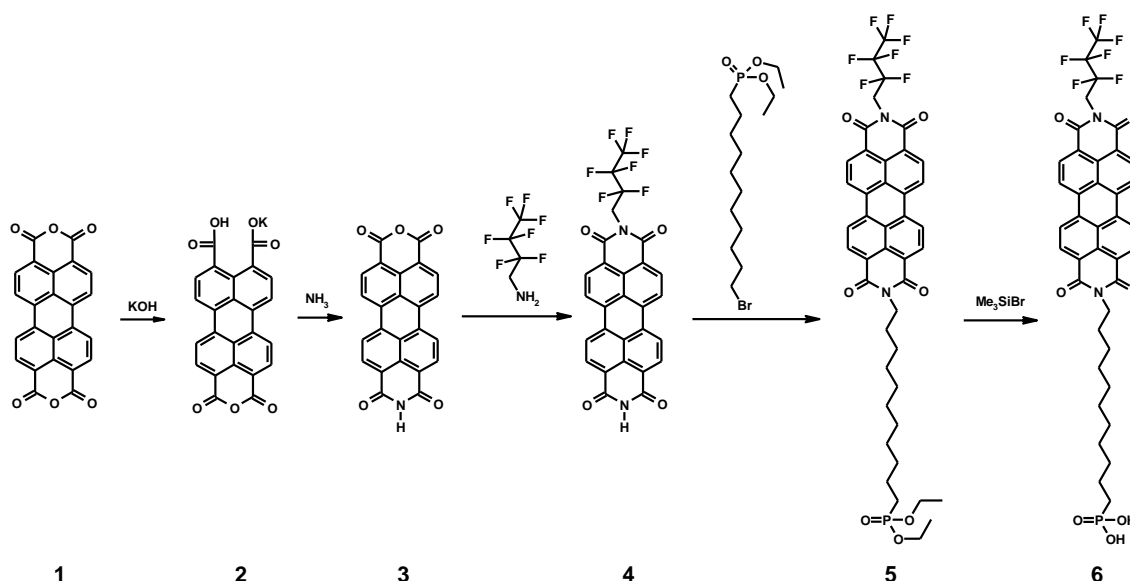


Figure 5: Overview of the synthetic strategy towards the target molecule PBIF-PA. Compounds 1-3 were synthesized according to a slightly modified literature procedure.^[27]

Preparation of N-(2,2,3,3,4,4,4-Heptafluoro-butyl)- perylene-3,4,9,10-tetracarboxylic bisimide 4.

Monoimide 3 (1 g, 2.55 mmol) and 2,2,3,3,4,4,4-Heptafluoro-butylamine (0.5 ml, 3.75 mmol) was heated together with 15 g Imidazole under argon in a sealed vessel at 140°C. After 8 hours the mixture was cooled to room temperature and poured into a mixture of 300 ml 2N HCl and 100 ml EtOH. The precipitate was filtered off, dried at 110°C in vacuum for 12 hours. 1.3 g (2.27 mmol, 89%) of a red solid was obtained, which was used without further purification.

EIMS(m/z): $[M]^+$ calculated for $C_{28}H_{11}F_7N_2O_4$, 572.40; found, 572.

1H -NMR (300 MHz, $CDCl_3$ /Trifluoroacetic acid- D_1 , δ): 5.12 (t; 15.4 Hz; 2H; N- CH_2), 8.80 - 8.93 (m; 8H; aromatic-H).

Preparation of N-(2,2,3,3,4,4,4-Heptafluoro-butyl)-N`-(undecyl-11-phosphonic acid dieylester) perylene-3,4,9,10-tetracarboxylic bisimide 5.

Perylenebisimide 4 (500 mg, 0.87 mmol) and sodium hydride (43 mg, 65% dispersed in mineral oil, 1.15 mmol) were dissolved in 30 ml dry DMF and stirred at room temperature. After 6 h the solution was heated to 85°C. After additional 12 h 11-Bromo-undecyl-phosphonic acid diethyl ester^[28] (0.36 g, 0.97 mmol) were added. After additional 48 h the reaction mixture was cooled to room temperature, filtered and extracted with $CHCl_3$. The solvent was evaporated, the crude product redissolved in $CHCl_3$ and poured into methanol. The precipitate was filtered off and purified by flash chromatography (solvent gradient EtOAc/THF 10:1 \rightarrow THF). The resulting red solid was freeze dried with dioxane to yield 281 mg (0.33 mmol, 38%) of 5.

EIMS(m/z): $[M]^+$ calculated for $C_{43}H_{42}F_7N_2O_7P$, 863.79; found, 863

1H -NMR (300 MHz, $CDCl_3$, δ): 1.16 – 1.51 (m; 22H; aliphatic-H), 1.68 – 1.84 (m; 4H; 2x CH_2), 4.01 – 4.15 (m; 4H; 2xP- CH_2), 4.19-4.24 (t; J = 7.7 Hz; 2H; N- CH_2), 5.03 – 5.08 (t; 15.5 Hz; 2H; N- CH_2), 8.55 – 8.70 (m; 8H; aromatic-H).

^{13}C -NMR (75 MHz, $CDCl_3$, δ): 16.80, 22.73, 25.08, 26.94, 27.48, 28.43, 29.46, 29.71, 29.88, 30.88, 31.11 (aliphatic C), 41.09 (C-N), 61.69 (C-P), 61.77 (C-N), 122.55, 123.40, 123.78, 123.93, 129.52, 129.84, 131.67, 132.40, 134.41, 135.64, 163.31, 163.55 (aromatic and fluorinated C).

^{31}P -NMR (120 MHz, $CDCl_3$, δ): 32.75.

Preparation of PBIF-PA 6 N-(2,2,3,3,4,4,4-Heptafluoro-butyl)-N'-(undecyl-11-phosphonic acid) perylene-3,4,9,10-tetracarboxylic bisimide 6.

Perylenebisimide 5 (280 mg, 0.32 mmol) was dissolved under argon in 50 ml dry CH_2Cl_2 , cooled to 0°C and bromotrimethylsilane (1 ml, 7.58 mmol) was added dropwise through a syringe. After addition of the silane, the reaction mixture was allowed to warm up to room temperature. After 48 h stirring, 5 ml water was added. After additional 2 h, the mixture was poured into 50 ml of a mixture of methanol and water (1:1). The resulting precipitate was collected by filtration. To obtain a fluffy powder, the red solid was dissolved in trifluoroacetic acid (TFA), dropped into dioxane, and subsequently freeze dried to obtain 250 mg (0.31 mmol, 97%) of the phosphonic acid 6 which was used without further purification.

$^1\text{H-NMR}$ (300 MHz, CDCl_3/TFA , δ): 1.23 – 1.50 (m; 18H; aliphatic-H), 1.58 – 1.67 (m; 2H; 2xP-OH), 1.72 – 1.82 (m; 2H; CH_2), 1.87 – 2.00 (m; 2H; CH_2), 4.25 (t, 7.4 Hz; 2H; N- CH_2), 5.08 (t; 15.33 Hz; 2H; N- CH_2), 8.79 – 8.88 (m, 8H; aromatic-H).

Experimental Details

Specular X-ray reflectivity (XRR) measurements were performed on a Panalytical Empyrean Reflectometer set up with copper sealed tube, a $1/32^\circ$ primary slit, a 10mm beam mask and a multilayer mirror ($\lambda = 0.1542$ nm) on the primary side. A small receiving slit of 0.1 mm and a 3D Panalytical Pixcel detector were used on the secondary side. The experimental data were fitted with Parrat formalism^[29] using X'Pert Reflectivity 1.3 software (PANalytical). The surface roughness and the interface roughness of the specimen were determined using the Nevot and Croce approach.^[30]

Grazing incidence x-ray diffraction (GIXD) measurements were performed at the beamline W1 at the synchrotron HASYLAB, Germany. A wavelength of 0.11807 nm was used. The incidence angle of the primary beam was chosen at the optimum value $\alpha_i=0.15^\circ$ resulting in the best signal to noise ratio. The samples were investigated in an inert helium atmosphere provided by a stage with a domed x-ray window (DHS900, AntonPaar).^[31] The results of in-plane GIXD measurements are presented reciprocal space maps measured by a one dimensional position sensitive detector (Mythen 1K, Dectris).

References

- [1] Queffélec, C.; Petit, M.; Janvier, P.; Knight, D. A.; Bujoli, B. Surface Modification Using Phosphonic Acids and Esters. *Chem. Rev.* **112**, **2012**, 3777-3807.
- [2] Cheng, X.; Noh, Y.-Y.; Wang, J.; Tello, M.; Frisch, J.; Blum, R.-P.; Vollmer, A.; Rabe, J. P.; Koch, N.; Sirringhaus, H. Controlling Electron and Hole Charge Injection in Ambipolar Organic Field-Effect Transistors by Self-Assembled Monolayers. *Adv. Funct. Mater.* **15**, **2009**, 2407-2415.
- [3] Novak, M.; Schmaltz, T.; Faber, H.; Halik, M. Influence of self-assembled monolayer dielectrics on the morphology and performance of α,ω -dihexylquaterthiophene in thin film transistors. *Appl. Phys. Lett.* **9**, **2011**, 93302.
- [4] Ando, T.; Fowler, A. B.; Stern, F. Electronic properties of two-dimensional systems. *Rev. Mod. Phys.* **2**, **1982**, 437-672.
- [5] Dinelli, F.; Murgia, M.; Levy, P.; Cavallini, M.; Biscarini, F.; Leeuw, D. de. Spatially Correlated Charge Transport in Organic Thin Film Transistors. *Phys. Rev. Lett.* **11**, **2004**, 116802.
- [6] Liu, S. W.; Lee, C.-C.; Wen, J.-M.; Chen, C.-T. C. In situ vacuum measurement of the thickness dependence of electron mobility in naphthalenetetracarboxylic diimide-based field-effect transistors. *Appl. Phys. Lett.* **98**, **2011**, 023306.
- [7] Tulevski, G. S.; Miao, Q.; Fukuto, M.; Abram, R.; Ocko, B.; Pindak, R.; Steigerwald, M. L.; Kagan, C. R.; Nuckolls, C. Attaching Organic Semiconductors to Gate Oxides: In Situ Assembly of Monolayer Field Effect Transistors. *J. Am. Chem. Soc.* **46**, **2004**, 15048-15050.
- [8] Mathijssen, S. G. J.; Smits, E. C. P.; van Hal, P. A.; Wondergem, H. J.; Ponomarenko, S. A.; Moser, A.; Resel, R.; Bobbert, P. A.; Kemerink, M.; Janssen, R. A. J.; Leeuw, D. M. de. Monolayer coverage and channel length set the mobility in self-assembled monolayer field-effect transistors. *Nat. Nanotech.* **10**, **2009**, 674-680.
- [9] Mottaghi, M.; Lang, P.; Rodriguez, F.; Rumyantseva, A.; Yassar, A.; Horowitz, G.; Lenfant, S.; Tondelier, D.; Vuillaume, D. Low-Operating-Voltage Organic Transistors Made of Bifunctional Self-Assembled Monolayers. *Adv. Funct. Mater.* **4**, **2007**, 597-604.
- [10] Hutchins, D. O.; Acton, O.; Weidner, T.; Cernetic, N.; Baio, J. E.; Ting, G.; Castner, D. G.; Ma, H.; Jen, A. K.-Y. Spin cast self-assembled monolayer field effect transistors. *Org. Electr.* **3**, **2012**, 464-468.
- [11] Smits, E. C. P.; Mathijssen, S. G. J.; van Hal, P. A.; Setayesh, S.; Geuns, T. C. T.; Mutsaers, K. A. H. A.; Cantatore, E.; Wondergem, H. J.; Werzer, O.; Resel, R.; Kemerink, M.; Kirchmeyer, S.; Muzafarov, A. M.; Ponomarenko, S. A.; Boer, B. de; Blom, P. W. M.; Leeuw, D. M. de. Bottom-up organic integrated circuits. *Nature.* **7215**, **2008**, 956-959.
- [12] Andringa, A. M.; Spijkman, M. J.; Smits, E. C. P.; Mathijssen, S. G. J.; van Hal, P. A.; Setayesh, S.; Willard, N. P.; Borshchev, O. V.; Ponomarenko, S. A.; Blom,

- P. W. M.; de Leeuw, D. M. Gas sensing with self-assembled monolayer field-effect transistors. *Org. Electr.* **11**, **2010**, 895-898.
- [13] de Leeuw, D. M.; Simenon, M.M.J.; Brown, A. R.; Einerhand, R.E.F. Stability of n-type doped conducting polymers and consequences for polymeric microelectronic devices. *Synt. Met.* **87**, **1997**, 53-59.
- [14] Novak, M.; Ebel, A.; Meyer-Friedrichsen, T.; Jedaa, A.; Vieweg, B. F.; Yang, G.; Voitchovsky, K.; Stellacci, F.; Spiecker, E.; Hirsch, A.; Halik, M. Low-Voltage p- and n-Type Organic Self-Assembled Monolayer Field Effect Transistors. *Nano Lett.* **1**, **2011**, 156-159.
- [15] Rumpel, A.; Novak, M.; Walter, J.; Braunschweig, B.; Halik, M.; Peukert, W. Tuning the Molecular Order of C60 Functionalized Phosphonic Acid Monolayers. *Langmuir.* **24**, **2011**, 15016-15023.
- [16] Ringk, A.; Li, X.; Gholamrezaie, F.; Smits, E. C. P.; Neuhold, A.; Moser, A.; van der Marel, C.; Gelinck, G. H.; Resel, R.; de Leeuw, D. M.; Strohriegel, P. N-Type Self-Assembled Monolayer Field-Effect Transistors and Complementary Inverters. *Adv. Funct. Mater.* **2012**, in press.
- [17] Yan, H.; Chen, Z.; Zheng, Y.; Newman, C.; Quinn, J. R.; Dötz, F.; Kastler, M.; Facchetti, A. A high-mobility electron-transporting polymer for printed transistors. *Nature.* **7230**, **2009**, 679-686.
- [18] Gholamrezaie, F.; Mathijssen, S. G. J.; Smits, E. C. P.; Geuns, T. C. T.; van Hal, P. A.; Ponomarenko, S. A.; Flesch, H.-G.; Resel, R.; Cantatore, E.; Blom, P. W. M.; Leeuw, D. M. de. Ordered Semiconducting Self-Assembled Monolayers on Polymeric Surfaces Utilized in Organic Integrated Circuits. *Nano Lett.* **6**, **2010**, 1998-2002.
- [19] Lodziana, Z.; Norskov, J. K.; Stoltze, P. The stability of the hydroxylated (0001) surface of alpha-Al₂O₃. *J. Chem. Phys.* **24**, **2003**, 11179-11188.
- [20] Chua, L.-L.; Zaumseil, J.; Chang, J.-F.; Ou, E. C.-W.; Ho, P. K.-H.; Sirringhaus, H.; Friend, R. H. General observation of n-type field-effect behaviour in organic semiconductors. *Nature.* **7030**, **2005**, 194-199.
- [21] Wapner, K.; Stratmann, M.; Grundmeier, G. Structure and stability of adhesion promoting aminopropyl phosphonate layers at polymer/aluminium oxide interfaces. *Int. J. Adhes. Adhes.* **28**, **2008**, 59-70.
- [22] Egginger, M.; Bauer, S.; Schwödiauer, R.; Neugebauer, H.; Sariciftci, N. S. *Monatsh. Chem.* Current versus gate voltage hysteresis in organic field effect transistors. **140**, **2009**, 735-750.
- [23] Krauss, T. N.; Barrena, E.; Zhang, X. N.; Oteyza, D. G. de; Major, J.; Dehm, V.; Würthner, F.; Cavalcanti, L. P.; Dosch, H. Three-Dimensional Molecular Packing of Thin Organic Films of PTCDI-C 8 Determined by Surface X-ray Diffraction. *Langmuir.* **22**, **2008**, 12742-12744.
- [24] Jones, B. A.; Facchetti, A.; Wasielewski, M. R.; Marks, T. J. Tuning Orbital Energetics in Arylene Diimide Semiconductors. Materials Design for Ambient Stability of n-Type Charge Transport. *J. Am. Chem. Soc.* **49**, **2007**, 15259-15278.

- [25] Geng, Y.; Wang, J.; Wu, S.; Li, H.; Yu, F.; Yang, G.; Gao, H.; Su, Z. Theoretical discussions on electron transport properties of perylene bisimide derivatives with different molecular packings and intermolecular interactions. *J. Mater. Chem. A*, **2011**, 134–143.
- [26] Nolde, F.; Pisula, W.; Müller, S.; Kohl, C.; Müllen, K. Synthesis and Self-Organization of Core-Extended Perylene Tetracarboxdiimides with Branched Alkyl Substituents. *Chem. Mater.* **18**, **2006**, 3715.
- [27] Wicklein, A.; Lang, A.; Muth, M.; Thelakkat, M. Swallow-Tail Substituted Liquid Crystalline Perylene Bisimides: Synthesis and Thermotropic Properties. *J. Am. Chem. Soc.* **131**, **2009**, 14442–14453.
- [28] Wang, X.; Lieberman, M. Zirconium–Phosphonate Monolayers with Embedded Disulfide Bonds. *Langmuir*. **18**, **2003**, 7346–7353.
- [29] Parratt, L. G. Surface Studies of Solids by Total Reflection of X-Rays. *Phys. Rev.* **95**, **1954**, 359.
- [30] Croce, P.; Névod, L. Étude des couches minces et des surfaces par réflexion rasante, spéculaire ou diffuse, de rayons X. *Rev. Phys. Appl. (Paris)* **11**, **1976**, 113-125.
- [31] Resel, R.; Tamas, E; Sonderegger, B; Hofbauer, P; Keckes, J. A heating stage up to 1173 K for X-ray diffraction studies in the whole orientation space. *J. Appl. Cryst.* **36**, **2003**, 80-85.

Supporting information for:

**N-Type Self-Assembled Monolayer Field-Effect Transistors
for Flexible Organic Electronics**

Content:

SAMFET device fabrication

Molecular modelling

X-ray photoelectron spectroscopy

X-ray reflectivity measurements

SAMFET device fabrication

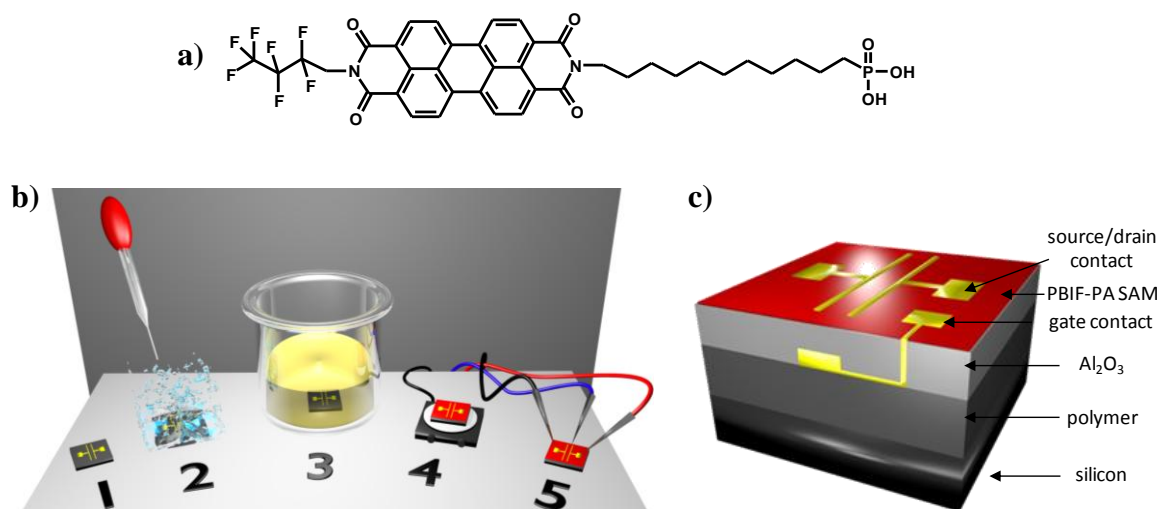


Figure S1: a) Chemical structure of PBIF-PA b) Illustration of the n-type SAMFET fabrication process. c) Scheme of SAMFET layout.

Bottom gate, bottom contact transistor substrates with an aluminium oxide dielectric were used for the SAMFET fabrication process. The substrate was cleaned by rinsing with isopropanol and hexane. Afterwards, the substrate was exposed to UV-ozone, which removed smallest amounts of organic residues and further activated the aluminium oxide. The cleaned substrate was put into a dilute solution of PBIF-PA in dimethylformamide (DMF). The solution had a concentration of 10^{-5} mol/L of PBIF-PA and was filtered through a $0.2 \mu\text{m}$ PTFE filter before use. The substrate was taken out of the solution after 24 hours and rinsed with DMF in order to remove residues from the surface. To remove DMF residues and to complete the condensation reaction of the phosphonic acid to aluminium oxide, the substrate was backed at 110°C for 20 min on a hotplate under inert conditions and subsequently measured. The chemical structure of PBIF-PA, the device fabrication process, and the SAMFET layout is depicted in figure S1.

Substrate fabrication

Bottom-gate/bottom-contact transistor substrates with patterned gate and interconnections were fabricated on flexible PEN foils. A proprietary foil on carrier process was used to laminate $25 \mu\text{m}$ heat stabilized PEN foils to a silicon monitor wafer. The gate was created by sputtering a thin gold layer and structuring it via photolithographic processes. On top a 100 nm thick Al_2O_3 layer was grown by atomic layer deposition (ALD) at 120°C using trimethylaluminum and H_2O as precursors. Next

vertical interconnections were created to enable contacting the gate. Finally the gold source and drain electrodes were deposited via sputtering and structured by conventional photolithography on top of the Al_2O_3 . The whole process was developed to remain below 150°C compatible for PEN foil. To facilitate the anchoring of the phosphonic acid to the dielectric, the Al_2O_3 was cleaned with solvents (acetone and isopropanol) and activated by UV-ozone treatment. After self-assembly of the semiconductor, the foil can be released from its carrier.

Molecular modelling

The intramolecular distances were calculated using Avogadro 1.0.3 software with the united force-field (UFF). The molecule PBIF-PA can be segmented into three different regions: a short fluorinated end capper (0.39 nm), the aromatic core (1.13 nm) and an aliphatic spacer (1.17 nm). All three layers and the calculated molecular length of 2.69 nm matches well with the lengths obtained the XPS and X-ray reflectivity measurements.

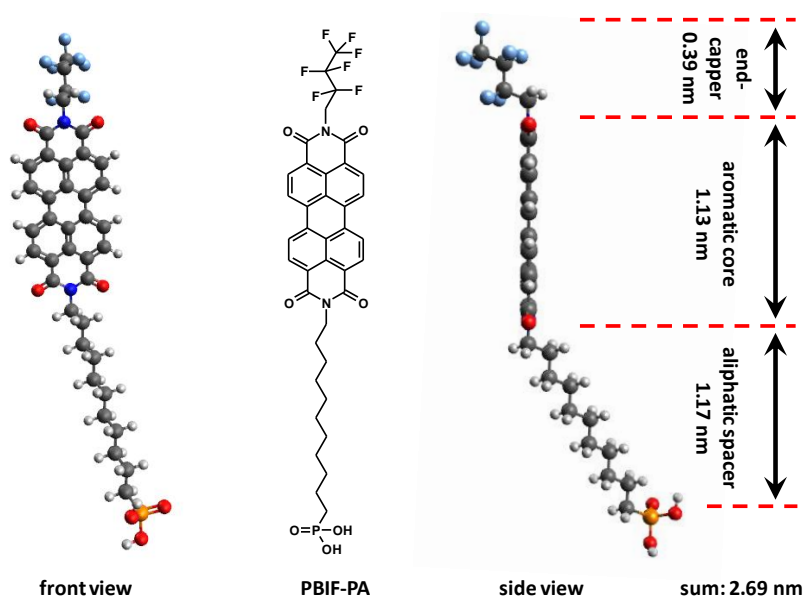


Figure S2. Illustration of the calculated intramolecular distances of PBIF-PA.

X-ray photoelectron spectroscopy (XPS)

Experimental details:

The measurements have been carried out in a Quantera SXMtm from Ulvac-PHI. The measurements have been performed using monochromatic $\text{AlK}\alpha$ -radiation and a

rectangular measurement area of $\approx 500 \times 250 \mu\text{m}$. By means of wide-scan measurements the elements present at the surface have been identified. The chemical state and the atomic concentrations of the elements present are determined from accurate narrow-scan measurements. Standard PHI-sensitivity factors^[1,2] were used to convert peak areas to atomic concentrations. As a result of this, it is possible that the concentrations deviate from reality in the absolute sense (generally not more than 20% relative).

Results and discussion:

XPS-analyses have been performed on the PBIF-PA samples to verify the presence of a monolayer of this material. First, survey spectra have been measured to determine which elements are present in the upper $\approx 7 \text{ nm}$ of the sample. These measurements demonstrated the presence of the elements Al, C, O, N, F and P. Next, angular resolved measurements have been done of the main peaks of the elements present at the surface; the take-off angle Θ was 80° , 20° and 80° . The apparent concentrations calculated from the peak areas are summarized in table S1. In this table is also shown which XPS line was measured, the peak position and the most likely chemical assignment.

Table S1: Apparent concentrations (at%) measured for two values of the take-off angle Θ . In the lower row, the concentration ratios $c_{\Theta = 80^\circ} / c_{\Theta = 20^\circ}$ are given. A large value of this ratio corresponds to a relatively large distance of the component from the outer surface.

Pos.	Θ ($^\circ$)	Al 2p	C 1s			F 1s		N 1s	O 1s	P 2s
		74.6	289, 291	28 5	288	688.4	685.6	400.4		191.0
		Al ₂ O ₃	CF ₂ , CF ₃	CH	N-C=O	CF ₂ , CF ₃	F	N-C=O		-PO ₃
B	80	20	2.0	27	2.5	7.2	1.6	1.4	37	0.8
B	20	8	4.8	47	5.5	13.7	0.7	2.6	18	0.8
B	80	20	2.3	29	2.2	5.0	1.7	1.4	37	0.7
<ratio 80 / 20>										
		2.7	0.4	0.6	0.4	0.4	2.3	0.5	2.1	0.9

Remarks to the results in table S1:

- The first and the second measurement for $\Theta = 80^\circ$ are in reasonable agreement except for the concentration of organic Fluor. The decrease of the concentration organic Fluor is a consequence of radiation damage.
- Based on the concentration ratios we conclude that the layer structure of the sample is as follows:

Al_2O_3 and F / P / organic layer containing C, O, and N / organic F and CF_2 , CF_3

To obtain insight into the thickness of the organic layer and the real concentrations, model calculations have been performed,^[3,4] for details about this method and the application to SAMFET-layers we refer to [5]. The results of the calculations are given in table S2.

Table S2: Results model calculations: values are given for the thickness of the organic layer, D_{org} , the coverage with P, N_p , and the real atomic concentrations in the organic layer. In the lower row the theoretical composition is given based on the molecular structure of PBIF-PA.

Θ	D_{org}	N_p	real concentrations in SAM-layer (in at%)					
($^\circ$)	(nm)	(at/cm^2)	C1s		F1s	N 1s	O1s	P 2s
			CF_2 , CF_3	C-H, NCO	CF_2 , CF_3		-org	-PO3
80	2.38	$2.1\text{E}+14$	3.8	75	10	3.1	6.2	2.4
20	2.69	$2.4\text{E}+14$	3.7	76	7	3.6	7.2	2.4
80	2.38	$2.0\text{E}+14$	4.3	78	6	3.1	6.1	2.3
theoretical composition (at%)			74		13	3.8	7.5	1.9
number of atoms / molecule			39		7	2	4	1
			C		F	N	O	P

Remarks to the results in table S2:

- The real concentrations derived from the measurements are in reasonable agreement with the theoretical composition, except for the concentration of F. This is related to loss of organic Fluor due to the irradiation of the sample with X-rays.

- Starting from the small angle results ($\Theta = 20^\circ$) a larger layer thickness D_{org} is found compared to the value of D_{org} obtained from the large angle results ($\Theta = 80^\circ$). An important assumption for the model calculations is the assumption that the IMFP (Inelastic Mean Free Path) of the electrons is independent of the directions the electrons are travelling. The present PFIB-PA layer clearly contains molecules all oriented into the same direction. Possibly the IMFP for electrons travelling in a nearly-perpendicular direction ($\Theta = 80^\circ$) is longer than the values for the IMFP used in the model calculations (and valid for a homogeneous organic material; see Ref. 5). For electrons travelling into a more glancing direction ($\Theta = 20^\circ$) the influence of the orientation of the molecules on the IMFP is expected to be negligible. By consequence, the model calculation starting from the measurements at 80° probably are less reliable. Remark: the conjecture that the IMFP in the PBIF-PA is dependent on the orientation of the electrons relative to the SAM-molecules is subject for further investigations.

X-ray reflectivity (XRR)

Two X-ray reflectivity measurements were performed to obtain the morphology of the SAM. In a first step the X-ray reflectivity measurement of a bare substrate was investigated. The known layer stack was used as input parameter to the fit of the experimental data. It consists of a native oxide silicon wafer with a coverage of 100 nm aluminium oxide. Additionally a top layer with low electron density had to be introduced to get a proper fit of the experimental data. This layer could result from adsorbed water due to handling of the substrate under ambient conditions. Figure S3 shows the X-ray reflectivity curve with the corresponding fit of the data, the fitting parameter are given in Table S3. The X-ray reflectivity curve of the SAM is depicted in Figure 2 of the manuscript. For fitting the SAM a three layer model was used according to the different electron densities within a single SAM, the fitting parameters of the substrate was kept identical to the bare substrate (except the top layer). Table S4 gives the fitting parameters of the SAM.

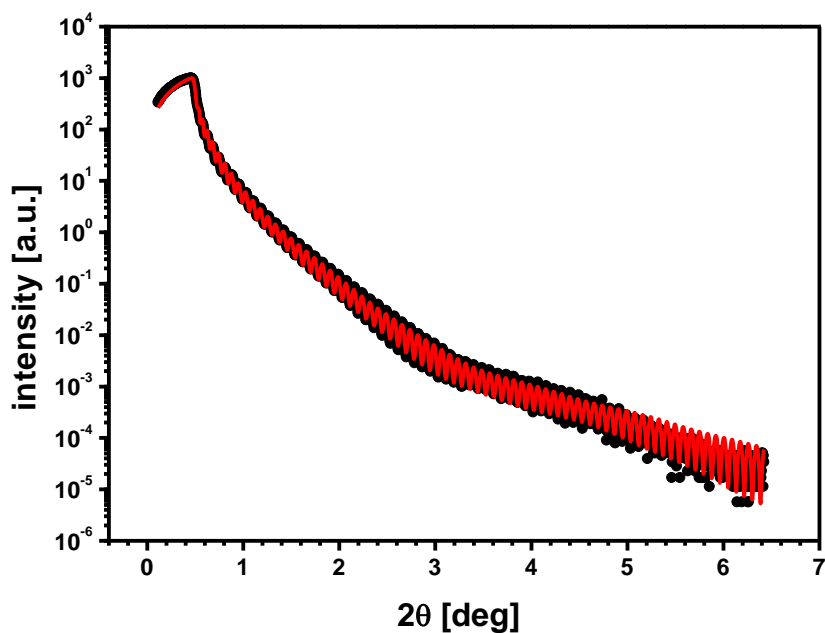


Figure S3: X-ray reflectivity curve (black dots) of the bare substrate together with a fit of the experimental data (red line).

Table S3: The fit parameters of the x-ray reflectivity curve from a bare substrate. The sequence of the inorganic layers is according to the preparation process of the substrate, a top layer had to be introduced to get a proper match to the experimental data.

Layer	thickness [nm]	roughness [nm]	electron density [nm ⁻³]
top layer	1.1	0.40	382
Al ₂ O ₃	103.0	0.65	854
SiO ₂	2.0	0.54	676
Si	∞	0.37	703

Table S4: The fit parameters of the X-ray reflectivity curve of a SAM with a three layer model. The parameters of the substrate was taken from the bare substrate (except the top layer) and kept fixed during the fit.

Layer	thickness [nm]	roughness [nm]	electron density [nm ⁻³]
fluorinated tail	0.60	0.18	225
aromatic core	0.93	0.13	403
alkyl spacer	1.15	0.30	206

Grazing incidence X-ray diffraction (GIXD)

A reciprocal space map of a PBIF-PA SAM taken by GIXD is given in Figure S4a. Integration of the scattered intensity along the z -component of the scattering vector q_z reduces the data to an intensity distribution as a function of the in-plane component of the scattering vector q_{xy} (Figure S4b). A broad diffraction feature is observed at around 18 nm^{-1} . The origin of this peak cannot be clearly assigned to the SAM or to the amorphous Al_2O_3 substrate, since either orientationally ordered pi-conjugated units as well as the amorphous aluminium oxide substrate shows a correlation peak at this value.^[6,7] Drop casted films of PBIF-PA reveal a strong tendency of the molecule to form layered structures with layers parallel to the substrate surface as observed by XRR. However, drop casted films do not show any crystalline diffraction peaks by GIXD.

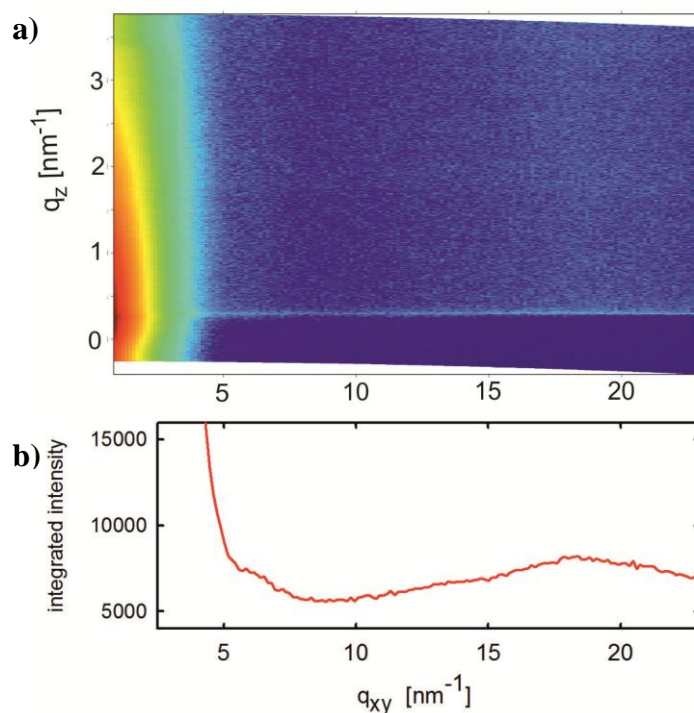


Figure S4: **a)** Reciprocal space map of a PBIF-PA SAM measured by grazing incidence x-ray diffraction (above). **b)** The scattered intensities are integrated along q_z ($q_z = 0 \dots 3.5 \text{ nm}^{-1}$) so that an intensity distribution as a function of the in-plane component of the scattering vector q_{xy} can be plotted.

Refernces

- [1] Moulder, J. F.; Stickle, W. F.; Sobol, P. E.; Bomben, K. D. Handbook of X-ray Photoelectron Spectroscopy, (Ed: J. Chastain), Perkin-Elmer Corporation, Physical Electronics, Eden Prairie, **1992**.
- [2] PHI-Multipak Software Manual Version 6.0 (Physical Electronics Division, Eden Prairie, **1998**.
- [3] van der Marel, C.; Yildirim, M.; Stapert, H. R. Multilayer approach to the quantitative analysis of X-ray photoelectron spectroscopy results: Applications to ultrathin SiO₂ on Si and to self-assembled monolayers on gold. *Vac. Sci. Technol. A*. **23**, **2005**, 1456.
- [4] van der Marel, C.; Verheijen, M. A.; Tamminga, Y.; Pijnenburg, R. H. W.; Tombros, N.; Cubaynes, F. Thickness and composition of ultrathin SiO₂ layers on Si. *Vac. Sci. Technol. A*. **22**, **2004**, 1572.
- [5] Ringk, A.; Li, X.; Gholamrezaie, F.; Smits, E. C. P.; Neuhold, A.; Moser, A.; van der Marel, C.; Gelinck, G. H.; Resel, R.; de Leeuw, D. M.; Strohriegl, P. N-Type Self-Assembled Monolayer Field-Effect Transistors and Complementary Inverters. *Adv. Funct. Mater.* **2012**, in press.
- [6] Lamparter, P; Kniep, R. Structure of amorphous Al₂O₃. *Physica B*, **405**, **1997**, 234-236.
- [7] Resel, R.; Kiebooms, R.; Vanderzande, D.; Stelzer F. Intermolecular order of poly(2,5-dimethyl *para*-phenylene vinylene) and poly(*paraphenylene vinylene*) - a comparison. *Monatsh. Chem.* **132**, **2001**, 433-440.

APPENDIX - N-TYPE SELF-ASSEMBLED MONOLAYER FIELD-EFFECT TRANSISTORS

Andreas Ringk,^{a,b} Xiaoran Li,^{c,d} Fatemeh Gholamrezaie,^{b,e,f} Edsger C. P. Smits^{c,*},
Alfred Neuhold,^g Armin Moser,^g Gerwin H. Gelinck,^c
Roland Resel,^g Dago M. de Leeuw,^{e,f} Peter Strohrriegl^{a,*}

^aMacromolecular Chemistry I, University of Bayreuth, 95440 Bayreuth, Germany

^bDutch Polymer Institute (DPI), P.O. Box 902, 5600 AX Eindhoven, The Netherlands

^cHolst Centre/TNO, High Tech Campus 31, 5656 AE Eindhoven, The Netherlands

^dDepartment of Chemical Engineering and Chemistry, Eindhoven University of
Technology P.O. Box 513, 5600 MB Eindhoven, The Netherlands,

^ePhilips Research Laboratories, High Tech Campus 4, 5656 AE Eindhoven,
The Netherlands

^fMolecular Electronics, Zernike Institute for Advanced Materials, University of
Groningen, Nijenborgh 4, 9747 AG Groningen, The Netherlands

^gInstitute of Solid State Physics, Graz University of Technology, Petersgasse 16, A-8010
Graz, Austria

Published in Proceedings of SPIE, **2012**

8478, 847813

DOI: 10.1117/12.929535

Reprinted with permission; Copyright © 2012 SPIE

Abstract:

Within this work we present the synthesis and applications of a novel material designed for n-type self-assembled monolayer field-effect transistors (SAMFETs). Our novel perylene bisimide based molecule was obtained in six steps and is functionalized with a phosphonic acid linker which enables a covalent fixation on aluminum oxide dielectrics. The organic field-effect transistors (OFETs) were fabricated by submerging predefined transistor substrates in a dilute solution of the molecule under ambient conditions. Investigations showed a thickness of about 3 nm for the organic layer which coincides to the molecular length. The transistors showed bulk-like electron mobilities up to $10^{-3} \text{ cm}^2/\text{Vs}$. Due to the absence of bulk current high on/off-ratios were achieved. An increase of the electron mobility with the channel length and XPS investigations point to a complete coverage of the dielectric with a dense monolayer. In addition, a p-type SAMFET based on a thiophene derivative and our new n-type SAMFET were combined to the first CMOS bias inverter based solely on SAMFETs.

Keywords: Self-assembled monolayer, n-type field-effect transistor, perylene bisimide, organic circuits, complementary inverter

1. Introduction:

Self-assembly is the spontaneous and autonomous organization of molecules into patterns¹. Self-assembling molecules usually contain an organic tail with one reactive group which is able to bind covalently to a surface. Dense and complete coverage can be achieved over large areas on a short time scale. The organic tails passivate the surface so that in many cases only one single monolayer is formed. Depending on the surface different anchor groups are used. The best known monolayers are thiols on gold. Organic acids or chlorosilanes are often used to modify inorganic oxides whereas silicon can be modified with materials having terminal double bonds by hydrosilylation². In such a way a monolayer is able to change the reactivity or polarity in order to passivate or protect the material surface.

Because the formation of self-assembled monolayers (SAMs) is a simple and quick method to achieve new material properties this technique arrived early in the broad field

of organic semiconducting devices. In organic solar cells monolayers of dye molecules on titanium dioxide are used for the absorption of light and an efficient charge transfer³. In organic light emitting diodes monolayers are used to modify indium tin oxide⁴. Also in organic field effect transistors (OFETs) SAMs are used to improve the performance. Common transistor substrates are based on silicon with a layer of silicon dioxide on top which is used as the dielectric. On this surface polar hydroxyl groups are present which have a negative influence on the charge transport especially for electrons⁵. In order to get rid of the polar groups, SAMs, for example chlorosilanes with long alkyl chains, are often used which react with the hydroxyl groups to create a non polar surface^[5]. The surface energy is also changing so that the monolayer can change the morphology of the semiconductor too⁶. It also has been shown that monolayers can be used as a thin dielectric resulting in transistors with very low operating voltages⁷. Because charge injection from the source electrode into the organic semiconductor plays a crucial role the electrodes, typically made of gold, can be covered with thiols in order to match the energy levels of the electrode and the organic semiconductor.⁸

It is known that charge transport in p- and n-type field-effect transistors occurs in an ultrathin accumulation layer close to the dielectric^{9,10}. This finding spurred interest in having a transistor with only one layer of a semiconducting molecule fixed to the dielectric surface by simple self-assembly (see Figure 1). A so called self-assembled monolayer field-effect transistor (SAMFET) was first demonstrated by Tulevski et al.¹¹ They attached a functionalized tetracene onto an aluminum oxide dielectric to form sub micron transistors. Meanwhile different other groups realized SAMFETs. Probably the best working SAMFETs are made from a thiophene derivative self-assembled onto a silicon dioxide surface¹². A dense, highly crystalline and well packed monolayer was formed to enable transistors with channel length up to 40 μm and hole mobilities of $10^{-2} \text{ cm}^2/\text{Vs}$. Additionally the first integrated circuits such as a 15 bit code generator were demonstrated using this bottom-up approach. Because the active channel in SAMFETs is only a single layer no bulk current occurs, which results in high on/off ratios up to 10^6 .

State of the art integrated circuits are mostly based on the well-established complementary metal oxide semiconductor (CMOS) technique, where pairs of p- and n-type transistors are combined in one device. The main advantages of CMOS-circuits are high noise immunity and low power consumption. Compared to p-type materials electron transporting transistors are more difficult to realize because of the high reactivity towards

enable the fixation to an aluminum oxide dielectric a phosphonic acid group is introduced to the perylene bisimide. Whereas homosubstituted PBIs can be synthesized in high yield in only one step from perylene-3,4,9,10-tetracarboxylic dianhydride (PTCDA), heterosubstituted PBIs are more difficult to realize. In principle two synthetic strategies are known¹⁶ to synthesize heterosubstituted PBIs. One of these routes was used for our synthesis and will be described in detail in the following chapter¹⁷.

PTCDA **1** is used as the starting material which is refluxed in a potassium hydroxide solution. During this reaction both anhydride groups are cleaved. Titration with acetic acid leads to the monopotassium salt **2**.

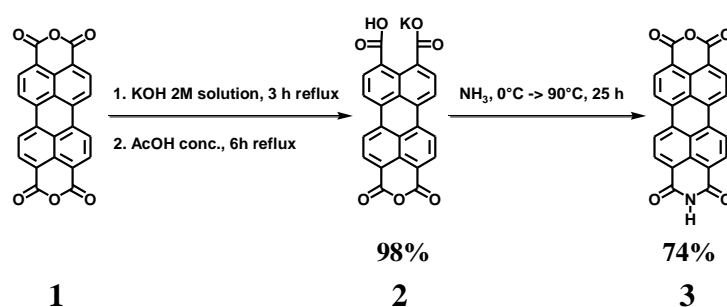


Figure 2: Synthetic strategy towards perylene monoimide anhydride.

The potassium salt **2** acts as a protective group so that in the following step ammonia reacts with the anhydride to form an imide group (Figure 2). After acidic workup the potassium group is transferred back into the anhydride to yield the asymmetric monoimide anhydride **3**.

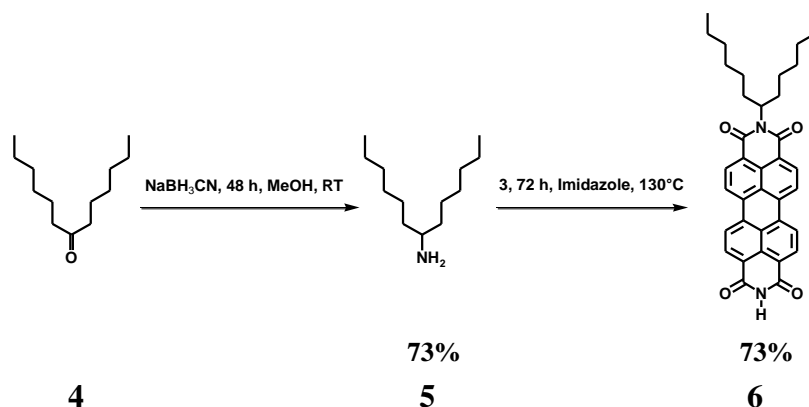


Figure 3: Synthetic strategy towards a heterosubstituted perylene bisimide.

Dihexylketone **4** reacts with sodium cyanoborohydride during a reductive amination reaction to the branched amine **5** (Figure 3)¹⁸. In the following step the amine **5** reacts with the previously synthesized perylene monoimide anhydride **3** to the heterosubstituted

perylene bisimide **6**. Due to the electron withdrawing character of the perylene core the proton of the bisimide **6** directly attached to the nitrogen can be removed with sodium hydride (Figure 4). The resulting anion reacts in an S_N2 -reaction with an excess of 1,11-dibromoundecane to form bisimide **7**.

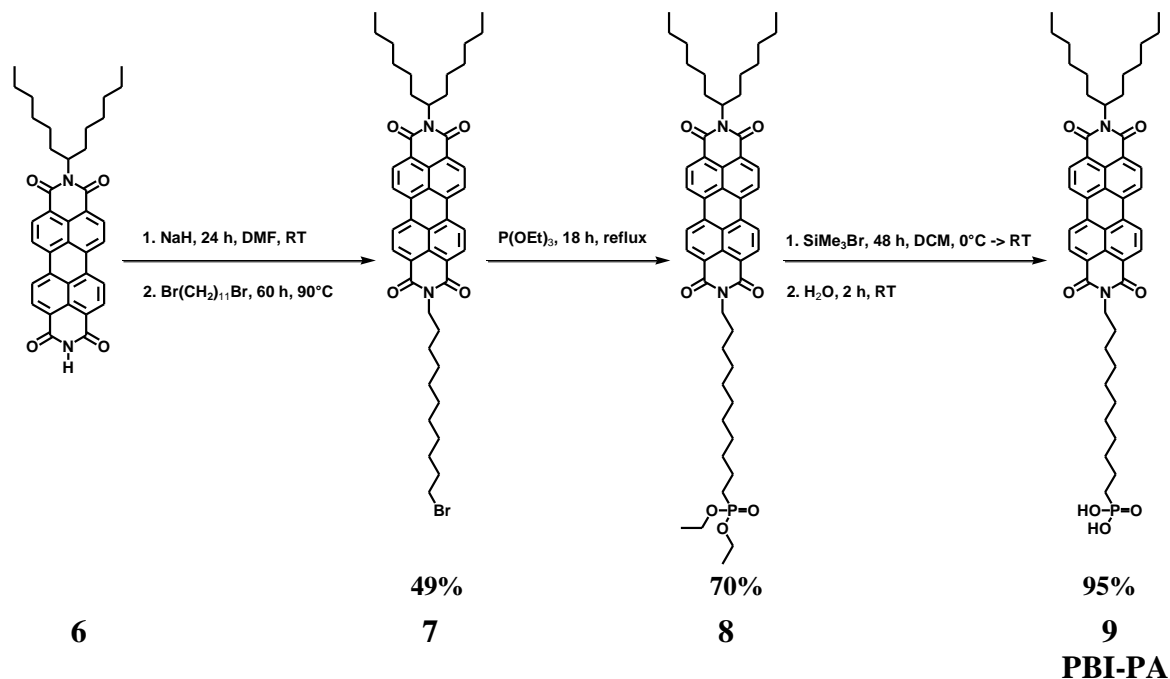


Figure 4: Synthetic strategy towards the target molecule PBI-PA 9.

The Michaelis-Arbusow reaction was used to transform bromide **7** into the phosphonic ester **8**. The phosphonic ester is cleaved using bromotrimethylsilane. After adding some water to the reaction mixture the phosphonic acid is generated and the target molecule PBI-PA **9** precipitates. Nuclear magnetic resonance (NMR) showed a complete conversion of the phosphonic ester **8** into the phosphonic acid PBI-PA **9**. The overall yield of the reaction sequence from **1** to **9** is 17 %.

UV-vis absorption and fluorescence measurements of PBI-PA in THF solution are depicted in figure 5. The absorption spectrum shows a maximum at 519 nm. Two additional blue-shifted vibrational satellites appear at 484 and 459 nm. The absorption edge is at 539 nm from which a band gap of 2.30 eV is calculated. After excitation at 484 nm the fluorescence spectrum shows an emission maximum at 529 nm. A second red-shifted peak appears at 568 nm with a shoulder at 611 nm.

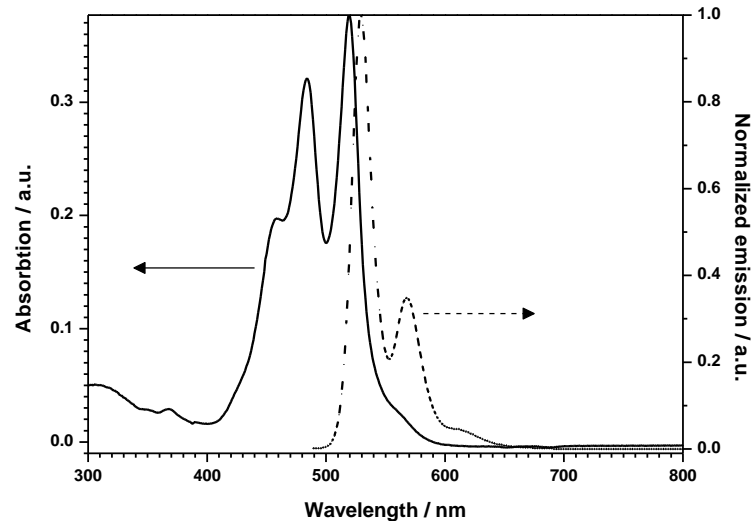


Figure 5: UV-vis absorption (solid line) and fluorescence (dotted line) spectra of PBI-PA in THF at room temperature. Concentration: 10^{-5} mol/L.

3. Device fabrication and measurements

For the device fabrication bottom gate/bottom contact transistor substrates were used having an aluminum oxide layer as dielectric and patterned gold source and drain electrodes. After a UV-ozone treatment the substrates were immersed into a 10^{-5} mol/L solution of PBI-PA in tetrahydrofuran (THF) under ambient conditions at room temperature. After 24 hours the substrates were rinsed with THF and baked on a hotplate at 110°C for 20 minutes to remove residual solvent. In Figure 6 an AFM height image captured inside a channel of a transistor is shown. A smooth surface comparable to the bare substrate is measured which is expected for a dense and homogenous monolayer. Some high islands of approximately 20 nm are also found which are supposed to be PBI-PA aggregates.

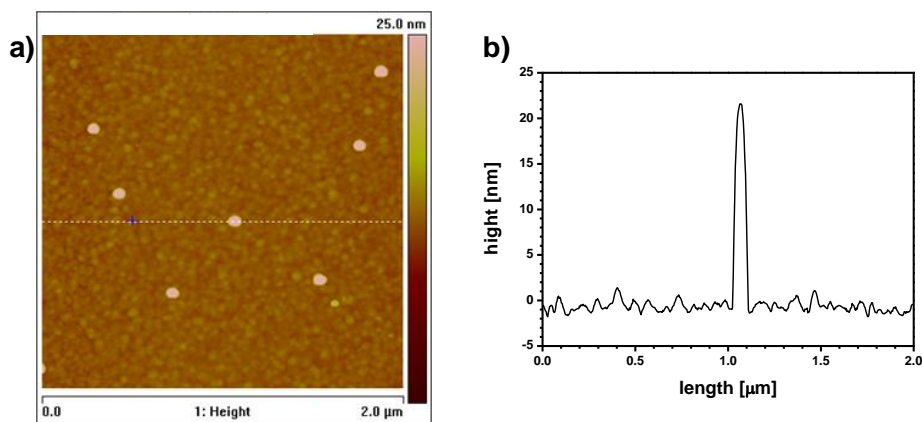


Figure 6: a) AFM height image of a PBI-PA SAMFET and b) the corresponding cross section.

To get information about the thickness X-ray photoelectron spectroscopy (XPS) and X-ray reflectivity (XRR) measurements were done. XPS studies show that a 3.1 nm thick organic layer is grown on top of the aluminum oxide dielectric. Additionally the XPS measurements revealed that the phosphorus is present within the whole organic layer. It is assumed that due to strong intermolecular π - π -stacking of the perylene cores not all phosphonic acid groups react with the surface which suggests some kind of tilted configuration of the molecules. Further informations are given by XRR investigations which also pointed out that a smooth and 3.0 nm thick organic layer is assembled on top of the dielectric. For simulations of the XRR measurements, the layer is segmented into three different interlayer's having a thickness from top to the bottom of 0.71 nm, 0.98 nm and 1.32 nm. XRR analysis also showed an enhanced electron density in the middle layer which suggests that here the aromatic core is present.

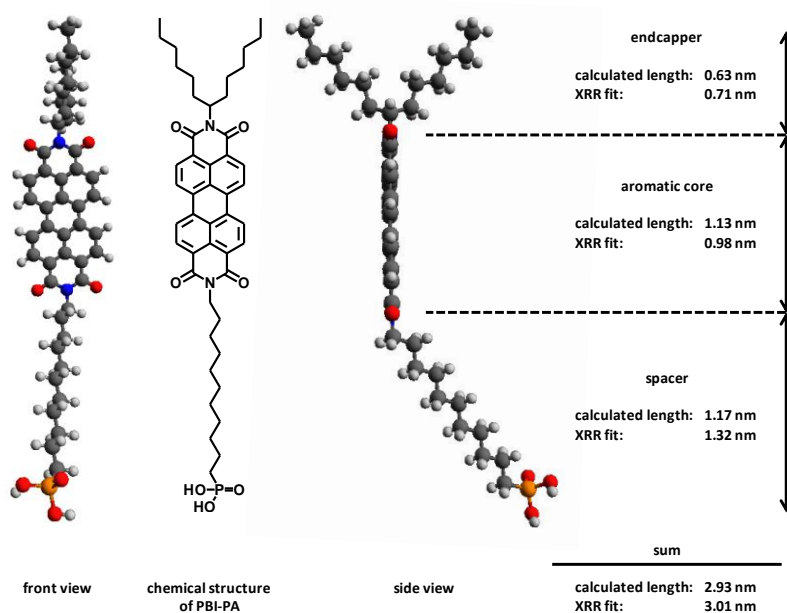


Figure 7: Calculated intramolecular distances of PBI-PA and results of XRR measurements.

Molecular modeling using Avogadro 1.0.3 software with the united force-field (UFF) was done to get informations about the length of the different molecular units inside the PBI-PA molecule. As shown in figure 7 the result of the experimental XRR investigations matches quite well with the theoretical thickness of the monolayer. The in-plane order of the monolayer was investigated by grazing incidence X-ray (GIXD). A broad reflex at $q_{xy} = 17.1 \text{ nm}^{-1}$ was found which revealed a perylene core-core distance of 0.36 nm. From the width of the diffraction peak (Δq_{xy}) of 2 nm^{-1} , the correlation length, or crystal size, was estimated to be 3.1 nm. This length corresponds to 9 perylene cores.

SAMFETs have been prepared by immersing predefined transistor substrates with an aluminum oxide dielectric and gold electrodes into a solution of PBI-PA like described before. All measured transistors showed field-effect behavior. Mobilities up to $10^{-3} \text{ cm}^2/\text{Vs}$ and high on/off-ratios of 10^5 were obtained. SAMFETs with channel length up to $100 \text{ }\mu\text{m}$ were obtained for the first time. The mobility increases with the channel length and saturates at a channel length of $40 \text{ }\mu\text{m}$ which is a fingerprint for SAMFETs with a completely covered surface^[19]. Typical transfer and output characteristics are shown in Figure 8. It is remarkable that all of the measured transistors worked (device yield = 100%). Also the fact that working SAMFETs can be prepared from a PBI-PA solution which has been stored for several weeks under ambient conditions demonstrates that PBI-PA is a robust molecule for the preparation of n-type SAMFETs.

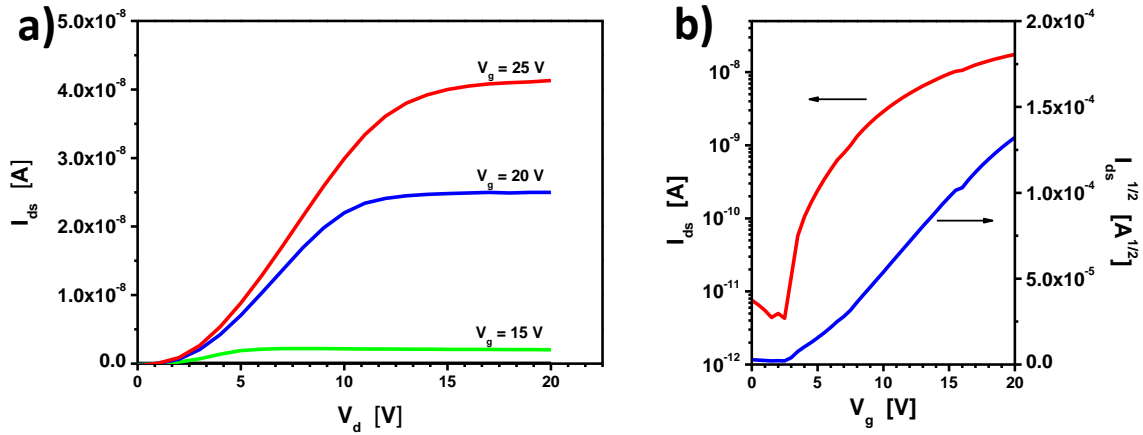


Figure 8: a) Transistor characteristics of a SAMFET based on PBI-PA with a channel length of $40 \text{ }\mu\text{m}$ and a channel width of $1000 \text{ }\mu\text{m}$. a) Output characteristics: the drain voltage is swept from 0 V to 20 V, the gate voltage is varied starting from 0 V to 25 V in 5 V per step. b) Transfer characteristics of the device in the saturation regime with a drain voltage of 20 V.

A bias inverter based on the complementary metal-oxide-semiconductor (CMOS) technology was built using a p-type and an n-type SAMFET on two substrates. The p-type SAMFET is based on a thiophene derivative connected covalently to silicon dioxide¹². PBI-PA on aluminum oxide was used for the n-type SAMFET. Both SAMFETs were connected in a complementary inverter configuration as depicted in figure 9b. The resulting inverter characteristics are shown in figure 9a. When the supply voltage (V_{dd}) was set at 30 V and the input voltage (V_{in}) was swept from 30 V to 0 V, a high gain value of ~ 15 with the “trip-point” at around 23 V of V_{in} and a noise margin of 7 V was obtained.

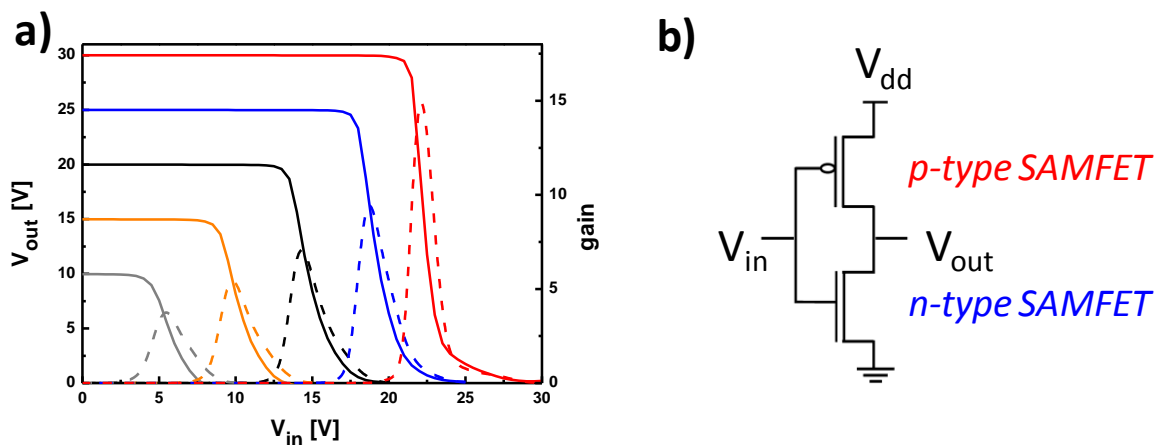


Figure 9: SAMFET based complementary inverter. (a) Device characteristics: The supply voltage (V_{dd}) was varied starting from 10 V to 30 V in 5 V per step. The dashed lines present the gains. (b) Diagram of the bias inverter.

4. Summary

In summary we synthesized a new perylene bisimide, having a semiconducting perylene bisimide core, a branched alkyl tail on one side to increase solubility and on the other side a linear alkyl tail with a phosphonic acid anchor group. The phosphonic acid anchor group enables a covalent fixation of the perylene bisimide to aluminum oxide surfaces. With this substance we were able to fabricate highly reproducible monolayer field-effect transistors by simple self-assembly under ambient conditions. High on/off-ratios of 10^5 and mobilities up to 10^{-3} cm^2/Vs were achieved. Besides the transistors a CMOS bias inverter based solely on SAMFETs was realized for the first time and showed a large noise margin of 7 volts and a high gain of 15.

5. Acknowledgement

The work of Andreas Ringk and Fatemeh Gholamrezaie forms part of the research programme of the Dutch Polymer Institute (DPI), projects 624 and 627. We gratefully acknowledge Dr. C. van der Marel (Philips Research Laboratories, Eindhoven) for the XPS analysis and fruitful discussions. We are grateful to Bas van der Putten (Holst Centre) for technical assistance, to Ingo Salzmänn (Humboldt University Berlin) for help with the X-ray measurements and the Austrian Science Foundation FWF:[P21094].

6. References

- [1] Whitesides, G. M.; Grzybowski, B. Self-Assembly at All Scales. *Science*. **295**, **2002**, 2418-2421.
- [2] Linford, M. R.; Fenter, P.; Eisenberger, P. M.; Chidsey, C. E. D, J. Alkyl monolayers on silicon prepared from 1-alkenes and hydrogen-terminated silicon. *J. Am. Chem. Soc.* **117**, **1995**, 3145-3155.
- [3] O'Regan, B.; Grätzel, M. A low-cost, high-efficiency solar cell based on dye-sensitized colloidal TiO₂ films. *Nature*. **353**, **1991**, 737-740.
- [4] Besbes, S.; Ltaief, A.; Reybier, K.; Ponsonnet, L.; Jaffrezic, N.; Davenas, J.; Ben Ouada, H. Injection modifications by ITO functionalization with a self-assembled monolayer in OLEDs. *Syn. Met.* **138**, **2003**, 197-200.
- [5] Chua, L.-L.; Zaumseil, J.; Chang, J.-F.; Ou, E. C.-W.; Ho, P. K.-H.; Sirringhaus, H.; Friend, R. H. General observation of n-type field-effect behaviour in organic semiconductors. *Nature*. **434**, **2005**, 194-199.
- [6] Novak, M.; Schmaltz, T.; Faber, H.; Halik, M. Influence of self-assembled monolayer dielectrics on the morphology and performance of α,ω -dihexylquaterthiophene in thin film transistors. *Appl. Phys. Lett.* **98**, **2011**, 093302.
- [7] Collet, J.; Tharaud, O.; Chapoton, A.; Vuillaume, D. Low-voltage, 30 nm channel length, organic transistors with a self-assembled monolayer as gate insulating films. *Appl. Phys. Lett.* **76**, **2000**, 1941-1943.
- [8] Cheng, X.; Noh, Y.-Y.; Wang, J.; Tello, M.; Frisch, J.; Blum, R.-P.; Vollmer, A.; Rabe, J. P.; Koch, N.; Sirringhaus, H. Controlling Electron and Hole Charge Injection in Ambipolar Organic Field-Effect Transistors by Self-Assembled Monolayers. *Adv. Funct. Mater.* **19**, **2009**, 2407-2415.
- [9] Dinelli, F.; Murgia, M.; Levy, P.; Cavallini, M.; Biscarini, F.; de Leeuw, D. M. Spatially Correlated Charge Transport in Organic Thin Film Transistors. *Phys. Rev. Lett.* **92**, **2004**, 116802.
- [10] Liu, S.-W.; Lee, C.-C.; Wen, J.-M.; Chen, C.-T. In situ vacuum measurement of the thickness dependence of electron mobility in naphthalenetetracarboxylic diimide-based field-effect transistors. *Appl. Phys. Lett.* **98**, **2011**, 023306.
- [11] Tulevski, G. S.; Miao, Q.; Fukuto, M.; Abram, R.; Ocko, B.; Pindak, R.; Steigerwald, M. L.; Kagan, C. R.; Nuckolls, C. Attaching organic semiconductors to gate oxides: In situ assembly of monolayer field effect transistors. *J. Am. Chem. Soc.* **126**, **2004**, 15048–15050.
- [12] Smits, E. C. P.; Mathijssen, S. G. J.; van Hal, P. A.; Setayesh, S.; Geuns, T. C. T.; Mutsaers, K. A. H. A.; Cantatore, E.; Wondergem, H. J.; Werzer, O.; Resel, R.; Kemerink, M.; Kirchmeyer, S.; Muzafarov, A. M.; Ponomarenko, S. A.; de Boer, B.; Blom, P. W. M.; de Leeuw, D. M. Bottom-up organic integrated circuits. *Nature*. **455**, **2008**, 956-959.

- [13] de Leeuw, D. M.; Simenon, M. M. J.; Brown, A.R.; Einerhand, R. E. F. Stability of n-type doped conducting polymers and consequences for polymeric microelectronic devices. *Synthetic Metals*. 87, **1997**, 53-59.
- [14] Novak, M.; Ebel, A.; Meyer-Friedrichsen, T.; Jedaa, A.; Vieweg, B. F.; Yang, G.; Voitchovsky, K.; Stellacci, F.; Spiecker, E.; Hirsch, A.; Halik, M. Low-voltage p- and n-type organic self-assembled monolayer field effect transistors. *Nano Lett.* 11, **2011**, 156–159.
- [15] Jones, B. A.; Facchetti, A.; Wasielewski, M. R.; Marks, T. J. Tuning orbital energetics in arylene diimide semiconductors. Materials design for ambient stability of n-type charge transport. *J. Am. Chem. Soc.* 129, **2007**, 15259–15278.
- [16] Wicklein, A.; Lang, A.; Muth, M.; Thelakkat, M. Swallow-tail substituted liquid crystalline perylene bisimides: Synthesis and thermotropic properties. *J. Am. Chem. Soc.* 131, **2009**, 14442–14453.
- [17] Ringk, A.; Li, X.; Gholamrezaie, F.; Smits, E. C. P.; Neuhold, A.; Moser, A.; Gelinck G. H.; Resel, R.; de Leeuw D. M.; Strohriegl, P. N-type self-assembled monolayer field-effect transistors and complementary inverters. (submitted).
- [18] Holman, M. W.; Liu, R.; Adams, D. M. Single-molecule spectroscopy of interfacial electron transfer. *J. Am. Chem. Soc.* 125, **2003**, 12649–12654.
- [19] Mathijssen, S. G. J.; Smits, E. C. P.; van Hal, P. A.; Wondergem, H. J.; Ponomarenko, S. A.; Moser, A.; Resel, R.; Bobbert, P. A.; Kemerink, M.; Janssen, R. A. J.; de Leeuw, D. M. Monolayer coverage and channel length set the mobility in self-assembled monolayer field-effect transistors. *Nature Nanotech.* 10, **2009**, 674-680.

Andreas Ringk, Xiaoran Li, Fatemeh Gholamrezaie, Edsger C. P. Smits, Alfred Neuhold, Armin Moser, Cees Van der Marel, Gerwin H. Gelinck, Roland Resel, Dago M. de Leeuw, Peter Strohriegl

“N-Type Self-Assembled Monolayer Field-Effect Transistors and Complementary Inverters”

Advanced Functional Materials, 23, 16, **2012**, 2016–2023.

DOI: 10.1002/adfm.201202888.

Andreas Ringk, Xiaoran Li, Fatemeh Gholamrezaie, Edsger C. P. Smits, Alfred Neuhold, Armin Moser, Gerwin H. Gelinck, Roland Resel, Dago M. de Leeuw, Peter Strohriegl

“N-Type Self-Assembled Monolayer Field-Effect Transistors”

Proceedings of SPIE, **2012**, 8478, 847813.

DOI: 10.1117/12.929535

Simon Bubel, **Andreas Ringk**, Peter Strohriegl, Roland Schmechel

“N-Type Perylene To Fill Voids In Solution Processed Nanoparticulate Zinc Oxide Thin Films”

Physica E, 44, **2012**, 2124–2127.

DOI: 10.1016/j.physe.2012.06.027

Andreas Ringk,^{a,b} W. S. Christian Roelofs,^c Edsger C. P. Smits^{d,*}, Cees van der Marel,^e Ingo Salzmann,^f Alfred Neuhold,^g Gerwin H. Gelinck,^d Roland Resel,^g Dago M. de Leeuw,^h Peter Strohriegl^{a,*}

“N-Type Self-Assembled Monolayer Field-Effect Transistors for Flexible Organic Electronics”

Organic Electronics, 14, 5, **2013**, 1297–1304.

DOI: [org/10.1016/j.orgel.2013.02.016](https://doi.org/10.1016/j.orgel.2013.02.016)

Conference talks:

“N-Type Self-Assembled Monolayer Field-Effect Transistors - Towards SAM-CMOS Circuits“

SPIE conference, Organic Field-Effect Transistors XI,

San Diego, USA, 14 August, **2012**.

“N-Type Self-Assembled Monolayer Field-Effect Transistors”

6th Winterschool on Organic Electronics, Self-Assembly and Hybrid Devices, Planneralp, Austria, 07 March, **2012**.

Additional talks:

“Self-Assembled Monolayers for FET Applications”

Dutch Polymer Institute - Functional Polymer Systems Review Meeting,

Eindhoven, The Netherlands, 29 October, **2012**.

“Self-Assembled Monolayers for FET Applications”

Dutch Polymer Institute - Functional Polymer Systems Review Meeting,

Eindhoven, The Netherlands, 03 April, **2012**.

“Air Stable N-Type Field-Effect Transistors”

Dutch Polymer Institute - Functional Polymer Systems Review Meeting,

Eindhoven, The Netherlands, 29 March, **2011**.

“Air Stable N-Type Field-Effect Transistors”

Philips - Project Meeting,

Eindhoven, The Netherlands, 28 March, **2011**.

“Hetero Substituted Perylenebisimides for the Application in Field-Effect Transistors”

Dutch Polymer Institute - Functional Polymer Systems Review Meeting,
Noordwijkerhout, The Netherlands, 13 October, **2010**.

“Air Stable N-Type Field-Effect Transistors”

Dutch Polymer Institute - Functional Polymer Systems Review Meeting,
Arnhem, The Netherlands, 16 March, **2010**.

“Air Stable N-Type Field-Effect Transistors”

Dutch Polymer Institute - Functional Polymer Systems Review Meeting,
Utrecht, The Netherlands, 24 September, **2009**.

“Air Stable N-Type Field-Effect Transistors”

Dutch Polymer Institute - Functional Polymer Systems Review Meeting,
Amsterdam, The Netherlands, 23 March, **2009**.

“Air Stable N-Type Field-Effect Transistors”

Dutch Polymer Institute - Functional Polymer Systems Review Meeting,
Amsterdam, The Netherlands, 04 October, **2008**.

Poster presentations:

Andreas Ringk, Xiaoran Li, Edsger Smits, Fatemeh Gholamrezaie, Gerwin Gelinck,
Dago de Leeuw, Peter Strohrriegl

“N-Type Self-Assembled Monolayer Field Effect Transistors - Towards SAM-CMOS-
Circuits”

Dutch Polymer Institute - Functional Polymer Systems Mini-Symposium,
Maastricht, The Netherlands, 05 – 06 October, **2012**.

Andreas Ringk, Peter Strohrriegl

“Air stable N-Type Field-Effect Transistors based on Diphenquinones”

9th International Symposium on Functional π -Electron Systems,
Atlanta, USA, 25 May, **2010**.

DANKSAGUNG/ACKNOWLEDGMENT

An dieser Stelle möchte ich mich bei allen bedanken die in irgendeiner Art und Weise zu dem Gelingen dieser Arbeit beigetragen haben bedanken.

Allen voran danke ich meinem Doktorvater Prof. Dr. Peter Strohrig für die Bereitstellung einer äußerst interessanten, vielseitigen und abwechslungsreichen Themenstellung (die jeden Tag zum SAM'sTag machten) sowie seiner steten Hilfsbereitschaft zu jeder beliebigen Minute.

Bei dem Lehrstuhlinhaber, Prof. Dr. Hans-Werner Schmitt, bedanke ich mich für die Bereitstellung eines ausgezeichnet ausgestatteten Laborplatzes.

Bei meinen Kollaborationspartnern der Universität Duisburg/Essen, Prof. Dr. Roland Schmechel und Dr. Simon Bubel bedanke ich mich für die gute Zusammenarbeit.

I would also like to thank my collaboration partners from the Netherlands, especially, Edsger C. P. Smits for enabling my stays at the Holst Centre in Eindhoven, his supervision, his support, and for lots of fruitful discussions.

Special thanks, also to Xiaoran Li for his effort, measurements and for the nice time in the Holst Labs with approximately thousand litres of tomato soup per week.

Thanks to Gerwin H. Gelinck for the desk in his group, and for his helpful discussions.

I am very grateful to Prof. Dr. Dago M. de Leeuw that he has given me the opportunity to work in his lab and for his help with a range of various issues. Thanks, also, to Fatemeh Gholamrezaie for her help in the Philips labs.

Many thanks to Cees van der Marel for the XPS measurements.

Last, but definitely not least, thousand thanks to Christian W. S. Roelofs for his effort to get nice, flexible SAMFETs.

Dank u wel!

Ein großer Dank gilt auch Prof. Dr. Roland Resel, Alfred Neuhold und Armin Moser für deren Röntgenuntersuchungen an den SAMs.

Vielen Dank auch an meine Praktikanten Christina Saller, Markus Herling, Philipp Knauer und Thomas Wittmann für deren Synthesen und Messungen während diverser Praktika.

Meinem kleinen, großen Bruder, Daniel Ringk, danke ich für die schnelle Durchsicht dieser Arbeit.

Für die freundschaftliche und harmonische Zusammenarbeit im Labor und außerhalb möchte ich mich bei den 595ern Andrea Jahreis, Christina Saller, Daniel Wagner, Esther Rothmann, Irene Bauer, Michael Rothmann, Pamela Schörgel und Philipp Knauer herzlichst bedanken.

Dem gesamten Lehrstuhl MCI danke ich für eine freundschaftliche Zusammenarbeit. Ein ganz besonderer Dank gilt hierbei der weltbesten Doris der Welt (=Doris Hanft). Ein großes Dankeschön auch an Katharina Neumann, Klaus Kreger und Robin Pettau für zahlreiche GPC-Messungen sowie an Ruth Lohwasser für die MALDI-Messungen.

Unzählige Stunden, viele hilfreiche Diskussionen, Anregungen und Spaß zusammen mit den in Bayreuth gewonnen Freunden, sei es im Kemiellabor, Kaffezimmer oder in der Freizeit außerhalb der Universität, werden die Doktorandenzeit für mich garantiert unvergesslich machen. Daher möchte ich den Leutz aus der AC, CSG, EP, MCII, OC, PC und nicht zu vergessen meinen Freunden aus der guten alten Heimat „Berndshausen und Umgebung“, die hier nicht alle namentlich erwähnt sind und trotzdem, wenn auch nicht immer im fachlichen Sinne, einen beachtlichen Beitrag zu dieser Arbeit beigetragen haben, Danke! sagen.

Zuletzt bedanke ich mich bei meiner Familie und ganz speziell bei meinen Eltern die mich im Laufe meines Studiums und der Doktorarbeit stets unterstützt und motiviert haben.

Mercredi !!!

Erklärung

Hiermit erkläre ich, dass ich die Arbeit selbständig verfasst und keine anderen als die angegebenen Hilfsmittel verwendet habe.

Ferner erkläre ich, dass ich nicht versucht habe, anderweitig mit oder ohne Erfolg, eine Dissertation einzureichen oder mich der Doktorprüfung zu unterziehen.

Bayreuth, Dezember 2012

Andreas Ringk